Chapter 1

Introduction

Molecular oxygen is an essential component for every aerobic organism on Earth. Including humans, all respiring life forms require oxygen to generate energy based on biochemical combustion of glucose producing CO_2 and H_2O. In spite of this fundamental necessity, the irony regarding molecular oxygen is that it has a cytotoxic nature. It has long been known that elevation of oxygen concentration in the atmosphere can cause severe cell damage, which is called the Paul Bert effect [1]. This poisoning effect of oxygen has been a mystery for a long time and has only been identified relatively recently as with the understanding of free radicals and their biological roles. The fact is that oxygen can react with certain metal containing components in our body, producing highly reactive and toxic forms of oxygen, called collectively "Reactive Oxygen Species (ROS)".

ROS include various types of oxygen-derived molecules, such as, oxygen free radicals (superoxide, hydroxyl radicals), peroxides (hydrogen peroxide), energetically excited molecular oxygen (singlet oxygen), and is sometimes more widely termed to include reactive nitrogen oxide species (such as nitric oxide and peroxynitrite). Chemically, the ROS can be understood as the intermediates of sequential single electron reduction of oxygen towards water (oxygen → superoxide anion → hydrogen peroxide → hydroxyl radical → water) [2-4]. The ROS are inevitable

byproducts of any aerobic metabolism in biology. In more detail, ROS are generated from various endogenous sources, such as electron leakage in cellular respiration through an electron transport chain in mitochondrial metabolism [2-4] and interaction of stimulants with membrane receptors in phagocytotic cells, as a host defense system against parasites and foreign objects [5-8]. The toxicity of ROS must be controlled to avoid non-specific collateral damage to normal cells and thus the ROS are delicately balanced in cells with antioxidants and antioxidant enzymatic activities (such as superoxide dismutases, and peroxidases) [2-4].

The ROS can also be introduced to the body exogenously. Radiation and photosensitization are good examples [9,10]. In radiation, when a water molecule, which is a major constituent of biological systems, is exposed to radiation, the high energy of radiation can ionize the water molecule, and the excited water ions can produce ROS by incorporating with other water molecules. In photosensitization, some specific photoactive drugs (photosensitizers) are introduced to the system. When photosensitizers are illuminated with light with a certain wavelength, they can be energetically excited by absorbing photon energy, and then go back to their ground state by transferring the energy to oxygen molecules, resulting in singlet oxygen. These methods for artificial ROS generation have been enthusiastically utilized in medicine for treatment of malignant diseases that are hardly curable with conventional therapy or surgical methods.

It has been widely accepted that the ROS can readily oxidize diverse biomolecules, interrupting their cellular functions and, eventually, inducing cell death [11,12]. There have been a number of works reporting the connection of ROS with many normal and abnormal physiological events. In normal condition, ROS participate in

ageing, cell cycle and death, host defense system, cell signaling and so on [3,13]. When the balance between ROS and antioxidants are broken, they cay be related with diverse pathogenic conditions, such as, ischemia and blood reperfusion injury, neurodegenerative diseases, and cancer [14-16].

Although our knowledge about mechanisms and functions of ROS in biology has been rapidly expanded by decades of effort, large parts of them still remain enigmatic yet. It is mainly due to the extreme reactivity and unstable nature of ROS. ROS have very short lifetime typically in the range of nano seconds to mili seconds, which means very short diffusion distance. Also, the lifetime of ROS can be even shorter in biological environments because they can be rapidly quenched by reacting with various biomolecules non-specifically. It implicates that the effect induced by ROS activities should be confined in very small space in very short time span. This unique property requires extraordinarily high sensitivity of the mean for detecting / observing ROS related mechanisms and functions. Furthermore, the mechanisms of ROS activity in biology are often the consequence of a combination among multiple types of ROS and the reactions among them are closely interconnected and interconvertible. It implicates that the detection materials or methods must also be specific to certain types of ROS, in addition to the requirement of high sensitivity. Because of these obstacles, more accurate, quantitative, and comprehensive investigations about ROS biofunctions are highly challenging, thus shackling all ROS research and its potential applications.

Optical sensing with fluorescence indicators is a powerful tool for investigating the mechanisms of biological events in living organisms, on the macroscopic or microscopic scale, and has been widely used for ROS research [17]. Fluorescence

indicators enable visualization of biological events, based on their optical property changes specific to certain analytes, with good sensitivity. Fluorescence can be and has been widely utilized for bioimaging, spectroscopy, quantitative analysis, flow cytometry and so on. Also, fluorescence techniques are easily applied to *in vitro/in vivo* measurements, are typically non invasive, and there are a large variety of fluorescence indicators for various analytes. However, fluorescence also has some drawbacks that have been limiting the application of this technique. The fluorescence indicator dyes can readily interact with cellular components, chemically or physically. The method requires sufficient amounts of dye molecules to obtain recognizable responses; this might interrupt the cellular function and even could be toxic. Also, the optical properties of fluorescence indicators are often influenced by other environmental factors, such as pH, temperature, solubility and protein content. Furthermore, these dyes are not free from photobleaching and can be commonly interfered with by other molecules that are similar to the goal analytes. These disadvantages can be even more crucial when we want to investigate the ROS which usually are uncontrollable, short-lasting analytes.

In order to optimize the efficiency of the fluorescence based optical sensing technique, and to overcome those drawbacks, the encapsulation of the fluorophores inside a protective matrix has been developed. A most widely studied method is that of optical fiber based biosensors [18]. The fiber optic sensors are usually fabricated by incorporating the sensing moiety on the tip of the fiber, using polymerized matrix entrapping for the fluorophores. These sensors can be used to monitor local changes of analytes, by simply probing with the sensor tip in the wanted region. The confinement of sensing fluorophores inside small spaces of polymeric matrixes provides a sufficient

intensity of response and, at the same time, reduces the chemical perturbation to the cellular function by administrating the dye into the system. This fiber optic sensor has further progressed with miniaturizing the size of the sensor in order to monitor smaller objects like cells or organelles. Many tricks to develop fine tips of optical fibers, typically in the submicron size,have been derived, including modified pipette pulling methods. The smaller size of the pulled optical fiber enabled the detection of intracellular events [19]. However, in spite of its small size, the fiber stem still needs to be connected to the tip and thus the sensor tip must be internalized with puncturing and, thus, damaging the cellular membrane, so as to monitor intracellular analytes. On the microscopic scale, this damage and the physical perturbation induced by piercing with the fiber tip cannot be neglected and the natural cellular event should be influenced.

Because of the above, the miniaturization of optical sensors needs to be even further advanced. The Kopelman research group has pioneered the nanoparticle type optical sensors, named PEBBLEs (Photonic Explorers for Biomedical uses with Biologically Localized Embeddings). PEBBLEs were first developed by then a member of our group, Dr. Heather A. Clark, in 1998 [20]; they can be defined comprehensively as biocompatible nanoparticles containing photo-chemically functional molecules. Typically being in the 20 nm to few 100's nm size in diameter, particles made of various organic/inorganic materials have been developed as PEBBLEs, and a number of biologically important analytes have been successfully detected with PEBBLE technology. For example, PEBBLE nano sensors or probes for ions (proton, calcium, potassium, copper, zinc, etc.) [21-24], small molecules (oxygen, glucose, etc.) [25,26], free radicals (hydroxyl radical, superoxide, single oxygen, etc.) [27-29] have been

developed. More recently, by coating the half sphere of a PEBBLE with magnetic metal and monitoring the rotation of this half coated PEBBLE blinking, using external magnetic force or Brownian motion, the recognizability (signal to noise ratio) of this PEBBLE nanosensor can be dramatically improved and the application of PEBBLE sensors has been expanded to monitoring physical parameters, such as viscosity of the medium, velocity, temperature, and so on [30,31].

PEBBLEs can have diverse important advantages over "naked" molecular probes and other conventional optical sensors. The small size of PEBBLEs in nm dimension can dramatically reduce physical perturbation to cellular function and viability. The encapsulation of the detecting materials inside of the protective matrix can minimize chemical/biological perturbations to the cell. Also, the biocompatible matrix can protect the functional molecules inside from unwanted non-specific reaction with biomolecules in the biological systems, maintaining the functionality intact. Encapsulation inside the PEBBLE matrix can widen the tolerance of the material properties, for instance when the materials in their naked form could not be used for the biological system because of inappropriate properties or toxicity, in spite of their other excellent properties. Another important benefit of PEBBLE technology is its potential multifunctionality. More than one type of functional molecule can be embedded together in one PEBBLE, giving simultaneously capabilities for different goals. Furthermore, the PEBBLE surface can be easily modified: by conjugating secondary functional units such as peptides or antibodies for homing to specific targets; or by attaching a second fluorescence label, thus avoiding fluorescence energy transfer between different dyes; or by attaching polyethyleneglycol (PEG) to improve biocompatibility and colloidal stability of the PEBBLEs.

Several different materials for PEBBLE matrix have been used, including polyacrylamide (PAA) [23,24,26], poly-decylmethacrylate (PDMA) [22], sol-gel silica [27], organically modified silicate (Ormosil) [25,29]. The Ormosil matrix will be mainly focused on here. Ormosil particles are the most recently introduced PEBBLE matrix, with typical size in the range of 100 – 300 nm in diameter, developed by Hah *et al*. [32]. Ormosil nanoparticles can be synthesized based on the combination of the microemulsion technique and the sol-gel method, and has been used for the oxygen detecting PEBBLE nanosensor [25] and for singlet oxygen detecting PEBBLE nanoprobes [29]. This matrix is relatively hydrophobic, because of its organic component, but is still applicable to aqueous media. Thus, the Ormosil matrix is capable of encapsulating both water-soluble dyes and water-insoluble dyes. Also, the matrix is composed of 2 different layers, with a phenyl group rich inner layer, with relatively low density, and a methyl group rich outer layer, with relatively higher density. The mix of these two different 3-dimensional networks, with different mesh size, provides the advantage that larger amounts of dye molecules can be efficiently contained, without significant dye leaching, which is a typical problem for different nanoparticles. Also, the Ormosil nanoparticle is known for having a hollow structure in its core region. Although the hollow structure can have some importance for other applications, it was found that only a negligible portion of the Ormosil nanoparticles have the hollow inside in our typical size PEBBLEs (around 100 nm in diameter); thus the hollow structure has only little relevancy to our work here.

In this body of works, 3 different research projects, all based on PEBBLE nanosensors with an Ormosil matrix, but designed for different ROS, will be discussed. The first project is about the development of singlet oxygen detecting Ormosil PEBBLE

nanoprobes with improved sensitivity, the second project is about the development of hydrogen peroxide detecting Ormosil PEBBLE with enhanced selectivity, and the last project is about the application of Ormosil PEBBLE for near infrared photo-acoustic bioimaging, and for photodynamic therapy based on singlet oxygen generation from the PEBBLE.

In chapter 2, singlet oxygen detecting Ormosil PEBBLE will be discussed. Singlet oxygen is an electronically excited state of molecular oxygen, in which one electron is moved to a higher energy orbital. Whether singlet oxygen is normally generated *in vivo* and how it occurs, if so, are still in debate. However, singlet oxygen has been mainly studied in artificially generated systems, based on the photodynamic effect. This photosensitization principle has been utilized for treatment of cancer, clinically called photodynamic therapy (PDT) and PDT has raised much interest as an alternative cancer treatment. Singlet oxygen is highly reactive and very short lived. Thus, quantitative investigation of single oxygen is quite challenging and has been rarely achieved so far. Although several molecular probes that are sensitive towards singlet oxygen are already available, the sensitivity of water-soluble probes which are appropriate for biomedical use is often insufficient. In our research, a new singlet oxygen probe, 1,3-diphenylisobenzofuran, which is significantly more sensitive than water-soluble probes, and has been used only in organic media, because of its strong hydrophobicity, was introduced by encapsulation into Ormosil PEBBLE. It will be shown here that this PEBBLE has better sensitivity towards singlet oxygen. Also, using the improved sensitivity of these PEBBLEs, a method for direct quantification of singlet oxygen, for in vitro photodynamic therapy systems, is developed.

In chapter 3, a simple but novel technique, using Ormosil PEBBLE to obtain improved hydrogen peroxide selectivity, will be described. H_2O_2 is the most stable ROS, having a few seconds long lifetime, and thus readily detectable. Thus the biological roles of H_2O_2 have been relatively well investigated, such as phagocytosis, a host defense system, and oxidative intracellular signaling. However, there have been demands for better H_2O_2 detection, because most H_2O_2 sensitive probes are susceptible to other ROS as well. Our group has attempted to develop PEBBLE sensors/probes sensitive towards a specific type of ROS, but has experienced unsuccessful results. It has been suspected that the PEBBLE matrix might be hindering the entrance of ROS and that the ROS are quenched before reaching the dye molecules inside. Applying judiciously these ideas, it is described here how Ormosil PEBBLE containing a sensitive but non-specific ROS probe became capable of detecting H_2O_2 selectively, by using the screening effect of the PEBBLE matrix.

In chapter 4, a new application of PEBBLE technology for bioimaging is proposed and explained: photoacoustic bioimaging, based on a near infrared photosensitizer embedded into Ormosil PEBBLEs. The near infrared (NIR) region (700-1000 nm in wavelength) is a hot area for biomedical optics, because biological tissues have minimal absorption in this region, thus allowing the deepest penetration of light. Also in relation with ROS, a new modality of PDT, using a new generation of photosensitizers with near IR absorption, can improve treatment efficiency. In association with NIR bioimaging, the resolution of optical or opto-acoustic imaging techniques can be enhanced for even deeper locations of tissue, without invasive surgical procedures, to obtain high quality information. We have shown that these two distinct applications could

be merged into a single discipline application, by developing near IR absorbing photosensitizers encapsulated into Ormosil PEBBLEs, thus aiming for synergistic outcomes: simultaneous photoacoustic cancer diagnostics and photodynamic therapy.

Through the above 3 researches, I would like to propose a more active concept of nanoparticle applications. Beyond simple passive functions as a sensor, carrier or protector of functional molecules, nanoparticles can become excellent activator/effector tools to achieve diagnostic/therapeutic goals, by dynamically enhancing, limiting, or complementing the properties of the functional contents inside.

References

1. P. Bert, La pression Barometrique, Paris, 1878
2. *Free Radicals in Biology* V 1, Edited by William A. Pryor, Academic Press (1976)
3. Matthew B. Grisham, *Reactive Metabolites of Oxygen and Nitrogen in Biology and Medicine*, R. G. Landes Company (1992)
4. Manfred K. Eberhardt, *Reactive Oxygen Metabolites: Chemistry and Medical Consequences*, CRC Press (2001)
5. B. M. Babior, Oxygen-dependent microbial killing by phagocytes, *N. Eng. J. Med.* (1978) v298(12), 659-668
6. R. Oren., M. L. Karnovsky *et al*., Metabolic Patterns in Three Types of Phagocytizing Cells, *J. Cell Biol.* (1963) v17(3), 487-501
7. M. L. Karnovsky, J. Lazdins, and S. Simmons, Metabolism of mononuclear phagocytes at rest and during phagocytosis, in *Mononuclear Phagocytes*, Edited by R. van Furth, Blackwell Scientific Publications (1975)
8. C. F. Nathan and R. K. Root, Hydrogen Peroxide Release from Mouse Peritoneal Macrophages: Dependence on Sequential Activation and Triggering, *J. Exp. Med.* (1977) v146,1648-1662
9. J. Weiss, Radiochemistry of aqueous solutions, *Nature* (1944), v153, 748-750
10. *Free Radicals in Biology* V 2, Edited by William A. Pryor, Academic Press (1976)
11. Dougherty T. J. *et al.* (1998). Review: Photodynamic therapy. *J. Natl. Cancer. Inst.* 90(12), 889-905
12. Moore J. V., West C. M. L., and Whitehurst C. (1997) The biology of photodynamic therapy, *Phys. Med. Biol.* 42(5), 913-935
13. S. G. Rhee, H_2O_2, A Necessary Evil for Cell Signaling, *Science* (2006) v312, 1882-1883
14. Kon T. *et al.* (2004) Singlet oxygen quenching activity of human serum. *Redox Report* 9(6), 325-330.
15. Reilly P.M. *et al.*(1991) Pharmacological Approach to Tissue Injury Mediated by Free Radicals and Other Reactive Oxygen Metabolites. *Am. J. Surg.* 161(4), 488-503
16. Kovacic P. *et al.* (2001) Mechanisms of Carcinogenesis: Focus on Oxidative Stress and Electron Transfer. *Curr. Med. Chem.* 8(7), 773-796
17. R. P. Haugland, The handbook 10^{th} edition, chapter 18, Invitrogen corp. (2008)
18. M. D. Marazuela and M. Cruz Moreno-Bondi, Fiber-Optic Biosensors: an Overview, *Anal. Bioanal. Chem.* (2002), v372, 664-682

19. W. Tan, R. Kopelman *et al*. Development of Submicron Chemical Fiber Optic Sensors, *Anal. Chem.* (1992) v64, 2985-2990

20. H. Clark, R. Kopelman, M. Philbert *et al*. Subcellular Optochemical Nanobiosensors: Probes Encapsulated by Biologically Localized Embedding (PEBBLEs), *Sensors and Actuators* B, (1998), v51, 12-16

21. H. Clark, R. Kopelman, M. Philbert et al. Optical Nanosensors for Chemical Analysis Inside Singlet Living Cells Part 2: Sensors for pH and Calcium and the Intracellular Application of PEBBLE Sensors, *Anal. Chem.* (1999) v71, 4837-4843

22. M. Brasuel, R. Kopelman, M. Philbert et al. Fluorescent Nanosensors for Intracellular Chmiecal analysis: Decyl Methacrylate Liquie Polymer Matrix and Ion-Exchange-Based Potassium PEBBLE Sensors with Real-Time Application to Viable Rat C6 Glioma Cells, *Anal. Chem.* (2001) v73, 2221-2228

23. E. J. Park, R. Kopelman et al. Ratiometric Optical PEBBLE Nanosensors for Real-Time Magnesium Ions Concentrations inside Viable Cells, *Anal. Chem.* (2003), v75, 3784-3791

24. J. Sumner, R. Kopelman et al. A fluorescent PEBBLE Nanosensor for Intracellular Free Zinc, *Analyst* (2002) v127, 11-16

25. Koo Y. L., Cao Y., Kopelman R. *et. al.* (2004) Real-Time Measurements of Dissolved Oxygen Inside Live Cells by Organically Modified Silicate Fluorescent Nanosensors. *Anal. Chem.*, 76(9), 2498-2505

26. M. King and R. Kopelman, Development of a Hydroxyl Radical Ratiometric Nanoprobe, *Sens. Act.* B, (2003) v90, 76-81

27. H. Xu, R. Kopelman et al. Fluorescent Nano-PEBBLE Sensors for the Real-Time Measurement of Glucose Inside Living Cells, *Analyst* (2002) v127, 1471-1477

28. M. King, Development of Ratiometric Nanoprobes and Nanosensors for the Detection of the Hydroxyl Radical, Hydrogen Peroxide and Superoxide, Dissertation Thesis, University of Michigan, Department of Chemistry, 2005

29. Y. Cao, R. Kopelman *et al.*, Ratiometric Singlet Oxygen Nano-optodes and Their Use for Monitoring Photodynamic Therapy Nanoplatforms. *Photochem. Photobiol.* (2005) v81(6), 1489-1498

30. J. Anker, C. Behrend, and R. Kopelman, Aspherical MagMOONs (Magnetically Modulated Optical Nanoprobes), *J. App. Phys.* (2003) v93, 6698-6700

31. C. Behrend, R. Kopelman et al., Metal Capped Brownian Modulated Optical Nanoprobes (MOONs): From Aqueous to Biological Microenrivonments, *J. Phys. Chem.*, (2004) v108, 10408-10414

32. H. J. Hah, S. M. Koo *et al.*, Simple preparation of monodisperse hollow silica particles without using templates. *Chem. Comm.*, (2003) (14), 1712-1713

Chapter 2

PEBBLE nanoprobes for singlet oxygen detection and application to *in vitro* photodynamic therapy

Introduction

Singlet oxygen ($^1O_2$), lowest excited electronic state of molecular oxygen, is one of the most reactive species in chemical and bio-chemical reactions. It is believed that singlet oxygen plays important roles in ageing processes, as well as in inflammatory diseases [1], ischemia/reperfusion injury [2], and cancer [3]. Singlet oxygen can interrupt cellular functions by oxidizing various biomolecules, such as membrane lipids, proteins, and DNA [4,5,6]. Accumulation of these oxidative stresses can trigger a cell death mechanism [7,8]. This reactivity of singlet oxygen has been utilized in some medical treatments, such as photodynamic therapy (PDT) [4,7-9].

Although quantitative information of the singlet oxygen can offer valuable information needed for exploring the mechanism related with singlet oxygen in biology as well as for improving the treatment efficiency of PDT, our knowledge largely remains at a qualitative stage. This is mainly due to difficulties in singlet oxygen detection, induced by the unique properties of singlet oxygen, which include a

remarkably reduced lifetime in aqueous media (about 2 μs or shorter), non-specific reactions with other molecules, and existence at only very low levels in physiological system. Only a few quantitative determinations of singlet oxygen levels generated from PDT in biological environments have been reported but they are still based on indirect values such as phosphorescence lifetime from singlet oxygen or singlet oxygen quantum yield, not based on direct quantification of singlet oxygen [10,11,12]. Effective means to detect singlet oxygen are still absent.

One of the widely used methods for the detection of singlet oxygen is introducing singlet oxygen sensitive chemical probes. This type of dyes can effectively quench singlet oxygen molecules by producing endoperoxides that show changes of their optical property (usually fluorescence), which can be quantitatively analyzed. Because this chemical detection depends on a permanent chemical change that is proportional to the cumulative amount of singlet oxygen, singlet oxygen can be detected even at very low levels. Based on this methodology, a number of studies have been established to evaluate the singlet oxygen generation by various photosensitizers in various solvents, using a variety of singlet oxygen probes. We have attempted to utilize this technique as well, with the water-soluble singlet oxygen probe, anthracene-9,10-dipropionic acid (APDA) [13]. However, we found that ADPA, for which the reactivity towards singlet oxygen is known to be only about 1.0×10^8 $M^{-1}s^{-1}$ [13,14], was not sensitive enough to evaluate singlet oxygen generation quantitatively in some practical situations [15]. We thus looked for a more sensitive singlet oxygen probe, so as to improve on the performance of ADPA. PEBBLE nanoprobes containing singlet oxygen chemical probe can be a good candidate for sensitive singlet oxygen probes and the feasibility of such a nanoparticle type probe

has been qualitatively demonstrated in previous work on 9,10-dimethylanthracene (DMA) encapsulated PEBBLEs from our lab [15]. The underlying rationale is that the hydrophobic probe can be applied to an aqueous system by encapsulating it into water suspended Ormosil nanoparticles, while still maintaining its higher sensitivity. Furthermore, the nanoparticle type probe has the advantages of PEBBLE sensors in biomedical applications, such as protection of the dye from cellular enzymes, prevention of sequestration of the dye into subcellular compartments, prevention of the dye from being pumped out of the cell (as in MDR, multiple drug resistance) and avoidance of interference with normal cell functions [16,17]. Furthermore, a much better selectivity towards singlet oxygen with respect to other reactive oxygen radical species, such as hydroxyl and superoxide, can be achieved because the latter cannot penetrate the nanoparticle matrix as will be described in chapter 3.

Specifically, in order to further increase the PEBBLE nanoprobe's sensitivity towards $^1O_2$, we have developed a singlet oxygen probes made of Ormosil matrix with encapsulated 1,3-diphenylisobenzofuran (DPIBF), which is one of the most sensitive fluorescence probes known for singlet oxygen detection in organic solvents [18-22]. The sensitivity of DPIBF towards singlet oxygen ranges from 8 to 47.1 x 10^8 $M^{-1}s^{-1}$, which is even higher than that of DMA (0.5 ~ 9.1 x 10^8 $M^{-1}s^{-1}$), not to mention ADPA [21,13,14]. It should be noted that, in spite of its excellent sensitivity, the use of DPIBF in biological systems has been strictly limited due to its poor water-solubility.

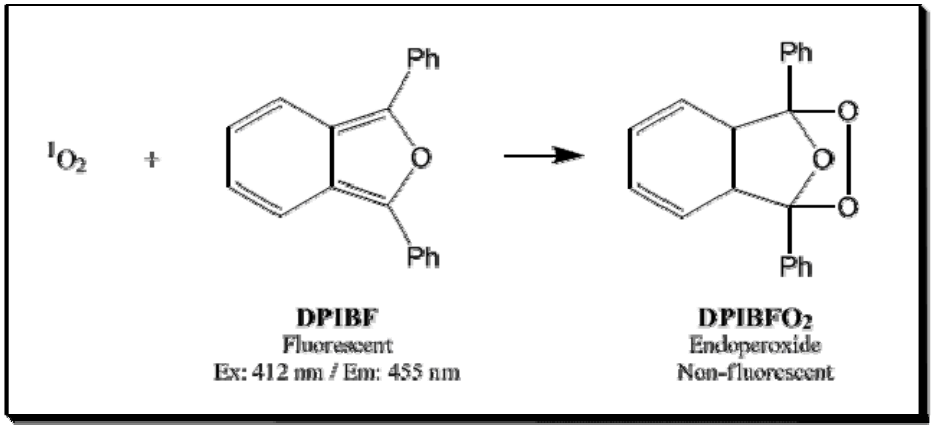

<Figure 2.1: The reaction mechanism of DPIBF with singlet oxygen. Fluorescent DPIBF can be transformed to non-fluorescent endoperoxides (DPIBFO2) by reacting with singlet oxygen.>

In this study, the DPIBF Ormosil singlet oxygen probes were prepared, characterized and tested for measuring singlet oxygen produced from the photosensitization of methylene blue, which is a well known photosensitizer, in aqueous solution. The sensitivity of the DPIBF Ormosil PEBBLE nanoprobe had to be re-determined because the $^1O_2$ sensitivity of this probe appeared changed from its free dye form, due to the nanoparticle encapsulation. Re-evaluation of this PEBBLE nanoprobe's $^1O_2$ sensitivity was achieved by comparing the nanoprobe's kinetic behavior with that of a model system. The reaction between photosensitized methylene blue (MB) and a micelle form of DPIBF, solubilized by sodium dodecylsulfate (DPIBF-SDS micelle) in aqueous media, was employed as such a model system, a system for which the reaction kinetics had been investigated by both Usui *et al.* [21] and by Gorman *et al.* [22].

This work describes how the use of the DPIBF Ormosil PEBBLE nanoprobes, with re-determined sensitivity, enabled us to quantify the amount of singlet oxygen generated from PDT systems in terms of direct values of concentration. The steady-state singlet oxygen concentrations generated from MB free dye under various conditions were

successfully measured using this DPIBF Ormosil PEBBLE nanoprobe. Also, this new technology was introduced to evaluate the efficiency of PDT based on dynamic nanoplatforms (DNPs), which are photosensitizer embedded polyacrylamide nanoparticles incorporated with specific tumor targeting, developed by our group as an advanced photodynamic therapy system.

Experimenal

Reagents

Methylene Blue (MB), 1,3-diphenylisobenzofuran (DPIBF), sodium dodecyl sulfate (SDS), phenyltrimethoxysilane (PTMS), and methyltrimethoxysilane (MTMS) were obtained from Aldrich (Milwaukee, WI) and used without further purification. Solvents for PEBBLEs synthesis and analysis including nitric acid, ammonium hydroxide and ethanol were obtained from Aldrich as well. MB DNP for in vitro PDT, prepared by incorporating the MB dye to PAA matrix by covalent bonding, was provided by Dr. Hoejin Hah in our group.

Synthesis of DPIBF Ormosil PEBBLE nanoprobes

The synthesis of the Ormosil nanoparticles was achieved following previously described methods [15,23,24]. Specifically, 31 mL of deionized (DI) water and 34 μL of nitric acid were mixed in a 100 mL round bottom flask. The solution was set in a water bath with heating on a VWR signature hot plate stirrer, model 575 (West Chester, PA), to maintain the reaction temperature at 60 ºC; then 2.4 mg of DPIBF was dissolved into 0.08

mL of PTMS and the PTMS solution was added to the heated solution. The solution was magnetically stirred at 1000-1300 RPM for 20 minutes, in order to form fine PTMS droplets and to obtain sufficient hydrolysis of PTMS under acidic conditions. 6 mL of ammonium hydroxide was quickly added to the solution, so as to convert the acidic environment to a basic environment in order to initiate condensation. The reaction mixture was stirred for 2 hours with heating, until the solution looked half cloudy. Then, 0.16 mL of MTMS was added into the reaction mixture and the reaction was run further for 1 or 2 hours until the solution become milky. The product was rinsed 3 times with a DI water/95 % ethanol (50:50) mixture to purify resulting PEBBLEs removing unwanted remnants, with a 0.1 μm pore size Osmonics MAGNA nylon filtration membrane (Minnetonka, MN), with suction, and the product was allowed to air-dry.

SEM imaging

DPIBF embedded Ormosil PEBBLE nanoprobes were suspended in water to give a 0.1 mg/mL concentration and then sonicated for several minutes. A droplet of this suspension was placed on an SEM stub, dried by air, and layered using a sputter gold coater for 100 seconds. SEM images of DPIBF embedded Ormosil PEBBLE nanoprobes were taken with a Phillips/FEI XL30 Scanning Electron Microscope (SEM) (Hillsboro, OR).

Optical instrumentation

Non-biological measurements of the DPIBF fluorescence emission spectrum to estimate the embedded dye amount in the nanoparticles and to detect singlet oxygen, and

the illumination of the photosensitizer to generate singlet oxygen have all been performed with a Jovin Yvon SPEX fluoromax-3 spectrofluorometer (Edison, NJ), using a xenon arc lamp as the light source. The DPIBF emission spectra were monitored in the range of 420 – 620 nm, with a 412 nm excitation wavelength and with a slit width of 2 nm, for both the excitation and emission spectra. Singlet oxygen generation was achieved by illuminating the MB-DPIBF mixture at 660 nm (beam power about 2 mW), which is the excitation wavelength for MB [25,26], for 5 minutes, with slit widths of 10 nm and 2 nm, for excitation and emission, respectively. The measured power of the illuminating beam was about 2 mW. Spectral data of DPIBF emission were acquired by the Datamax software provided by the manufacturer of the spectrofluorometer.

The UV-VIS absorption spectra of the mixtures of MB with various concentrations and DPIBF-SDS micelles and nanoprobes were measured in the range of 400 nm – 800 nm with a Shimadzu UV-VIS spectrophotometer (Columbia, MD). The absorption intensity was used to calculate the number of absorbed photons (I_{abs}).

For the *in vitro* PDT experiment, an Olympus IMT II fluorescence microscope hooked with Xenon arc lamp set in Lambda DG-4 filter changer was mainly used. The microscope was incorporated with an Acton Research Spectrograph for spectral measurements and a Hamamatsu charge-coupled device (CCD) for fluorescence imaging. Luxeon /o high power red LED was used as an illumination source for PDT. A customized violet filter set was used to measure fluorescence emission spectra of DPIBF embedded Ormosil PEBBLEs. The cell damage by PDT was monitored by propidium iodide (PI) staining in cell viability assay, using standard green filter set.

Determination of dye loading into Ormosil matrix

The amount of DPIBF dye molecules encapsulated in the Ormosil nanoparticles was estimated by the following method: The DPIBF Ormosil PEBBLE nanoprobes were suspended in a water-ethanol (50:50) mixture and sonicated for several minutes, to prevent aggregation of the relatively hydrophobic ormosil particles, giving a 0.1 mg/mL concentration. A 0.1 mg/mL of blank Ormosil particles, suspended in a water-ethanol mixture, was prepared for the subtraction of background light scattering due to the nanoparticle matrix. DPIBF dye was weighed and dissolved in the prepared Ormosil blank particles suspension and was diluted to various known DPIBF concentrations by adding more blank Ormosil solutions. The fluorescence emission spectra of the prepared DPIBF free dye – blank Ormosil particle solutions, as well as a DPIBF embedded Ormosil PEBBLE nanoprobes suspension (unknown), were measured with the spectrofluorometer. The DPIBF concentration vs. fluorescence intensity calibration curve was constructed by the results from known DPIBF free dye solutions, with subtraction of signal from blank Ormosil particle solutions, and the concentration of the embedded DPIBF in the Ormosil PEBBLE nanoprobes was estimated, based on this calibration curve.

Dye leaching

In order to make sure that singlet oxygen detection occurs truly inside of the nanoparticle matrix, not outside of nanoprobes by leakage of dye molecules, dye leaching must be examined before further investigation. A 0.1 mg/mL DPIBF Ormosil PEBBLE nanoprobes solution in water was prepared and a part of the solution was filtered, using a

filter membrane with very small pore size (Whatman Anodisc filter membrane, 0.02 um pore), to remove nanoparticles from the solution. The leakage of DPIBF molecules was evaluated by measuring, with fluorometer, DPIBF's fluorescence emission of the nanoprobes solution and of the filtrate.

Singlet oxygen detection by DPIBF embedded Ormosil PEBBLE nanoprobes and DPIBF-SDS micelles in aqueous media

A stock solution of DPIBF embedded Ormosil PEBBLE nanoprobes with concentration 0.2 mg/mL) was prepared. Another stock solution for comparison, a 10 μM DPIBF-SDS micelles in water, was prepared as well following the procedures described by Usui and Gorman [21,22]. Briefly, DPIBF was solubilized with 0.1 M SDS warm aqueous solution with slow stirring until the dye is sufficiently solubilized. The concentration of the DPIBF–SDS micelle sample was chosen to be roughly equivalent to the DPIBF in PEBBLE nanoprobes solution, as determined earlier (about 10 uM).The photosensitizer, MB, was dissolved in water and diluted to give various concentrations (10, 5, 1, 0.5, and 0.1 μM). Then 0.2 mL of DPIBF-SDS micelles or DPIBF nanoprobes stock solution was added to 2 mL of each MB in water solution, in polypropylene cuvettes, to give final concentrations for MB (0.091, 0.455, 0.909, 4.545, and 9.091 μM), for DPIBF-SDS micelle (0.909 μM), and for DPIBF Ormosil PEBBLE nanoprobes (0.018 mg/mL). The decay of the DPIBF fluorescence, due to reacting with singlet oxygen, was monitored by measuring the fluorescence intensity at 0 sec, 20 sec, 40 sec, 1 min, 2 min, 3 min, 4 min, and 5 min time points, with magnetic stirring, so as to maintain a sufficient oxygen supply, based on the setup described above.

DPIBF auto-oxidation studies

The auto-oxidation effect, which is the oxidation of DPIBF by normal oxygen without photosensitization, of DPIBF free dye and DPIBF Ormosil PEBBLE nanoprobes, was examined under same experimental configurations without photosensitizer MB, with various compositions of water-EtOH mixtures, with increasing water contents of 0 %, 25 %, 50 %, 75 %, and nearly 100 %. The emission change was monitored around 453 nm, with 412 nm excitation wavelength, at 0 sec, 20 sec, 40 sec, 1 min, 2 min, 3 min, 4 min, and 5 min time points, following the procedures of singlet oxygen detection described above.

Singlet oxygen sensitivity comparison with ADPA free dye and DMA Ormosil PEBBLE nanoprobes

In order to confirm the improved singlet oxygen sensitivity of DPIBF Ormosil PEBBLE nanoprobes, the reaction rate of DPIBF Ormosil PEBBLE nanoprobes was compared with the rate of previously used singlet oxygen probes in our lab, ADPA free dye and DMA Ormosil PEBBLE nanoprobes. Solutions of 10 μM ADPA free dye, 0.2 mg/mL DMA Ormosil PEBBLE nanoprobes, and 0.2 mg/mL DPIBF Ormosil PEBBLE nanoprobes were each mixed into 2 mL of 5 μM MB free dye solution. The fluorescence emission change of each type of probe was monitored for 5 minutes while each solution was illuminated under the same conditions, with a 660 nm excitation beam used for singlet oxygen generation from MB free dye.

Analysis of reaction kinetics of MB-DPIBF photosensitization system

In order to determine the sensitivity of DPIBF Ormosil PEBBLE nanoprobes in aqueous solvent, the reaction kinetics of singlet oxygen generation from MB and its connection with singlet oxygen quenching by DPIBF is necessary to be considered carefully. The understanding of this reaction kinetics enables the quantification of important parameters in the PDT system, such as singlet oxygen quantum yield and the steady-state singlet oxygen concentration, in addition to the singlet oxygen sensitivity of the given probe. The mechanism of MB photosensitization has been investigated previously by Junqueira's work [27] and the reaction kinetics was applied to our own system following Moreno's method [13], with minor modifications.

$^1MB \rightarrow {}^3MB^*$	I_{abs} (rate of photon absorption by system)
$^3MB^* \rightarrow {}^1MB$	k_d (sensitizer triplet deactivation)
$^3MB^* + {}^3O_2 \rightarrow {}^1MB + {}^1O_2$	$k_{^1O_2}$ (singlet oxygen generation)
$^1O_2 +$ solvent $\rightarrow {}^3O_2 +$ solvent	k_{sol} (solvent quenching)
$^1O_2 +$ DPIBF $\rightarrow {}^3O_2 +$ DPIBF	k_p (physical quenching)
$^1O_2 +$ DPIBF $\rightarrow$ $DPIBFO_2$	k_c (chemical quenching)
DPIBF $\rightarrow$ Y	k_y (non-singlet oxygen involved reaction)

$k_p + k_c \approx k_c$ (In case of DPIBF, k_p is generally negligible in various solvents [28])

This reaction scheme can be expressed by the following differential equations:

$$d[^1\mathrm{MB}]/d\mathrm{t} = -I_{\mathrm{abs}} + (k_{\mathrm{d}} + k_{^1\mathrm{O}_2}[^3\mathrm{O}_2])[^3\mathrm{MB}^*] \quad (1)$$

$$d[^3\mathrm{MB}^*]/d\mathrm{t} = I_{\mathrm{abs}} - (k_{\mathrm{d}} + k_{^1\mathrm{O}_2}[^3\mathrm{O}_2])[^3\mathrm{MB}^*] \quad (2)$$

$$d[\mathrm{DPIBF}]/d\mathrm{t} = -(k_{\mathrm{c}}[^1\mathrm{O}_2] + k_{\mathrm{y}})[\mathrm{DPIBF}] \quad (3)$$

$$d[^1\mathrm{O}_2]/d\mathrm{t} = k_{^1\mathrm{O}_2}[^3\mathrm{O}_2][^3\mathrm{MB}^*] - \{k_{\mathrm{sol}} + k_{\mathrm{c}}[\mathrm{DPIBF}]\}[^1\mathrm{O}_2] \quad (4)$$

The steady-state can be assumed to occur when the photosensitization of MB was induced under illumination in a continuous wave (CW) mode and the reaction of DPIBF with singlet oxygen negligibly affects the overall reaction, which is represented as $k_{\mathrm{sol}} >> k_{\mathrm{c}}[\mathrm{DPIBF}]$. If a steady-state is assumed, $d[^1\mathrm{MB}]/d\mathrm{t}$, $d[^3\mathrm{MB}^*]/d\mathrm{t}$, and $d[^1\mathrm{O}_2]/d\mathrm{t}$ all equal to 0.

Thus,

$$I_{\mathrm{abs}} = (k_{\mathrm{d}} + k_{^1\mathrm{O}_2}[^3\mathrm{O}_2])[^3\mathrm{MB}^*] \quad (5)$$

$$k_{^1\mathrm{O}_2}[^3\mathrm{O}_2][^3\mathrm{MB}^*] = \{k_{\mathrm{sol}} + k_{\mathrm{c}}[\mathrm{DPIBF}]\}[^1\mathrm{O}_2] \quad (6)$$

The singlet oxygen quantum yield is defined as

$$\Phi_{^1\mathrm{O}_2} = \frac{k_{^1\mathrm{O}_2}[^3\mathrm{O}_2][^3\mathrm{MB}^*]}{(k_{\mathrm{d}} + k_{^1\mathrm{O}_2}[^3\mathrm{O}_2])[^3\mathrm{MB}^*]} \quad (7)$$

from (5), (6), and (7),

$$\{k_{\mathrm{sol}} + k_{\mathrm{c}}[\mathrm{DPIBF}]\}[^1\mathrm{O}_2] = \Phi_{^1\mathrm{O}_2} I_{\mathrm{abs}} \quad (8)$$

Thus the decay of [DPIBF] by illumination can be expressed by integrating equation (3):

$$[\mathrm{DPIBF}]_{t=t} = [\mathrm{DPIBF}]_{t=0} e^{(-kt)} \quad (3)'$$

$$k = k_c[^1O_2] + k_y \approx k_c[^1O_2] \quad (9)$$

(This assumption is valid because DPIBF is highly specific to singlet oxygen only [29] and the known side reaction (auto-oxidation) could be negligible and easily subtracted).

Under the condition of $k_{sol} >> k_c[\mathrm{DPIBF}]$, thus

$$\therefore\ k = \frac{k_c \Phi_{^1O_2} I_{abs}}{k_{sol} + k_c[\mathrm{DPIBF}]} \approx \frac{k_c \Phi_{^1O_2} I_{abs}}{k_{sol}} = \frac{\Phi_{^1O_2} I_{abs}}{\beta}\ ,\ (k_{sol} >> k_c[\mathrm{DPIBF}]) \quad (10)$$

The term $\beta(\frac{k_{sol}}{k_c})$ is defined as the ratio between the quenching rate constant by solvent and the quenching rate constant by the probe [18,30], and is often used as a parameter representing the sensitivity of the probe. The β of DPIBF Ormosil PEBBLE nanoprobes can be determined by comparing the reaction kinetics with that of a model system for which β is already known. Usui *et al.* and Gorman *et al.* have investigated the kinetics of the photosensized reaction between MB and DPIBF solubilized by an SDS micelle in aqueous environments and determined β for the DPIBF-SDS micelle. The comparison of reaction kinetics between the DPIBF Ormosil PEBBLE nanoprobes and the DPIBF-SDS micelles was achieved by comparing their *k* values:

From equation (10)

$$\frac{k_{\text{micelle}}}{k_{\text{nanoprobe}}} = \frac{\Phi_{^1O_2} I_{\text{abs,micelle}} / \beta_{\text{micelle}}}{\Phi_{^1O_2} I_{\text{abs,nanoprobe}} / \beta_{\text{nanoprobe}}} \quad (11)$$

$\Phi_{^1O_2}$ is a constant representing singlet oxygen generation efficiency of given photosensitizer ($\Phi_{^1O_2}$ of MB is 0.52 [31,32]). Equation (11) can be re-organized as follows.

$$\therefore \beta_{\text{nanoprobe}} = \frac{k_{\text{micelle}} I_{\text{abs,nanoprobe}}}{k_{\text{nanoprobe}} I_{\text{abs,micelle}}} \times \beta_{\text{micelle}} \quad (12)$$

This estimation is valid only when the micelles and nanoprobes show the same pattern of *k* value distribution in various MB concentrations. According to the definition of β, the more sensitive the probe is, the lower β becomes.

Determination of steady-state singlet oxygen concentration in various MB concentrations

If β of the DPIBF Ormosil PEBBLE nanoprobes is determined, in other words, if the reactivity (k_c) of DPIBF Ormosil PEBBLE nanoprobes towards singlet oxygen is known, the steady-state singlet oxygen concentration ($[^1O_2]_{s\text{-}s}$) can be calculated by analyzing *k* (decay rate constant of DPIBF Ormosil PEBBLE nanoprobes), which is measured from experiment. Based on the obtained k_c value for the DPIBF Ormosil PEBBLE nanoprobes, the steady-state singlet oxygen concentration was calculated by equation (9) as follows.

$$[^1O_2]_{s\text{-}s} = \frac{k}{k_c} \quad (12)$$

Preparation of C-6 glioma cells

A rat neural cell, C-6 glioma was cultured in Dulbecco's Modified Eagle Medium (DMEM) containing 10 % Fetal Bovine Serum (FBS) and 1 % Penicillin-Streptomycin-Neomycin (PSN) under 5 % CO2 atmosphere at constant 37 ˚C. Cells were split using trypsinization until passage 3 or higher, then used for experiments. Cells were plated on coverslips, adjusting to develop 2 different cell densities after 2 day incubation. Right before the actual PDT measurements, the number of cells on the coverslip of each density was counted on spare coverslips with hemacytometer using a trypan blue dye exclusion assay [33], which can selectively stain dead cells blue while not staining live cells.

In vitro **PDT with MB encapsulated polyacrylamide nanoparticles and singlet oxygen quantification**

C-6 glioma cells with 2 different densities were plated and cultured on 6 well plates. The coverslip of rat C-6 glioma cells was installed in a cell chamber with 1.75 mm inner diameter after rinsing with fresh cell media. A singlet oxygen generating MB PAA nanoparticles (especially, termed dynamic nanoplatforms (DNPs)) was suspended in the same cell media for 2 different DNP concentrations, 1 mg/mL and 0.1 mg/mL, for each cell density; overall 4 conditions (1 mg/mL MA PAA DNP with high cell density, 1 mg/mL MA PAA DNP with low cell density, 0.1 mg/mL MA PAA DNP with high cell density, and 0.1 mg/mL MA PAA DNP with low cell density). The cell chamber was filled with 1 mL of the cell media containing the MB PAA DNP, and the background

fluorescence spectrum was measured. DPIBF Ormosil PEBBLE nanoprobes suspended in cell media and 3 μL of Propidium Iodide (PI), which is a staining dye for dead cells, were added to monitor, simultaneously, singlet oxygen generation during illumination and cell death. Photosensitizer MB PAA DNPs were irradiated by a Luxeon Star /O red-LED with roughly 2 mW power at 660 nm wavelength for 5 minutes. During the 5 minute illumination, the fluorescence emission intensity changes of theDPIBF Ormosil PEBBLE nanoprobes were measured with a customized violet filter cube set (excitation: 415 nm centered bandpass filter and emission: a 450 or higher nm longpass filter with an appropriate dichroic mirror). Also, PI dead cell staining was monitored simultaneously with a standard green filter cube set (excitation: 546 nm centered bandpass and emission: 600 nm or higher long pass filter with dichroic mirror) for 1 hour, including the first 5 minutes for light illumination. The same procedures were repeated without cells under identical conditions, as a control, and the results were compared.

Post-PDT tumor regrowth assay

C-6 glioma cells with 2 different densities were prepared on 6-well plates without glass coverslips (high density: 144,000/mL and low density: 15,000/mL about a 10 time difference). For 4 sets of samples, for 4 day monitoring (day 0, 1, 2, and 3), a total of 56 wells of cells were plated (12 wells for high density-PDT treated (4 each for day 1, 2, and 3), 16 wells for high density-control (4 for day 0, 1, 2, and 3), 12 wells for low density-PDT treated (4 for day 1, 2, and 3), and 16 wells for low density-control (4 for day 0, 1, 2, and 3). A 1 mg/mL MB DNP concentration was used for PDT treatment for each cell

well and the cells were illuminated, by the same red-LED with 2 mW power at 660 nm, for 5 minutes.

The tumor regrowth after PDT was monitored by counting the number of total healthy cells from day 0 to day 3. Each cell well was rinsed with PBS buffer, trypsinized to lift the cells from the bottom, and then the number of cells in single well was counted using hemacytometry with trypan blue staining as previously mentioned. A total of 4 sets of wells for PDT treated cells and controls were measured each day and the results were averaged.

Results and Discussion

Synthesis of DPIBF Ormosil PEBBLE nanoprobes

DPIBF embedded Ormosil PEBBLE nanoprobes, roughly monodispersed in size (80-140 nm), were synthesized (Figure 2.2). The mechanism of the nanoparticle formation is based on the coupling of microemulsion and sol-gel principle, summarized as follows. The first monomer, PTMS forms fine droplets in the aqueous solution because of its hydrophobicity and the size of the droplets decreases by a combination of mechanical forces from stirring with hydrolysis of PTMS molecules in an acidic environment. After a sufficient period of hydrolysis (about 20 minutes), the pH of the solution is reversed to a basic condition by addition of excess ammonium hydroxide, so as to trigger condensation. During the condensation period, the 3 dimensional –Si (Phenyl)-O- network structures develop, entrapping DPIBF molecules inside. Introducing the second precursor, methyltrimethoxysilane (MTMS), makes the network structure

more compact by filling and covering the network with a silicate network with the methyl group, a smaller side group. The denser network prevents the leakage of the embedded DPIBF molecules.

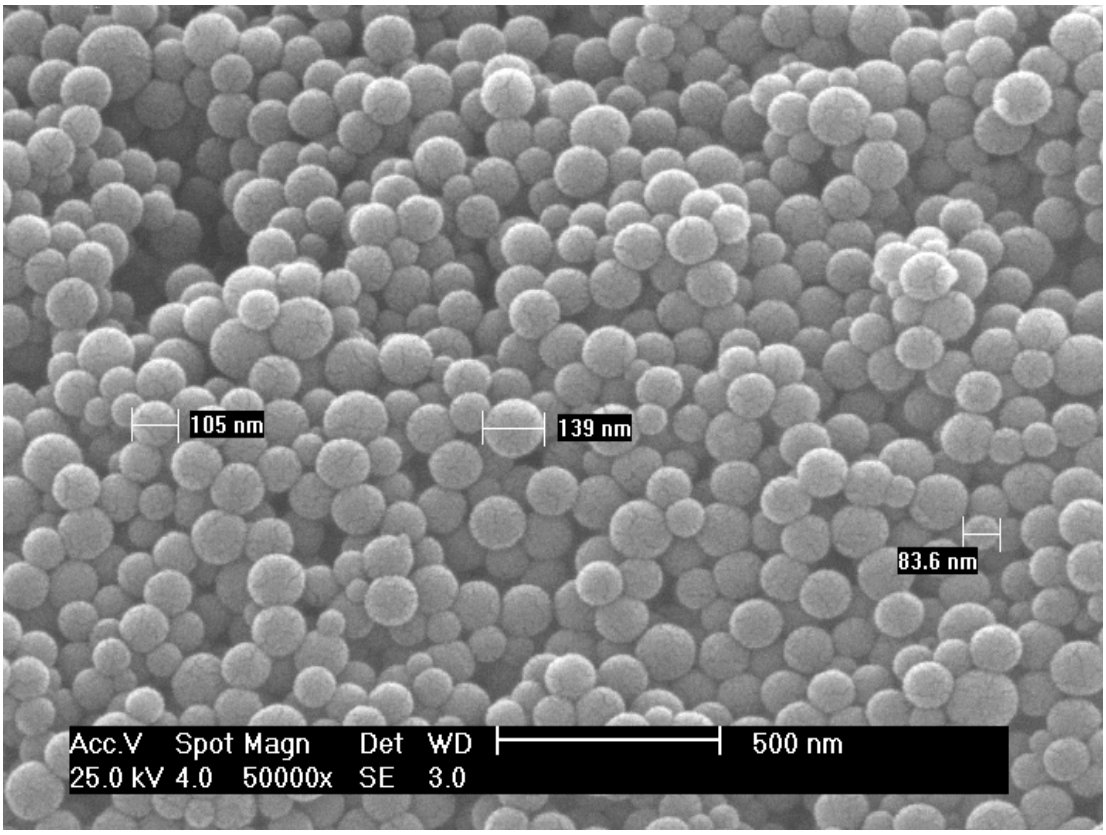

<Figure 2.2: SEM image of synthesized DPIBF embedded Ormosil PEBBLE nanoprobes showing an 80-140 nm diameter range. SEM image was obtained with XL 30 FEG SEM device with 40 seconds gold sputter coating on the sample surface.>

Amount of embedded DPIBF in Ormosil nanoparticles

The fluorescence intensity of DPIBF free dye solutions with different known concentrations was measured, in order to construct a calibration curve in the presence of blank Ormosil nanoparticles (Figure 2.3). Then, the amount of DPIBF loaded in the ormosil nanoparticles was estimated by comparing its fluorescence intensity to the

calibration curve. The fluorescence intensity of 0.1 mg/mL DPIBF Ormosil PEBBLE nanoprobes showed an equivalent intensity of 0.0027 mg/mL DPIBF free dye with blank Ormosil particles. The concentration of DPIBF in Ormosil PEBBLE nanoprobes suspension was roughly similar to 9.91 μM free dye solution when assuming that the Ormosil nanoparticle matrix does not affect the fluorescence intensity of the dye content.

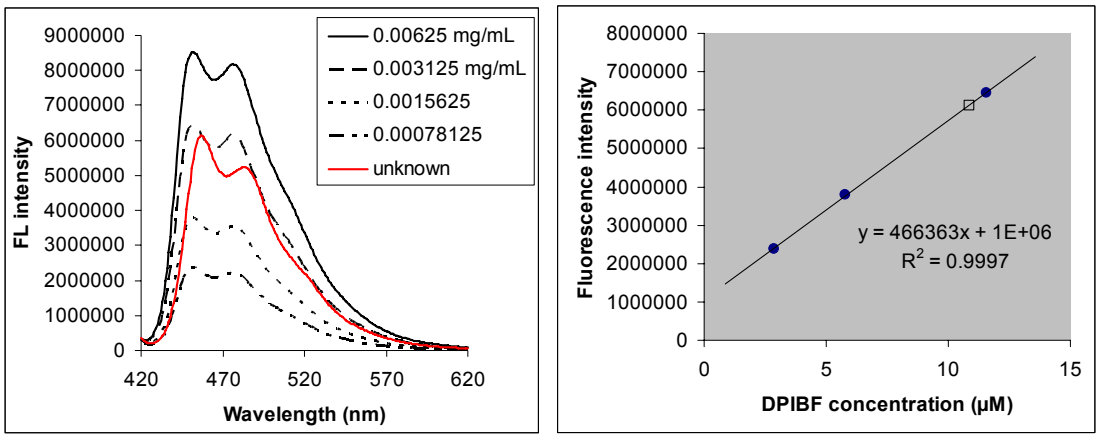

a) b)

<Figure 2.3: Determination of the amount of DPIBF embedded in the Ormosil PEBBLEs: a) fluorescence emission spectra of DPIBF with various known concentrations and unknown DPIBF Ormosil PEBBLE nanoprobes, b) fluorescence intensity vs. DPIBF concentration calibration curve for estimation of dye loading capacity; ●: known, □: unknown>

Dye leaching

As explained in chapter 1, the advantages of the Ormosil matrix over other matrixes we have used before are the ability to encapsulate both hydrophobic dyes and hydrophilic dyes and to contain the dye more tightly by compact 3 dimensional silicate networks, thus without significant dye leaching. The leaching out of the dye from the DPIBF ormosil PEBBLE nanoprobes was examined by filtrating the PEBBLEs, so as to remove all nanoparticles from the solutions. As shown in figure 2.4, the filtrate solution

exhibited only a trace of DPIBF fluorescence, indicating that the leaching out of the dye from the PEBBLE nanoprobes was negligible, as seen from the fact that the PEBBLE solution before filtration had a significant fluorescence intensity. This result confirmed that the DPIBF molecules are tightly contained inside the Ormosil matrix. Also, it implicated that the observed reaction between DPIBF and singlet oxygen had to occur only inside of the PEBBLE nanoprobes.

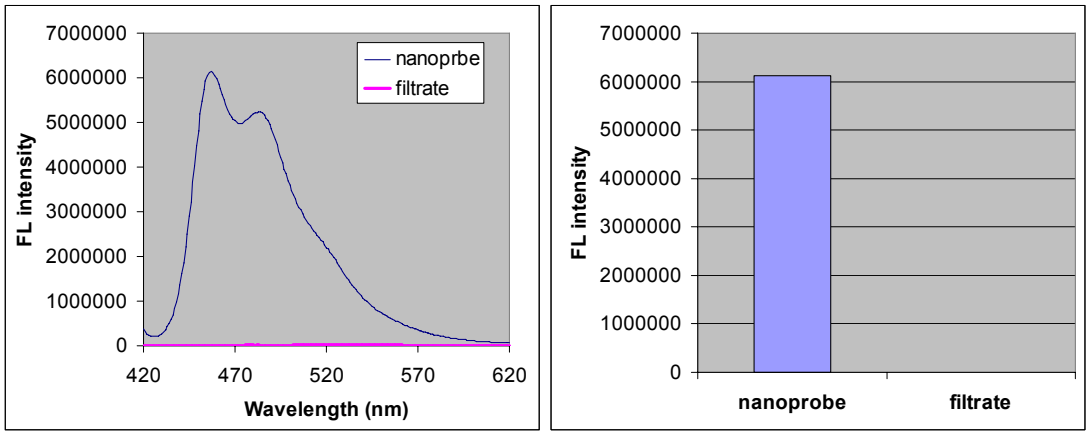

<Figure 2.4: Examination of dye leaching from PEBBLE nanoprobes: Comparison of DPIBF's fluorescence emission between a nanoprobe solution in DI water (blue line in left chart) and the filtrate solution in DI water (pink line in left chart), showing no dye leaching out of the nanoparticles and numerical comparison of fluorescence intensity at maximum peak>

Auto-oxidation studies

It should be noted that the calculation of *k* values may incur a considerable error if side reactions exist, as described at the end of the reaction scheme. A known side reactions is the auto-oxidation of DPIBF, which is defined as the reaction of DPIBF with dissolved ground state (normal) oxygen, thus resulting in the formation of o-dibenzoylbenzene even in the dark (without the photodynamic effect), at ambient temperature, as has been reported by Howard and Mendenhall [34]. Most previous

research on singlet oxygen detection with DPIBF as a probe was able to neglect the effect of auto-oxidation, because the work was performed in organic solvents, in which auto-oxidation is usually negligible.

The auto-oxidation of the DPIBF free dye and the DPIBF ormosil PEBBLE nanoprobes was tested in various mixtures of ethanol and water, as summarized in figure 2.5. In order to test whether there was auto-oxidation or not, experiments without illumination were repeated, using a sample solution after 20 minutes of nitrogen purging. No decrease of DPIBF fluorescence was observed (data not shown) in the absence of oxygen. This result indicates that the self initiated decrease of DPIBF emission was related to reaction with normal oxygen, defined as auto-oxidation. As shown in figure 2.5, auto-oxidation increased as the water content in the solvent increased, up to nearly pure water,(about 96 %, It looked dissolved with stirring for 5 minute measurement but aggregates were formed over time) for both DPIBF free dye and DPIBF Ormosil PEBBLE nanoprobes. However, the auto-oxidation effect of the nanoprobes was significantly less than that of DPIBF free dye. This is in accord with what we expected from a previous report saying that the auto-oxidation is related to the hydrophobicity of DPIBF and to the polarity of the solvent [35].

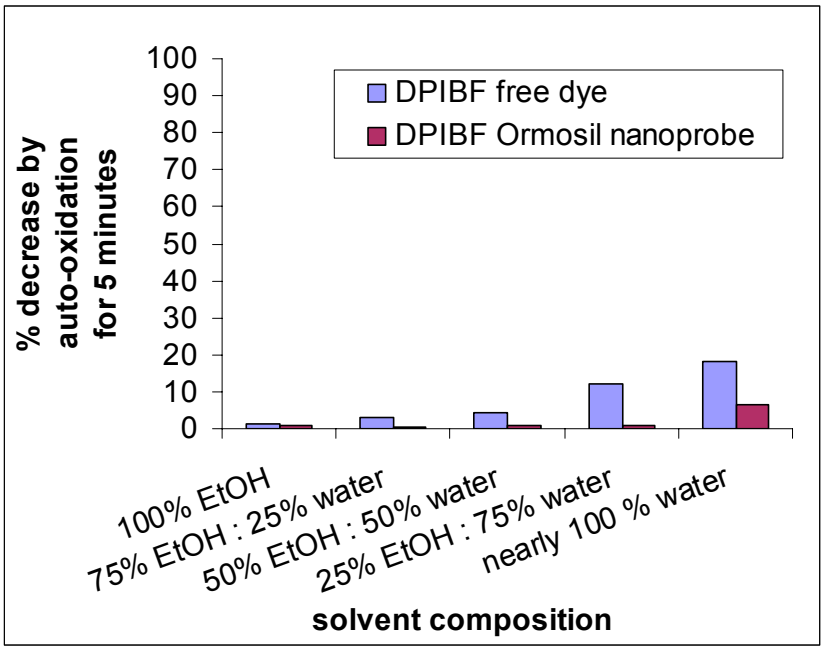

<Figure 2.5: Comparison of auto-oxidation between DPIBF free dye and DPIBF Ormosil PEBBLE nanoprobes in various compositions of water-EtOH mixtures. The reduction of DPIBF's and DPIBF Ormosil PEBBLE nanoprobes' fluorescence intensity at emission maxima (around 455 nm) were measured for 5 minutes with increasing water content. DPIBF free dye showed larger auto-oxidation effect as water content increased. PEBBLE nanoprobes exhibited significantly lower such effect than free dye in all solvent compositions>

This result reveals another advantage of the DPIBF Ormosil PEBBLE nanoprobes, namely that the PEBBLE nanoprobe is much more stable against auto-oxidation in near aqueous environments than is the free dye form, and thus more accurate evaluations of the singlet oxygen level can be obtained. Because the reaction rate constant of the side reactions (k_y) is not available and the auto-oxidation effect was practically negligible for DPIBF Ormosil PEBBLE nanoprobes, the inaccuracy induced by auto-oxidation was simply compensated for by subtracting the portion of auto-oxidation from the total decrease of DPIBF fluorescence emission, at each time point. Also, the background signal due to the light scattering of Ormosil particles was

subtracted as well. The determinations of all kinetic parameters (k, β, and steady-state singlet oxygen concentrations) were obtained after these corrections.

As a consequence of the above study, the DPIBF and DPIBF Ormosil PEBBLE nanoprobes have been stored and dealt with in a dark, nitrogen saturated environment, so as to avoid auto-oxidation. Fresh solutions must be used for every experiment.

Singlet oxygen sensitivity comparison with ADPA free dye and DMA Ormosil PEBBLE nanoprobes

DPIBF in the form of a molecular probe has significantly higher sensitivity towards singlet oxygen than ADPA free dye and DMA free dye (or DMA Ormosil PEBBLE nanoprobes) [30]. However, the encapsulation of DPIBF in an Ormosil matrix might have affected its sensitivity; thus the sensitivity of DPIBF Ormosil PEBBLE nanoprobes had to be evaluated so as to test whether using DPIBF Ormosil PEBBLE nanoprrpobes has any advantage over the previously used ADPA and DMA. ADPA, DMA Ormosil PEBBLE nanoprobes, and DPIBF Ormosil PEBBLE nanoprobes were examined under identical conditions of PDT, using 5 μM MB free dye in water, with 660 nm excitation for 5 minutes. The fluorescence changes of those 3 different singlet oxygen probes, by the reaction with singlet oxygen generated from the PDT system, were monitored and the results were plotted in a combined chart in figure 2.6, so as to compare their sensitivities towards singlet oxygen.

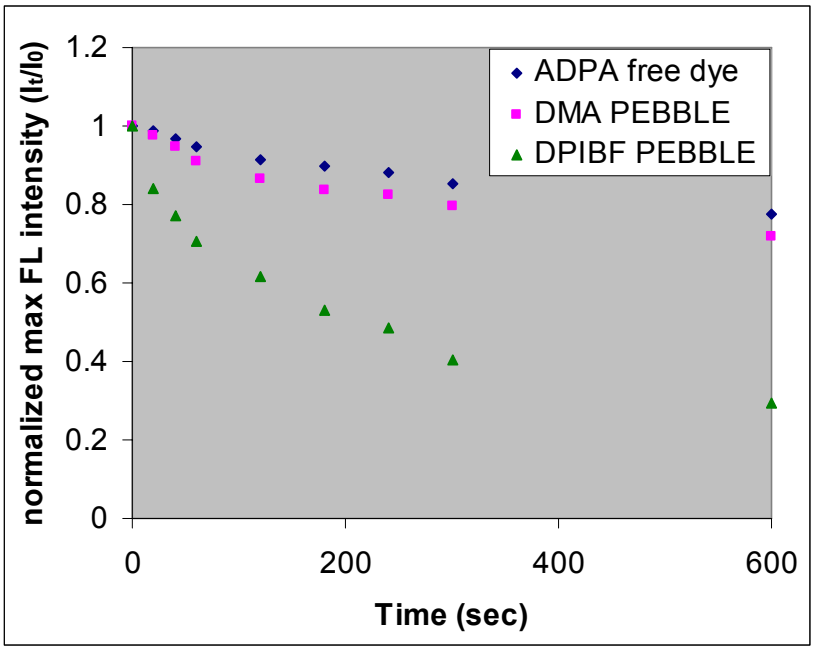

<Figure 2.6: Relative comparison of singlet oxygen sensitivity among ADPA free dye, DMA Ormosil PEBBLE nanoprobes, and DPIBF Ormosil PEBBLE nanoprobes under identical condition. Singlet oxygen was generated by 5 uM MB free dye in DI water by 660 nm irradiation for 5 minutes and quenched by these three singlet oxygen probes individually. The decay of fluorescence intensity for each probe was compared after the normalization of I_t (fluorescence intensity at time t) / I_0 (fluorescence intensity at time 0)>

DPIBF Ormosil PEBBLE nanoprobes exhibited a significantly faster decay compared to the other 2 probes, under identical conditions, clearly indicating better singlet oxygen sensitivity. The DMA Ormosil PEBBLE nanoprobes were only slightly faster than the ADPA free dye, not showing a notable sensitivity advantage of using it (even though it has other advantages (Cao [15])). The significantly improved sensitivity of DPIBF Ormosil PEBBLE nanoprobes implies that faster and more accurate detection would be now available, so that the weak change or slight difference in the response from singlet oxygen, which used to be unrecognizable with ADPA or DMA nanoprobes, could now become distinguishable.

Singlet oxygen detection by DPIBF embedded Ormosil PEBBLE nanoprobes and DPIBF-SDS micelles in aqueous media

While illuminating MB at a given concentration with 660 nm light, both the DPIBF-SDS micelles and DPIBF Ormosil PEBBLE nanoprobes exhibited an exponential decrease of fluorescence emission intensity, in the region of 450-500 nm, indicating the disappearance DPIBF molecules, due to the production of endoperoxides, $DPIBFO_2$ by reacting with singlet oxygen, as shown in Figure 2.7.

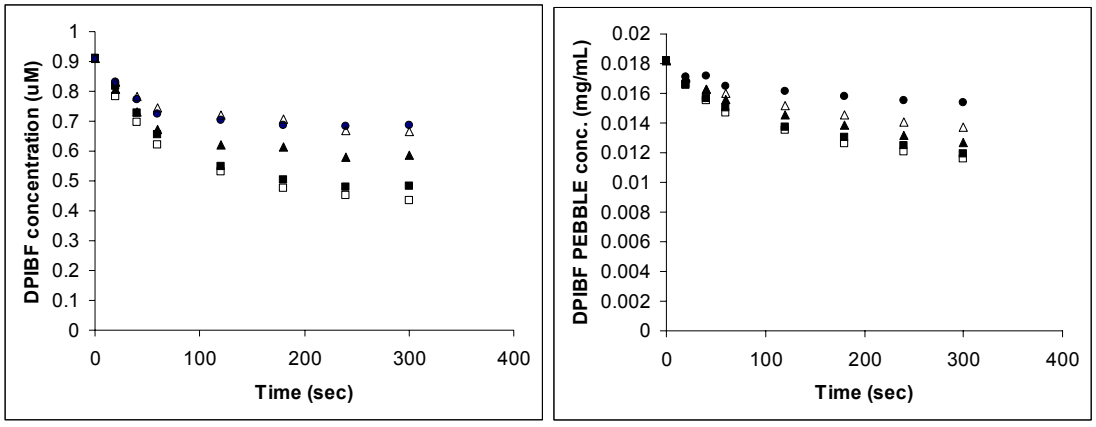

a) DPIBF-SDS micelles b) DPIBF Ormosil PEBBLE nanoprobes

<Figure 2.7: The exponential decay of DPIBF-SDS micelles' and DPIBF Ormosil PEBBLE nanoprobes' fluorescence intensity by reaction with singlet oxygen generated by photosensitizer MB in various concentrations in DI water. The results were normalized by converting the fluorescence intensity to concentration of each probe and the auto-oxidation and light scattering effects were subtracted. [a) DPIBF-SDS micelles, and b) DPIBF Ormosil PEBBLE nanoprobes , ■: 9.091 μM MB, □: 4.545 μM MB, ▲: 0.909 μM MB, Δ: 0.455 μM MB, and ●: 0.091 μM MB]>

The distribution of *k* values showed that DPIBF Ormosil PEBBLE nanoprobes behaved like DPIBF-SDS micelles at various singlet oxygen levels, proving that the DPIBF Ormosil PEBBLE nanoprobes can serve as a good singlet oxygen probe, though

the sensitivity towards singlet oxygen was somewhat reduced compared to the DPIBF-SDS micelle sample, as described in table 2.1 and figure 2.8. The reaction of DPIBF free dye with singlet oxygen in organic solvents was known to follow pseudo 1st order [29]. So, we presumed that DPIBF PEBBLE nanoprobes would follow the same order too. The rate of the decay in the early time regime was, roughly, shorter than 1 minute and matches a 1st order reaction kinetics without significant error, while the longer time period showed a gradual deviation from 1st order kinetics for both DPIBF-SDS micelles and DPIBF ormosil PEBBLE nanoprobes. This deviation may indicate that there is a population of DPIBF molecules deep inside the nanoparticles or micelles which cannot be reached quickly by the singlet oxygen generated outside, and thus maintains an intact fluorescence. This might be because of the limited diffusion distance by the short-lived singlet oxygen and, possibly, also due to the protective effect by the initially produced endoperoxides ($DPIBFO_2$ molecules) located in the outer part of the matrix. Therefore, the *k* value for determining β was calculated using the decay data taken from only 0-1 minute time period.

MB conc. (μM)	*k* (sec^{-1})	
	Micelles	Nanoprobes
9.091	0.0059	0.0031
4.545	0.0065	0.0036
0.909	0.0050	0.0027
0.455	0.0038	0.0021
0.091	0.0032	0.0014

<Table 2.1: Numerical comparison of 1st order fluorescence decay rate (*k*) by reaction with singlet oxygen between DPIBF-SDS micelles and DPIBF Ormosil PEBBLE nanoprobes in various situations examined>

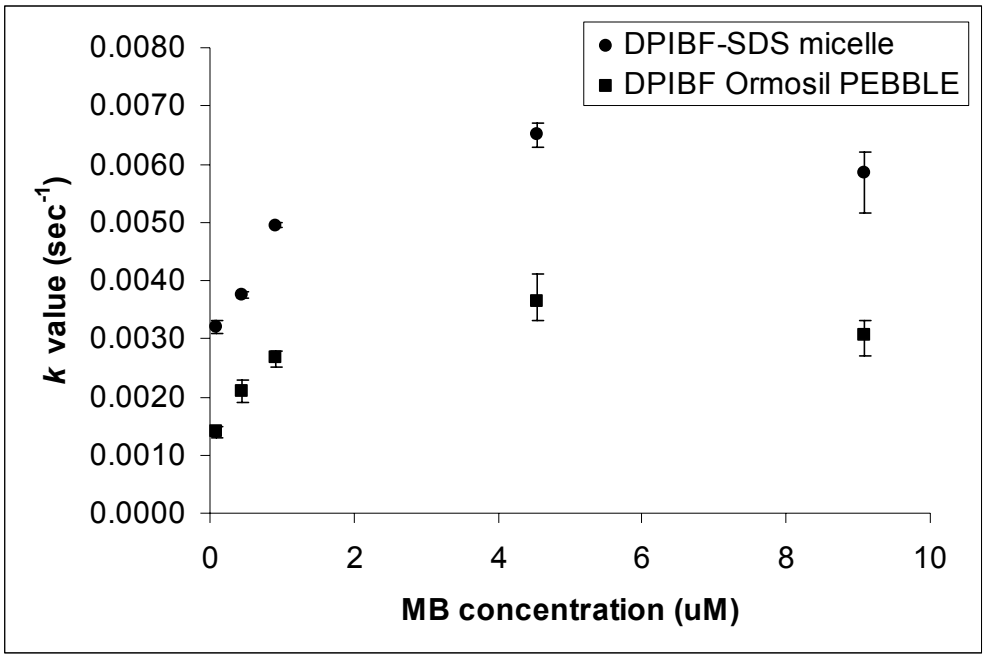

<Figure 2.8: Comparison of *k* values determined for DPIBF-SDS micelles and for DPIBF Ormosil PEBBLE nanoprobes in various photosensitizer MB's concentrations in 5 minutes photosensitization. It showed a consistent trend that DPIBF Ormosil PEBBLE nanoprobes have roughly 50 % reduced sensitivity towards singlet oxygen compared to DPIBF-SDS micelles in overall situations.>

Quantitative determination of singlet oxygen sensitivity for DPIBF Ormosil PEBBLE nanoprobes

The decay rate of DPIBF fluorescence (*k*) was calculated by fitting the data of the 0-1 minute time period to an first order exponential decay, expressed as equation (3)'. The *k* value for each MB concentrations was summarized in table 2.1 and their distribution was displayed in Figure 2.8. DPIBF Ormosil PEBBLE nanoprobes showed about 50 % smaller *k* values on average, than DPIBF-SDS micelles, and this discrepancy was consistently present over changes in MB concentration by up to 2 orders of magnitude. Thus, it can be reasonably concluded that the sensitivity towards singlet oxygen of the DPIBF Ormosil PEBBLE nanoprobes is in constant proportion to that of

the DPIBF-SDS micelles. The β factor for the DPIBF Ormosil PEBBLE nanoprobes was determined (1.94 x 10^{-4} M), using equation (12), based on the known β of the DPIBF-SDS micelles (1.1 x 10^{-4} M [21]). Also, the rate constant of the PEBBLE nanoprobes with singlet oxygen (k_c) was estimated from the definition of β. The estimation results and parameters used in this calculation (absorbance at 660 nm, number of absorbed photons (I_{abs}), β, and k_c) are shown in figure 2.9 and table 2.2-a).

MB conc. (μM)	I_{abs}		β (M)		k_c ($M^{-1}s^{-1}$)*	
	Micelles	nanoprobes	Micelles	nanoprobes	Micelles	Nanoprobes
9.091	1.70 x 10^{-5}	1.55 x 10^{-5}	1.10 x 10^{-04}	1.91 x 10^{-4}	47.1 x 10^{8}	26.2 x 10^{8}
4.545	1.13 x 10^{-5}	9.54 x 10^{-6}		1.68 x 10^{-4}		29.8 x 10^{8}
0.909	3.09 x 10^{-6}	3.06 x 10^{-6}		2.02 x 10^{-4}		24.8 x 10^{8}
0.455	2.03 x 10^{-6}	2.09 x 10^{-6}		2.05 x 10^{-4}		24.4 x 10^{8}
0.091	1.89 x 10^{-7}	1.55 x 10^{-7}		2.06 x 10^{-4}		24.2 x 10^{8}
			average	1.94 x 10^{-4}	average	25.9 x 10^{8}

a) * $\beta = \frac{k_{sol}}{k_c}$, k_{sol} = 5 x 10^{5} s^{-1} [19]

$^1O_2$ probes	Solvent	β	k_c
DPIBF-SDS micelle	H_2O	1.1 x 10^{-4} M	47.1 x 10^{8} $M^{-1}s^{-1}$
DPIBF Ormosil Nanoprobe	H_2O	1.9 x 10^{-4} M	25.9 x 10^{8} $M^{-1}s^{-1}$
Histamine	H_2O	2.5 x 10^{-3} M	2.0 x 10^{8} $M^{-1}s^{-1}$
2,5-dimethylfuran	H_2O	3.2 x 10^{-4} M	15.6 x 10^{8} $M^{-1}s^{-1}$
9,10-dimethylanthracene-micelle	H_2O	5.5 x 10^{-4} M	9.1 x 10^{8} $M^{-1}s^{-1}$
2,5-diphenyloxazole	H_2O / D_2O	1.6 x 10^{-3} M	1.6 x 10^{8} $M^{-1}s^{-1}$
Anthracene-9,10-dipropionic acid	H_2O	3.0 x 10^{-3} M	1.0 x 10^{8} $M^{-1}s^{-1}$

b)

<Table 2.2: Numerical summary of β and k_c values for DPIBF Ormosil nanoprobes. a) determination of β and k_c values for DPIBF Ormosil nanoprobes by comparison with known values of DPIBF-SDS micelles [21,30], and b) comparison of nanoprobe's sensitivity towards singlet oxygen with those of other common singlet oxygen probes [21]>

The estimated β is a value representing this PEBBLE nanoprobe's sensitivity towards singlet oxygen and the discrepancy in β from that of micelles reflects the lower effect of the nanoparticle matrix. In spite of the reduced sensitivity, the DPIBF Ormosil PEBBLE nanoprobes still have a considerably higher sensitivity than other common singlet oxygen probes in aqueous solvents, as demonstrated in table 2.2-b), exhibiting the advantage of using DPIBF Ormosil PEBBLE nanoprobes Also, PEBBLE nanoprobes can have advantages over SDS-micelles in non-sensitivity aspects, such as no fusion between micelles and no fusion with cell membranes, easier surface modification/functionalization, improved stability and so on.

Determination of steady-state singlet oxygen concentration

The steady-state singlet oxygen concentration can be defined as the concentration level formed from equilibrium between generation and deactivation of singlet oxygen under photosensitization with continuous illumination. It remains constant as long as the illumination is on. The steady-state singlet oxygen concentration was determined utilizing equation (9), based on the β value of DPIBF Ormosil PEBBLE nanoprobes estimated. Table 2.3 displays the steady-state singlet oxygen concentration. The steady-state singlet oxygen concentrations are proportional to the *k* values, giving 1.21×10^{-12} M at maximum and 0.58×10^{-12} M at minimum. It means that singlet oxygen exists on a constant pico-molar level at any moment during the illumination.

Also, it is notable that the change in steady-state singlet oxygen concentration was just by a factor of 2-3 during a change in MB concentration by a factor of 100. The steady-sate singlet oxygen concentration increased as the MB concentration increased up

to 4.545 μM MB. Then, it began to be reduced at higher MB concentrations. This indicates that there exists an optimal concentration of photosensitizer MB for generating singlet oxygen and a larger amount of photosensitizer does not necessarily mean more effective generation of singlet oxygen. This is clear quantitative evidence for the same conclusion derived in our previous qualitative study using DMA PEBBLEs [15].

MB conc. (μM)	Steady-state [$^1O_2$] (μM)
9.091	1.18×10^{-6}
4.545	1.21×10^{-6}
0.909	1.09×10^{-6}
0.455	0.86×10^{-6}
0.091	0.58×10^{-6}

<Table 2.3: Steady-state singlet oxygen concentrations produced by photosensitizer MB with various concentrations in aqueous media estimated by equation (12), $[^1O_2]_{s\text{-}s} = k/k_{c,nanoprobes}$ using measured fluorescence decay rate (k) and established sensitivity of DPIBF Ormosil nanoprobes (k_c)>

This "saturation" phenomenon could be understood by a hypothesis based on the formation of MB dimers, which do not generate singlet oxygen, which increases rapidly at higher MB concentrations. It has been well studied by Rabinowitch and Epstein [25], and Patil *et al.* [26] that MB molecules form dimers or oligomers at increasing concentration. Also, many researchers have reported that aggregation of photosensitizer dyes, including MB, can decrease their singlet oxygen quantum yield ($\Phi_{^1O_2}$), and this is most remarkable for hydrophobic photosensitizers in aqueous solvents [36-41]. Furthermore, we observed that the k value, which is directly proportional to the steady-

state singlet oxygen concentration, constantly increased with MB concentration in an organic solvent that effectively suppressed self-aggregation (data not included). The above supports the conclusion that aggregation of dye is responsible for the reduction of singlet oxygen generation at high concentration.

The above study points out clearly that only the steady-state singlet oxygen concentration can be considered as a true measure for cancer cell exposure to treatment in clinical PDT. In that sense, a measured steady-state singlet oxygen concentration should be regarded as a more important and accurate gauge for deciding on an appropriate dosage of photosensitizer and for evaluating the PDT efficiency, rather than other commonly used values, such as the singlet oxygen quantum yield of the given photosensitizer, and the light dose of PDT, both of which being only a limited predictive value, as they ignore practical complications in clinical PDT, such as aggregation of the dye and molecular transformations in the cell. Thus DPIBF embedded Ormosil PEBBLE nanoprobes can become a highly sensitive and effective way to determine the real important therapeutic parameters of PDT.

Singlet oxygen quantification for *in vitro* PDT using DPIBF Ormosil PEBBLE nanoprobes

Based on the determined sensitivity of DPIBF Ormosil PEBBLE nanoprobes towards singlet oxygen, the quantitative evaluation of the singlet oxygen generation was attempted for *in vitro* PDT using MB incorporated PAA DNP as photosensitizer. As described in earlier sections, the steady-state singlet oxygen concentration can be directly determined by monitoring the exponential decay of DPIBF fluorescence emission during

illumination. The PDT was performed under 4 different conditions, with combination of 2 different MB PAA DNP concentrations (1 mg/mL and 0.1 mg/mL) and 2 different cell densities (200,000/mL and 40,000/mL of C-6 glioma cells). Also, 2 control measurements for each MB DNP concentrations were repeated without the presence of cells, under identical situations. While the entire cell chamber was illuminated by red-LED with 2 mW power at 660 nm for 5 miutes, the fluorescence emission of DPIBF Ormosil PEBBLE nanoprobes was monitored. The spectral change of DPIBF Ormosil PEBBLE nanoprobes for each case was shown as below in figure 2.9.

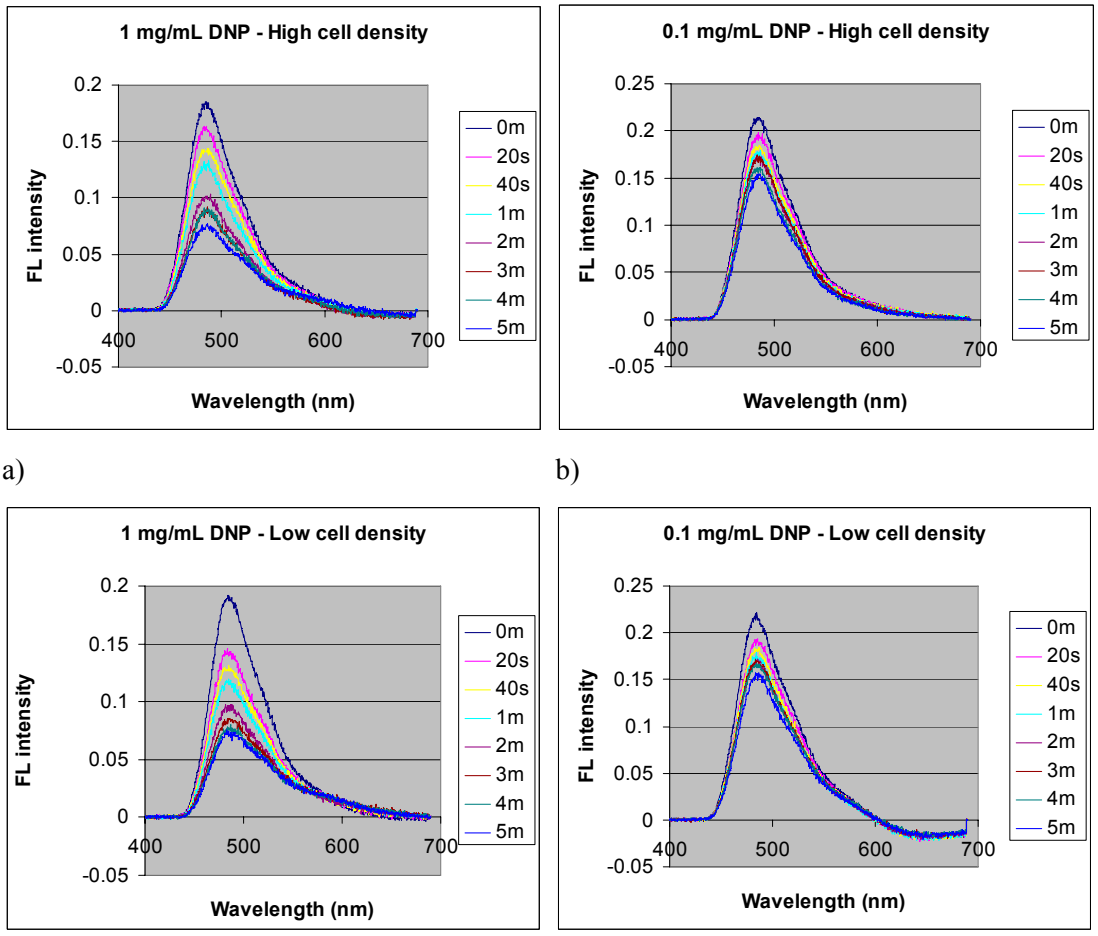

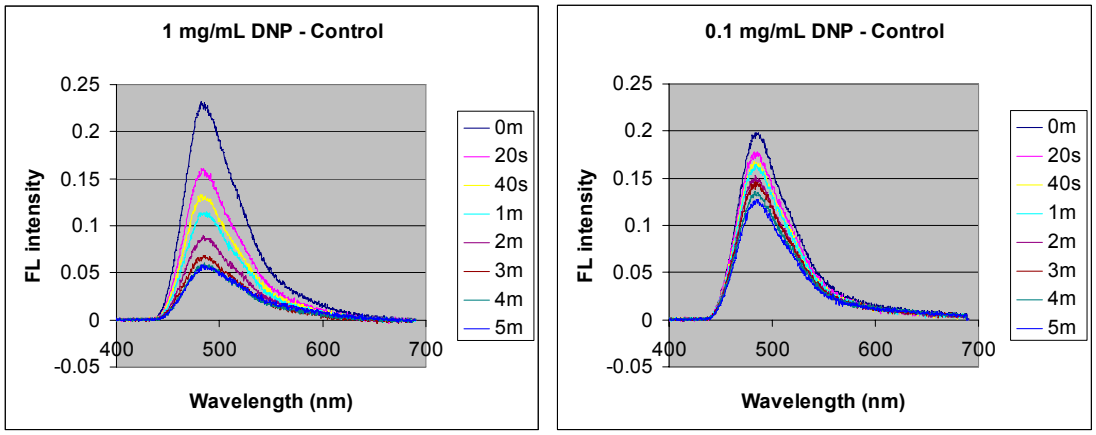

e) f)

<Figure 2.9: Fluorescence emission change of DPIBF Ormosil PEBBLE nanoprobes measured from in vitro PDT for C6 glioma cells using photosensitizer MB PAA DNPs for 5 minutes, 4 different conditions using 2 DNP concentrations and 2 cell densities were examined and control experiment for each DNP concentration was performed as well without the presence of cells. a) 1 mg/mL MB PAA DNP with high cell density, b) 0.1 mg/mL MB PAA DNP with high cell density, c) 1 mg/mL MB PAA DNP with low cell density, d) 0.1 mg/mL MB PAA DNP with low cell density, e) 1 mg/mL MB PAA DNP without cells (control), and f) 0.1 mg/mL MB PAA DNP without cells (control)>

By analyzing this decay of fluorescence emission with 1st order kinetics, the *k* value of each result was calculated as shown in figure 2.10 and the steady-state singlet oxygen concentration for each condition could be determined. It must be importantly noted that the *k* values obtained from controls without cells were consistently higher than k values obtained in the presence of cells for all conditions. It means that DPIBF Ormosil PEBBLE nanoprobes detected less amount of singlet oxygen when the cells were present. Because all other experimental conditions were identical except the presence of cells, this discrepancy should be induced by the presence of cells. It can be explained as due to the fact that a certain amount of singlet oxygen was consumed to attack the cells, resulting in a lower steady-state singlet oxygen concentration.

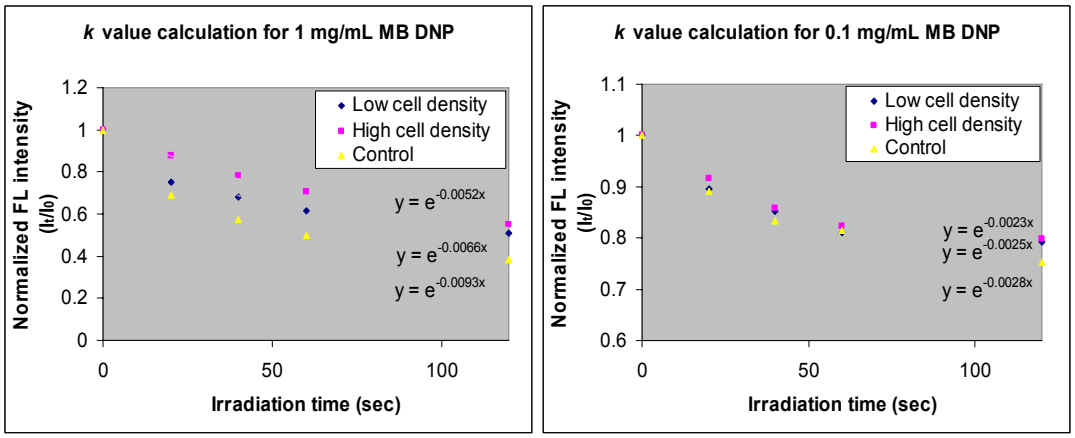

<Figure 2.10: *k* value determination for estimation of steady-state singlet oxygen concentrations for *in vitro* PDT experiment performed. The change of fluorescence intensity at emission maxima of DPIBF Ormosil PEBBLE nanoprobes were measured for 5 minutes and the obtained fluorescence intensity values were normalized as I_t (fluorescence intensity at time t) / I_0 (fluorescence intensity at time 0) for comparison. Right: PDT was performed with 1 mg/mL MB PAA DNPs in 3 sets of samples: high cell density, low cell density, and no cells (control). Left: PDT was performed with 0.1 mg/mL MB PAA DNPs in same 3 sets of samples. Besides DNP concentration and cell density, all other experimental conditions were identical>

From the calculation of steady-state singlet oxygen concentration for each case, the difference caused by cellular singlet oxygen consumption could be quantified as well, by simply subtracting the steady-state singlet oxygen concentration in the presence of cells from that of the control. The estimated singlet oxygen concentration and the cellular consumption for 4 different conditions are summarized in table 2.4.

In addition to the determination of steady-state singlet oxygen amounts consumed to attack cells present in the system, the singlet oxygen concentration can be even further applied to estimate how many singlet oxygen molecules were used to attack an individual cell (singlet oxygen molecules per cell), by normalizing it with the number of cells in each case. This calculation revealed that when the density of cells was lower, with the

same concentration of MB PAA DNP, the cells were attacked by more singlet oxygen. *Vice versa*, when the density of cells was higher, the cells were attacked by less singlet oxygen. As shown in table 2.4, the average c-6 cell at the lower density treated by PDT with 1 mg/mL of DNP was attacked by the most singlet oxygen molecules (about 21,000 singlet oxygens) and it was followed by the average cell at the higher density with 1 mg/mL (about 6,000 singlet oxygens), the cell at lower density with 0.1 mg/mL (about 1,900 singlet oxygens), and the cell at higher density with 0.1 mg/mL (about 600 singlet oxygens), respectively.

	MB DNP conc.	high cell density ($2x10^5$/mL)	low cell density ($4x10^4$/mL)	Control (no cell)
k value (sec^{-1})	1 mg/mL	0.0052	0.0066	0.0099
	0.1 mg/mL	0.0023	0.0025	0.0028
$[^1O_2]_{s\text{-}s}$ (M)	1 mg/mL	2.20×10^{-12}	2.80×10^{-12}	4.19×10^{-12}
	0.1 mg/mL	9.75×10^{-13}	1.06×10^{-12}	1.19×10^{-12}
$^1O_2$ consumed by single cell in steady-state	1 mg/mL	9.96×10^{-18} M/cell = 9.96×10^{-21} mole/cell = **5,997 /cell**	3.50×10^{-17} M/cell = 3.50×10^{-20} mole/cell = **21,054 /cell**	
	0.1 mg/mL	1.06×10^{-18} M/cell = 1.06×10^{-21} mole/cell = **638 /cell**	3.18×10^{-18} M/cell = 3.18×10^{-21} mole/cell = **1,914 /cell**	

<Table 2.4: Quantification of steady-state singlet oxygen and consumption by cells. Steady-state singlet oxygen concentration for all 6 experiments (1 mg/mL DNP – high cell density, 1 mg/mL DNP – low cell density, 1 mg/mL DNP – control, 0.1 mg/mL DNP – high cell density, 0.1 mg/mL DNP – low cell density, and 0.1 mg/mL DNP – control) were estimated using equation (12) from *k* values experimentally determined. From the difference between each control measurement and actual measurement, the steady-state singlet oxygen concentrations used for attacking cells were calculated for each case. Then, quantities of singlet oxygen used for attacking a single cell were calculated by dividing the determined concentration values by number of cells.>

When the MB PAA DNP concentration was also normalized by the number of cells, the relation between the normalized DNP concentration (mg/mLcell) and singlet oxygen consumption (singlet oxygen/cell) was found to be nearly linear, as shown in figure 2.11. This linear relation can be used as a calibration curve to predict the singlet oxygen quantity, which has been impossible to obtain because of uncontrollable property of singlet oxygen. In other words, based on this calibration curve, when we know the concentration of DNP (or the given photosensitizer in other situations) and the number of cancer cells or the volume of cancer tissue, we now can foretell how many singlet oxygen molecules would be consumed to attack the cancer cells or tissue.

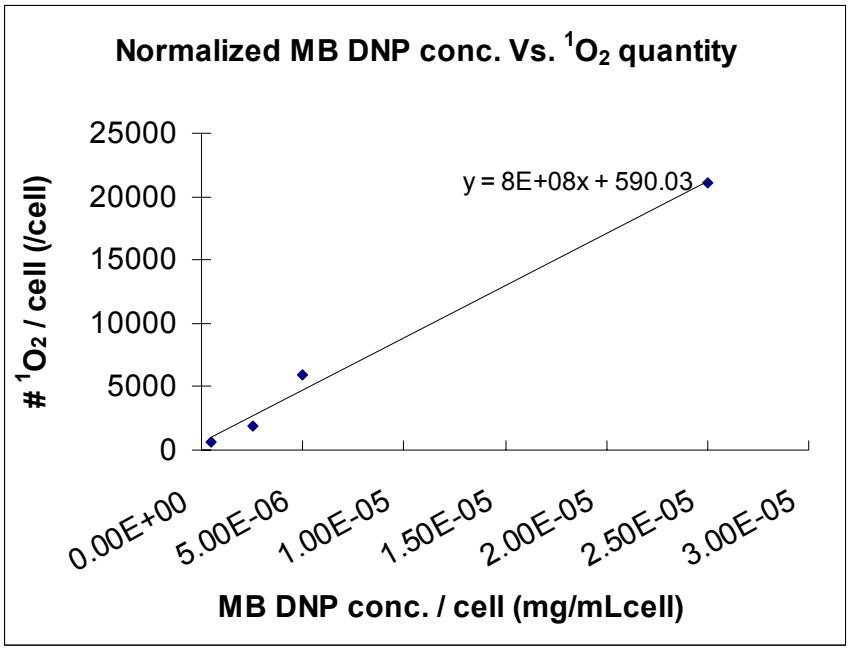

<Figure 2.11: Linear relationship between normalized concentration of photosensitizer MB PAA DNP and normalized consumption of singlet oxygen by cells determined from *in vitro* PDT experiments described above>

The fluorescence imaging based on PI staining, which selectively stains dead cells, also supported these results (figure 2.12). In the case of 1 mg/mL MB PAA DNP with

lower cell density, PI staining (shown as red spots) began to show up immediately after PDT for 5 minutes (or from sometime during PDT). On the other hand, 1 mg/mL MB DNP with higher cell density displayed PI stained cells only after 15 minutes (10 minutes after PDT was terminated). The same trend was observed for the 0.1 mg/mL MB PAA DNP concentration: 45 minutes for the lower cell density and 60 minutes for the higher cell density. In summary, the onset of cell death will be delayed under the same conditions of PDT when the cell density is increased. This result supports well the trend observed in quantification result above, showing cell density dependence for the cellular consumption of singlet oxygen: 'the less cells, the more damage and the more cells, the less damage'.

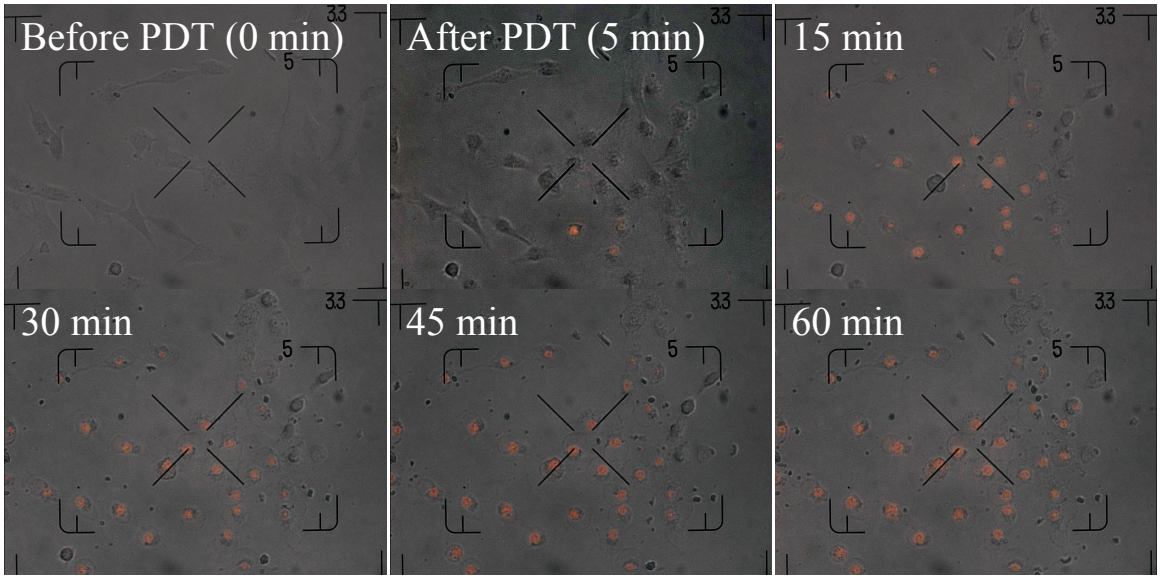

a) 1 mg/mL MB PAA DNP with low cell density, showing PI staining onset at 5 minutes.

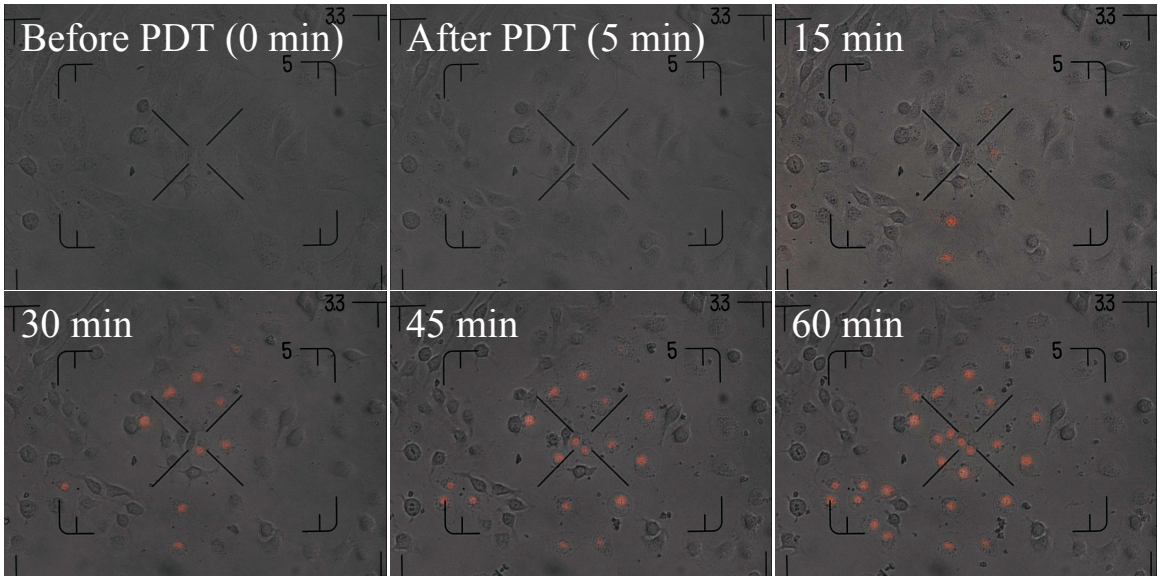

b) 1 mg/mL MB PAA DNP with high cell density, showing PI staining onset at 15 minutes.

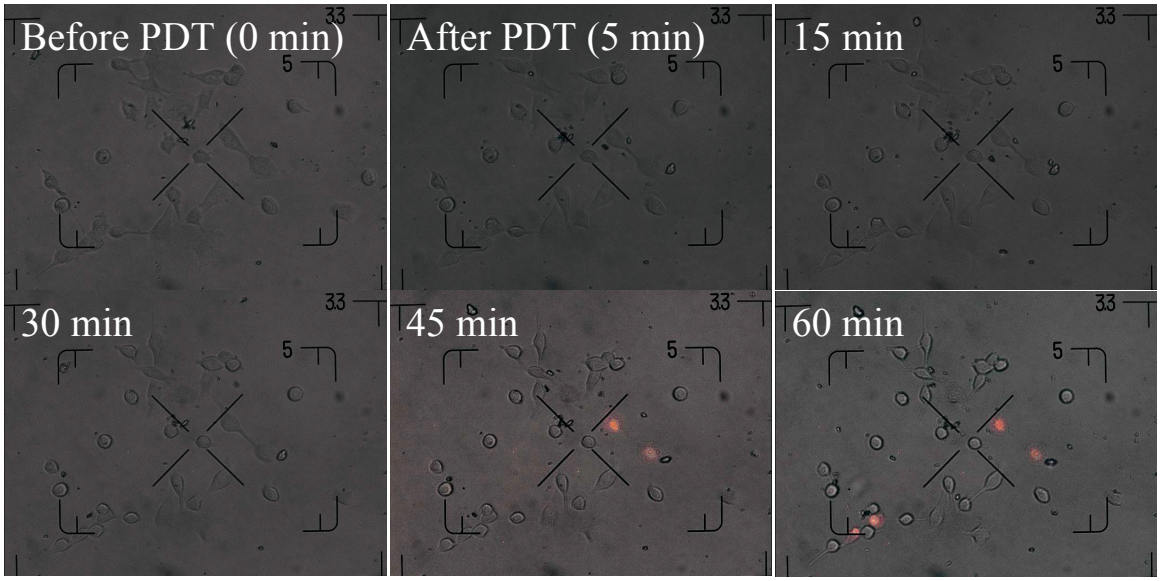

c) 0.1 mg/mL MB PAA DNP with high cell density, showing PI staining onset at 45 minutes.

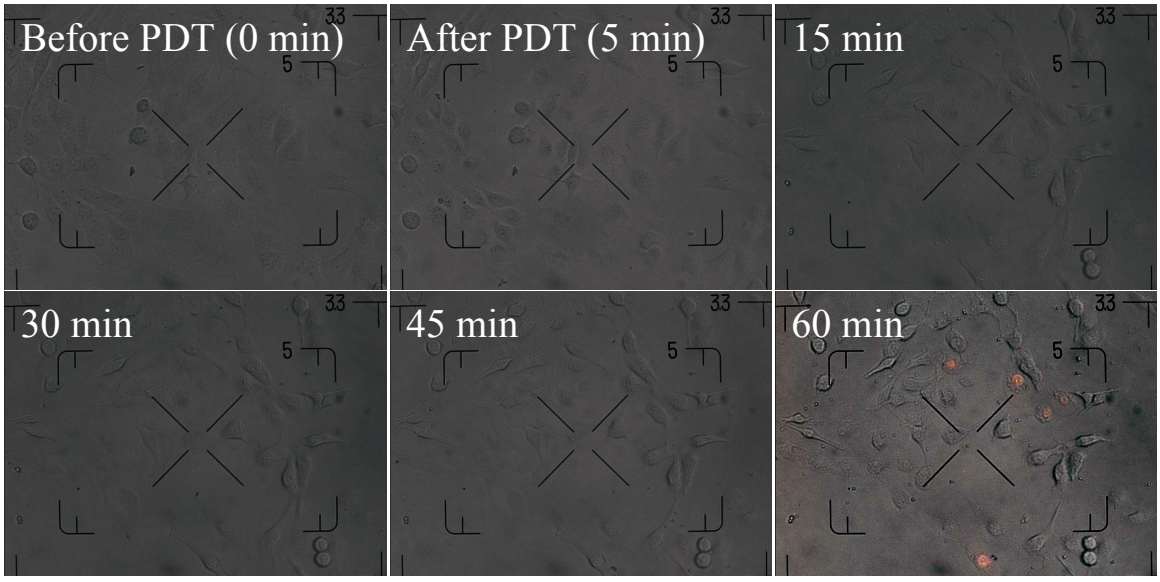

d) 0.1 mg/mL MB PAA DNP with high cell density, showing PI staining onset at 60 minutes.

<Figure 2.12: Bright field – fluorescence overlaid images to show cell damage indicated by PI staining, observed during *in vitro* PDT using MB PAA DNP for 5 minutes. The fluorescence of PI staining was measured in Olympus IMT II fluorescence microscope with standard green filter cube set. The cell density dependence of cell damage was indicated by delay of appearance of PI stained cells when there were more cells in the system under same concentration of DNPs.>

Post-PDT tumor regrowth

In previous sections, it was descried that DPIBF enabled the quantification of steady-steady singlet oxygen concentration and singlet oxygen consumption per individual cell. There is a critical question remaining to be answered, using this new ability obtained from DPIBF Ormosil PEBBLE nanoprobes, of importance for successful PDT: what is a sufficient quantity of singlet oxygen for killing completely the given tumor cells or tissue? In order to answer this question, the determination of singlet oxygen quantity must be correlated with the cell death profile.

Although PI staining is a widely used method for monitoring cell viability, it is based on cellular membrane damage allowing internalization of dye molecules to stain

the nucleus, and, in principle, this method shows rather how much cells were damaged were by the PDT treatment than how many cells actually died of it. After PDT was performed, some cells would be dead, but other cells might be able to recover and start growing back, eventually, causing the PDT to fail. Therefore, the cell growth after PDT needed to be monitored in another method over the long term. Thus post-PDT regrowth was examined on PDT treated cells for 3 days after PDT by monitoring the change in total number of surviving cells in a cell well using trypan blue staining. (Similar to PI staining, the trypan blue staining is also based on membrane damage not actual cell death. However, it was valid for our purpose because no dead cells were observed in our experiments, indicating that dead cells were lifted and disappeared from the system with only live cells remaining.) In order for correlating this with the singlet oxygen quantification results, the tests were performed for 2 different initial densities (high density: 144,000/mL; low density: 15,000/mL). Also, a control measurement without PDT treatment for each cell density was performed in parallel. The PDT was achieved in the same configurations used for the singlet oxygen quantification studies, i.e. with 1 mg/mL MB PAA DNP as a photosensitizer, red-LED with 2 mW power at 660 nm, and 5 minute illumination. The results are displayed in figure 2.13.

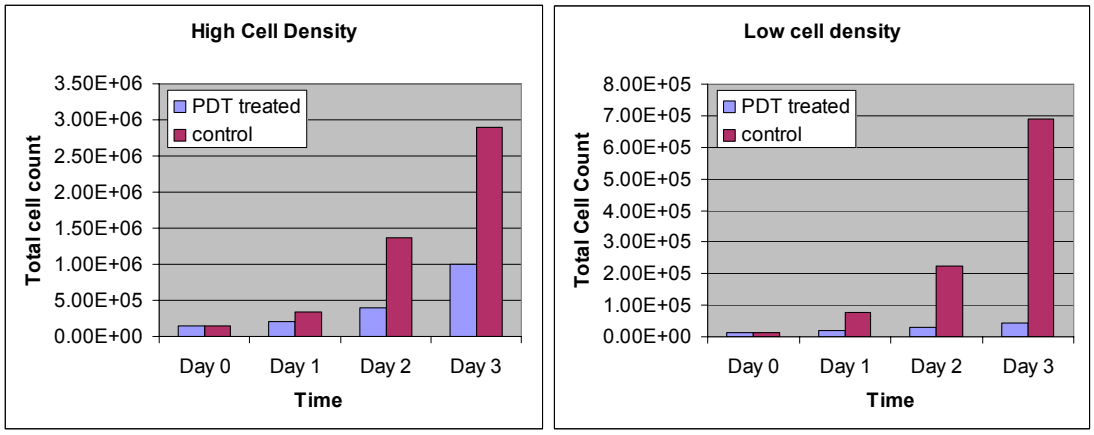

<Figure 2.13: Tumor regrowth profiles after *in vitro* PDT using MB PAA DNP for 5 minutes for 2 different cell densities and comparison with growth of non-treated cells (controls). The C6 glioma cells were continued to be cultured for 3 days after PDT treatment and the number of surviving cells were counted by hemacytometer with trypan blue exclusion. All the results were averaged out of 4 measurements for consistency. Significant reduction of cell numbers were observed from PDT treated cells compared to un-treated controls.>

As shown in figure 2.13, cells treated by PDT showed considerably slower regrowth than the controls, for both cell densities. As expected from the conclusions of the previous section, the lower cell density sample exhibited significantly slower regrowth than the higher cell density one, well supporting the idea of 'the less cells, the more damage and the more cell, the less damage'. In order to evaluate this effect numerically, the data from the two cell densities were normalized in one plot by setting the final cell count as 100 and the initial cell count as 0 (figure 2.14).

Over 3 days after PDT, the higher cell density samples showed about 31 % regrowth of cells, compared to untreated case. On the other hand, the low cell density samples showed only 4 % regrowth. If we correlate these data with the calibration curve in figure 2.11, the normalized MB-DNP concentration for the high cell density was 6.94 x 10^{-6} mg/mLcell on average and the steady-state singlet oxygen consumed to attack a

single cell under this condition could be 6,146/cell. This singlet oxygen consumption was able to suppress 69 % of cell regrowth for 3 days. In the same way, the normalized MB-DNP concentration for the low cell density was 6.67 x 10^{-5} mg/mLcell and the steady-state singlet oxygen used to attack a single cell was 53,923/cell and it could suppress 96 % of cell regrowth for 3 days, which is quite close to perfect cell killing. With accumulation of such correlation data, between singlet oxygen quantification and cell regrowth suppression, one might in the near future be able to determine a realistic threshold for the singlet oxygen quantity required to kill a single C-6 glioma cell.

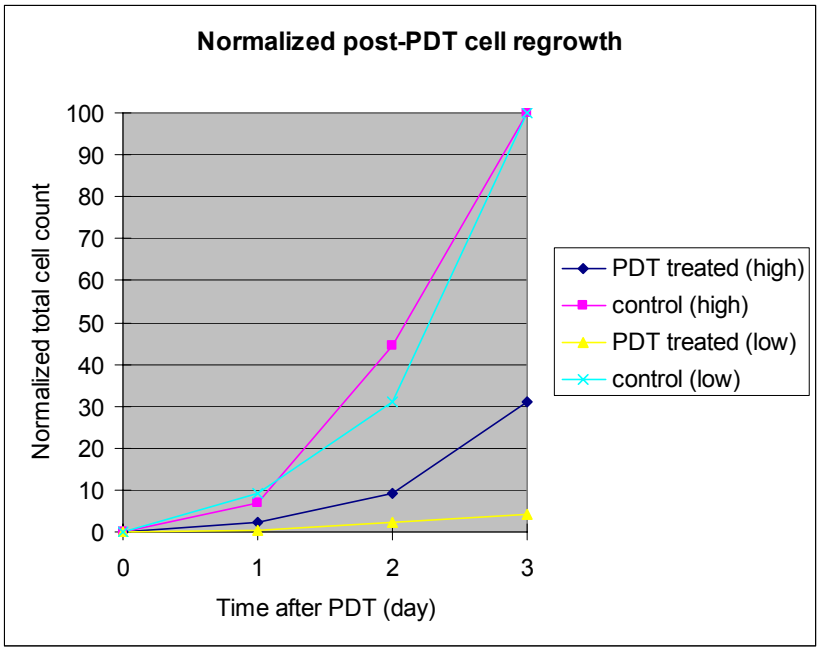

<Figure 2.14: A summary of cell regrowth profiles over 3 days after in vitro PDT. The number of cell for each case was normalized by adjusting the initial cell count (day 0) to 0 and final cell count (at day 3) of each control (un-treated cells) to 100. Both controls showed similar pattern of growth after normalization. The treated cells with high density showed 31 % regrowth and the ones with low density showed 4 % regrowth compared to controls, indicating significant suppression of cell growth by PDT treatment.>

To our best knowledge, we believe that the results described in this chapter, including direct quantitation of the steady-state concentration of singlet oxygen, under both non-biological and biological conditions, the quantitation of singlet oxygen consumed in attacking cells, the singlet oxygen calibration, and the correlation with cell death profiles, are reported for the first time in this scientific field.

Acknowledgements

The author thanks to valuable advice from Dr. Yong-Eun L. Koo, and kind cooperation and help from Dr. Hao Xu. This work was supported by NCI grant (N01-CO-37123).

References

1. Kon T. *et al.* (2004) Singlet oxygen quenching activity of human serum. *Redox Report* 9(6), 325-330.
2. Reilly P.M. *et al.*(1991) Pharmacological Approach to Tissue Injury Mediated by Free Radicals and Other Reactive Oxygen Metabolites. *Am. J. Surg.* 161(4), 488-503
3. Kovacic P. *et al.* (2001) Mechanisms of Carcinogenesis: Focus on Oxidative Stress and Electron Transfer. *Curr. Med. Chem.* 8(7), 773-796
4. DeRosa M. and Crutchley R. (2002) Photosensitized singlet oxygen and its applications. *Coordination Chemistry Reviews* 233-234, 351-371
5. Eberhardt M. (2001) *Reactive oxygen metabolites; chemistry and medical consequences*, CRC press
6. Shen H., Ong C. *et al.* (1996) Detection of elevated reactive oxygen species level in cultured rat hepatocytes treated with aflatoxin B_1. *Free radical biology and medicine*, 21(2), 139-146
7. Dougherty T. J. *et al.* (1998). Review: Photodynamic therapy. *J. Natl. Cancer. Inst.* 90(12), 889-905
8. Moore J. V., West C. M. L., and Whitehurst C. (1997) The biology of photodynamic therapy, *Phys. Med. Biol.* 42(5), 913-935
9. Brown S., Brown E., and Walker I. (2004), The present and future role of photodynamic therapy in cancer treatment. *The Lancet Oncology*, 5(8), 497-508
10. Steinbeck M. J., Khan A. U., and Karnovsky M. J. (1992) Intracellular singlet oxygen generation by phagocytosing neutrophils in response to particles coated with a chemical trap, *J. Biol. Chem.,* 267(19), 19, 13425-13433
11. Niedre M., Patterson M. S., and Wilson B. C. (2002) Direct near-infrared luminescence detection of singlet oxygen generated by photodynamic therapy in cells *In Vitro* and tissues *In Vivo*, *Photochem. Photobiol.* 75(4), 382-391
12. Dysart J. S., Singh G., and Patterson M. S. (2005) Calculation of singlet oxygen dose from photosensitizer fluorescence and photobleaching during mTHPC photodynamic therapy of MLL Cells, *Photochem. Photobiol.*, 81(1), 196-205
13. Moreno M., Kopelman R. *et al.* (2003) Production of singlet oxygen by $Ru(dpp(SO_3)_2)_3$ incorporated in polyacrylamide PEBBLEs. *Sensors and Actuators* B, 90(1-3), 82-89
14. Zahir K. O. and Haim A. (1992) Yields of singlet dioxygen produced by the reaction between the excited state of tris(bipyridine)ruthenium(II) and triplet dioxygen in various solvents. *J. Photochem. Photobiol.* A, 63(2), 167-172
15. Cao, Y, Koo Y. L., Koo S. M., and Kopelman, R., (2005) Ratiometric Singlet Oxygen Nano-optodes and Their Use for Monitoring Photodynamic Therapy Nanoplatforms. *Photochem. Photobiol.* 81(6), 1489-1498

16. R. Kopelman *et al.* (1998) Subcellular optochemical nanobiosensors: probes encapsulated by biologically localised embedding (PEBBLEs). *Sensors and Actuators* B, 51(1-3), 12-16

17. Xu H., Kopelman R. *et al.* (2004) Photoexcitation-Based Nano-Explorers: Chemical Analysis inside Live Cells and Photodynamic Therapy. *Isr. J. chem.* 44(1-3), 317-337

18. Foote C. S. and Denny R. W. (1971) Chemistry of singlet oxygen. XIII. Solvent effects on the reaction with olefins. *J. Am. Chem. Soc.* 93(20), 5168-5171

19. Merkel P. B. and Kearns D. R. (1972) Radiationless decay of singlet molecular oxygen in solution. Experimental and theoretical study of electronic-to-vibrational energy transfer. *J. Am. Chem. Soc.*, 94(21), 7244-7253

20. Young R. H., Brewer D., and Keller R. A. (1973) Determination of rate constants of reaction and lifetimes of singlet oxygen in solution by a flash photolysis technique. *J. Am. Chem. Soc.*, 95(2), 375-379

21. Usui Y., Tsukada M., and Nakamura H. (1978) Kinetic studies of photosensitized oxygenation by singlet oxygen in aqueous micellar solutions. *Bull. Chem. Soc., Jap.* 51(2), 379-384

22. Gorman A. A., Lovering G., and Rodgers M. A. J. (1976) The photosensitized formation and reaction of singlet oxygen, O2*(1Δ), in aqueous micellar systems. *Photochem. Photobiol.* 23(6), 399-403

23. Hah H. J., Lee Y. E. *et al.* (2003) Simple preparation of monodisperse hollow silica particles without using templates. *Chem. Comm.* (14), 1712-1713

24. Koo Y. L., Cao Y., Kopelman R. *et. al.* (2004) Real-Time Measurements of Dissolved Oxygen Inside Live Cells by Organically Modified Silicate Fluorescent Nanosensors. *Anal. Chem.*, 76(9), 2498-2505

25. Rabinowitch E. and Epstein L. (1941) Polymerization of Dyestuffs in Solution. Thionine and Methylene Blue. *J. Am. Chem. Soc.* 63(1), 69-78

26. Patil K., Pawar R., and Talap P. (2000) Self-aggregation of Methylene Blue in aqueous medium and aqueous solutions of Bu_4NBr and urea. *Phys. Chem. Chem. Phys.*, 2(19), 4313-4317

27. H.C. Junqueira, M. S. Baptista *et al*. (2002) Modulation of methylene blue photochemical properties based on adsorption at aqueous micelle interfaces, PCCP, v4, 2320-2328

28. Merkel B. B. and Kearns D. R. (1975) Rate constant for the reaction between 1,3-diphenylisobenzofuran and singlet oxygen. *J. Am. Chem. Soc.* 97(2), (1975), 462-463

29. Rao P. S., Mueller J. S. *et al.* (1988) Specificity of oxygen radical scavengers and assessment of free radical scavenger efficiency using luminol enhanced chemiluminescence. *Biochem. Biophys. Res. Comm.*, 150(1), 39-44

30. Wilkinson F., Helman W. P. and Alberta B. R. (1995) Rate constants for the decay and reactions of the lowest electronically excited singlet state of molecular oxygen in solution. An expanded and revised compilation. *J. Phys. Chem. Ref. Data* 24: 663-1021, (http://allen.rad.nd.edu/compilations/SingOx/SingOx.htm)

31. Nemoto M., Kokubun H., and Koizumi M. (1969), Determination of S*-T transition Probabilities of some xanthene and thiazine dyes on the basis of T-energy transfer. II. Results in the aqueous solution, *Bull. Chem. Soc. Jap.* 42(9), 2464-2470

32. Wilkinson F. (1975), in *Organic Molecular Photophysics*, John Wiley, New York, v2 152-155

33. hemacytometry protocol

34. Howard J. A. and Mendenhall G. D. (1975), Autoxidation and photooxidation of 1,3-diphenylisobenzofuran. Kinetic and product study. *Can. J. Chem.* 53(14), 2199-2201

35. Aubry J. M. et al. (2003) Reversible binding of oxygen to aromatic compounds, Acc. Chem. Res. 36(3), 668-675

36. Fernandez J. M., Bilgin M. D., and Grossweiner L. I. (1997) Singlet oxygen generation by photodynamic agents. *J. Photochem. Photobiol.* B, 37(1-2), 131-140

37. Renikuntla B. R. *et al.* (2004) Improved photostability and fluorescence properties through polyfluorination of a cynine dye, *Organic Letters*, 6(6), 909-912

38. Konishi T. *et al.* (2003) Improvement of quantum yields for photoinduced energy/electron transfer by isolation of self-aggregative zinc tetraphenyl porphyrin-pendant polymer using cyclodextrin inclusion in aqueous solution, *J. Phys. Chem.* B, 107(41), 11261-11266

39. Damoiseau X. *et al.* (2001) Increase of photosensitizing efficiency of the bacteriochlorin *a* by liposome-incorporation, *J. Photochem. Photobiol.* B, 60(1), 50-60

40. Zenkevich E. *et al.* (1996) Photophysical and photochemical properties of potential porphyrin and chlorine photosensitizers for PDT, *J. Photochem. Photobiol.* B, 33(2), 171-180

41. Gabrielli D. *et al.* (2004) Binding, aggregation, and photochemical properties of methylene blue in mitochondrial suspensions, *Photochem. Photobiol.* 79(3), 227-232

Chapter 3

Development of Ormosil PEBBLE Nanoprobes for Improved Hydrogen Peroxide (H_2O_2) Selectivity and Application to Macrophage Activation Studies

Introduction

This chapter describes a simple method for converting a non-specific ROS sensitive molecular probe into a hydrogen peroxide selective one, by incorporating the probe molecules inside PEBBLEs made with an Ormosil matrix. Hydrogen peroxide (H_2O_2) is one of the reactive oxygen species (ROS) and plays important roles in cellular functions that are based on oxidant-antioxidant balance. H_2O_2 is well known as a key component of phagocytotic host defense systems [1-4] and one of the important mediators in redox based cell signaling [5-8]. The H_2O_2 can be produced in biology from biological oxidation by various oxidase activities, mainly based on divalent reduction of molecular oxygen or dismutation of superoxide radicals. The latter has been intensively investigated in relation with superoxide dismutase (SOD) mechanisms. When superoxide radicals are generated, SOD rapidly scavenges them, producing H_2O_2. On the other hand, H_2O_2 can be a precursor of diverse secondary ROS when certain conditions are met, such as hydroxyl radicals (·OH) in the presence of metal ions, hypochlorous acid (HOCl) in the presence of myeloperoxidases (MPO), singlet oxygen ($^1O_2$), and

and peroxynitrite ($ONOO^-$) [9-11]. The mechanisms are summarized as below.

<Generation of H_2O_2 in biological environment>

$2\ O_2^- + H^+ \rightarrow H_2O_2 + O_2$ (catalyzed by SOD)

< H_2O_2 mediated ROS generation>

$H_2O_2 + Fe^{2+} \rightarrow Fe^{3+} + \cdot OH + \cdot OH^-$ (Fenton reaction)

$H_2O_2 + Cl^- \rightarrow HOCl + OH^-$ (Catalyzed by MPO)

$HOBr(or\ Cl) + H_2O_2 \rightarrow {}^1O_2 + H^+ + Br^-(or\ Cl^-) + H_2O$

$H_2O_2 + NO_2^- \rightarrow H_2O + ONOO^-$

The cytotoxicity of H_2O_2 has been generally an accepted fact, though the accurate mechanism is not clearly understood yet. Recently, H_2O_2 has been investigated as a mediator for the further generation of secondary ROS that are more reactive and toxic, rather than for its own properties and functions. Actually, H_2O_2 is the least reactive ROS, thus exhibiting relatively mild toxicity, and, concomitantly, the most stable/longest lasting one [9]. This stability makes the detection of H_2O_2 relatively easy, compared to the detection of other ROS. Taking into account its interrelation with other ROS, and its stability, H_2O_2 has been drawing interest because a qualitative or quantitative understanding of H_2O_2 can provide important information for understanding the mechanisms of other ROS as well, while their direct detection can be difficult. However, the investigation of the H_2O_2 mechanism and function, *in vitro and in vivo,* still remains

challenging, mainly due to the absence of H_2O_2 specific materials and methods of detection.

Applications of PEBBLE nanosensor/probes for specific reactive oxygen species have been explored by our group previously. PEBBLEs for the detection of singlet oxygen [12], superoxide radicals [13], H_2O_2 [13], and hydroxyl radicals [14] have been attempted, with only partial success. For instance, the previously developed singlet oxygen detecting PEBBLEs showed good specificity towards singlet oxygen and good stability. However, their sensitivity, which is the key property for singlet oxygen detection, was barely improved compared to other molecular probes; also, change of sensitivity due to the encapsulation inside the PEBBLE matrix was not investigated. Consequently, this limited the use of these PEBBLEs to an only relative evaluation of singlet oxygen in non-biological systems (These drawbacks were overcome as described in Chapter 2). PEBBLEs for the detection of superoxide radicals and of H_2O_2 were derived based on an indirect measurement of the oxygen consumed by the generation of O_2^- or H_2O_2, instead of monitoring them directly. This methodology can lead to biased results, especially when multiple types of ROS are generated, which is typical under physiological conditions. Thus it could be valid only for simplified systems for specific ROS. PEBBLEs with higher sensitivity and better specificity are still needed for ROS detection.

King described a hydroxyl radical PEBBLE sensor [13,14], where the hydroxyl radical could only be detected on the surface of the PEBBLEs because of its extremely short lifetime, and thus his hydroxyl radical PEBBLE sensor was made by conjugating the hydroxyl radical sensitive probe molecules onto the surface of the PEBBLEs. It

showed that ·OH cannot penetrate PEBBLE matrix. Also, we have experienced loss of sensitivity in various ROS detecting molecular probes, when they were encapsulated in a PEBBLE matrix. This lesson can be inversely interpreted to show that hydroxyl radicals and other ROS can be blocked from reaching probes that are encapsulated inside a nanoparticle matrix. Based on this idea, a methodology to improve the specificity of ROS detecting probes is suggested, that is, using nanoparticle as a screening device for unstable reactive oxygen species and thus make PEBBLE sensors with improved selectivity towards the more stable ROS, such as hydrogen peroxide.

2',7'-dichlorofluorescin diacetate (DCFDA) is one such non-specific (i.e. universal) molecular probe for ROS; thus it has been most widely used to study oxidative burst [15-17]. As summarized in figure 3.1, DCFDA does not have optical signatures when it is in its original lipophilic form, enabling this dye molecule easily to permeate cellular membranes. Once it is internalized into cells, this dye is trapped inside by losing its diacetate group, due to the intracellular esterase activity, thus turning into a hydrophilic and slightly fluorescent form (2',7'-dichlorofluorescin dihydroxide, DCFH). This procedure has been often called *activation* because it was believed that the dye becomes sensitive towards ROS in its DCFH form. The DCFH can effectively be oxidized by various ROS, such as H_2O_2, ·OH, O_2^-, NO·, and $ONOO^-$, generating a strongly fluorescent fluorescein derivative, dichlorofluorescein (DCF) [18].

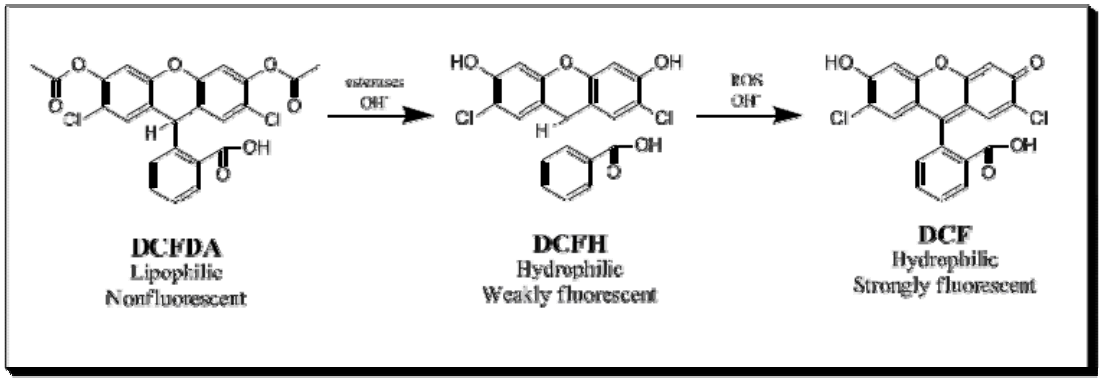

<Figure 3.1: Schematic for ROS detection mechanism of DCFDA free dye in biological systems. Lipophilic DCFDA can readily penetrate cell membrane and be trapped by being transformed to hydrophilic DCFH. DCFH can be oxidized by ROS producing strong fluorescent product DCF>

The reaction of this dye with ROS can be catalyzed by the activity of peroxidases, heme-containing enzymes, and intracellular ferrous ion. Thus, the reactive oxygen assay using DCFDA has been typically performed in association with horseradish peroxidase (HRP) [15,16]. Although the mechanisms of this dye are relatively well investigated, it is still not clear how this dye is oxidized by various ROS and other oxidants. Its application has been strictly limited whenever a specific type of ROS needed to be monitored, because of this dye's poor specificity. The auto-oxidation of DCFDA by illumination or other conditions, as well as the enzymatic oxidation of this dye by HRP alone, without ROS, were other well known drawbacks [16,18]. Also, DCFDA is sensitive to pH. Under acidic conditions, this dye loses its sensitivity towards ROS as well as its fluorescent property. On the other hand, under basic conditions, it can lose its diacetate groups, forming an activated fluorescent product and, according to our experience, the base can eventually complete the oxidation of this dye forming DCF somehow [18].

In this chapter, the development of PEBBLE nanoprobes containing DCFDA with Ormosil matrix, using a new post-loading technique, is described. Also, experimental

evidence is provided to show that the H_2O_2 selectively of this PEBBLE nanoprobe was improved. In vitro H_2O_2 detection in live macrophages, using these PEBBLE nanoprobes, is described as well.

Experimental

Materials

2',7'-dichlorofluorescin diacetate (DCFDA), 2',7'-dichlorofluoresein (DCF), phenyltrimethoxysilane (PTMS), methyltrimethoxysilane (MTMS), aminopropyltrimethoxysilane (APTMS), ammonium hydroxide, nitric acid, chloroform, , potassium superoxide, peroxidase from horse radish (type VI), *N*-formyl-Methiony-*L*-Leucyl-*L*-Phenylalanine (fMLP) were purchased from Sigma-Aldrich (St. Louis, MO) and used without further purification. Hydrogen peroxide (30%) was obtained from Acros Organics (Morris Plains, NJ). Peroxynitrite was obtained from Cayman Chemical, (Ann Arbor, MI), Alexa 568 succinimidyl ester, sulfo-succinimidyl 4-[*N*-maleimidomethyl]cyclohexane-1-carboxylate (sulfo-SMCC), cysteine capped TAT peptide were purchased from Invitrogen (Carlsbad, CA), Pierce Biotechnology (Rockford, IL), and SynBioSci (Livermore, CA), respectively. All chemicals for macrophage culture including A-DMEM, Glutamax, FBS, and P/S were purchased from Invitrogen and mixed following the recipe provided by Youxhin Zhang in Dr. Joel Swanson's group in University of Michigan, Department of Microbiology and Immunology.

Optical instrumentation

The fluorescence emission intensity of DCFDA free dye and dye embedded PEBBLE nanoprobes and its response towards H_2O_2 or other ROS was monitored with a Horiba Jovin Yvon fluoromax-3 fluorospectrometer (Kyoto, Japan) equipped with xenon arc lamp. Typical measurements were performed by recording the fluorescence emission intensity of DCFDA, in a time resolved acquisition mode, for 5 minutes, with excitation wavelength at 505 nm and emission wavelength 523 nm, with slit widths of 2 nm for both excitation and emission.

The fluorescence in *in vitro* cellular measurements was measured with an Olympus IMT II fluorescence microscope (Lake Success, NY), incorporated with an Acton Research (Trenton, NJ) Spectrograph spectrometer and a Hamamatsu HC230 charge coupled device (CCD) (Hamamatsu, Japan) [20,25]. The fluorescence emission spectra of DCFDA free dye or the nanoprobes were measured using a standard blue filter cube from Omega Optical (Brattleboro, VT). Also, the intracellular distribution of the nanoprobes was visualized based on a second dye labeling (Alexa 568), using a standard green filter cube from Omega Optical.

Preparation of Ormosil nanoparticles

Ormosil nanoparticles were synthesized, without addition of DCFDA dye, following the method described in our previous literature [12,19,20], and the procedures were the same as described in chapter 2. In addition to the previous method, a third monomer with primary amine group, aminopropyltrimethoxysilane (APTMS) was added to functionalize the surface of the Ormosil particles for future conjugation with dyes and

targeting moieties. One hour after addition of APTMS, the final product was rinsed by filtering the solution 3 times with an excess amount of de-ionized water. The product Ormosil nanoparticles were recovered after drying.

DCFDA encapsulation by post-loading

Hydrophobic DCFDA, the dye in its hydrophobic parent form and blank Ormosil nanoparticles (1:10 weight ratio between dye and nanoparticle respectively) were suspended together in 0.5 mL of chloroform. This suspension was mixed into an excess amount of DI water (about 150 mL) and the mixture was vigorously shaken to disperse chloroform droplets of very small size. Then, the whole mixture was opened to air, allowing evaporation of chloroform for 1 or 2 hours, while ultrasonicated to avoid coagulation of the chloroform droplets. The mixture was occasionally shaken again until the chloroform was sufficiently removed by vaporization. The final product particles were recovered after a number (usually more than 5 times) of filtrations, sufficient to remove possible unbound dye molecules. The product was re-suspended in phosphate buffer with physiological pH, to give a 1 mg/mL concentration. This stock solution was stored frozen at -20 ˚C in 0.5 mL aliquots; it was thawed and diluted to 0.1 mg/mL concentration right before the experiments.

H_2O_2 response and concentration dependency

A 0.1 mg/mL DCFDA Ormosil PEBBLE nanoprobe suspension in phosphate buffer (pH 7.2) was prepared. 20 μL of H_2O_2 solutions with various concentrations (from

3% to 0.003 %) were mixed with 2 mL of the PEBBLE nanoprobe solutions, to give a concentration range from 8.7 μM to 8.7 nM of final H_2O_2. The DCFDA Ormosil PEBBLE nanoprobe's response towards H_2O_2 was monitored by time-resolved acquisition of fluorescence emission, with 505 nm excitation and 523 nm emission wavelengths, for 5 minutes after addition of H_2O_2 with stirring.

Dye leaching

In order to make sure that the DCFDA Ormosil PEBBLE nanoprobe's response towards H_2O_2 occurs truly inside of the nanoparticle matrix, the dye leaching needed to be examined. 0.1 mg/mL DCFDA loaded Ormosil nanoprobes in phosphate buffer were prepared. An 2 mL aliquot of this nanoprobe solution was filtered through an Amicon filtration system with 100 kDa molecular weight cut-off (MWCO), so as to remove Ormosil nanoparticles from the solution, and the filtrate was taken for an H_2O_2 response test. A 0.3 % H_2O_2 solution was added to the nanoprobe solution and filtrate solution. Then, the fluorescence emission intensity change for each was monitored for 5 minutes with the same optical configuration described above.

Interference by enzymes and other ROS

- Horseradish Peroxidase (HRP) interference: The interference from HRP was examined by monitoring the change of DCFDA loaded Ormosil nanoprobe's fluorescence emission upon introduction into the DCFDA Ormosil PEBBLE nanoprobe solution of HRP alone, H_2O_2 alone, and HRP and H_2O_2 combined. A 10 μL solution of

0.1 mg/mL HRP suspended in PBS buffer with pH 7.2 (final concentration about 10 μM) and 20 μL of 0.3 % H_2O_2 (final concentration about 870 nM) were added separately or together to each 2 mL of nanoprobe solution, with stirring, to achieve instant homogeneity. The change of the DCFDA fluorescence for each case was monitored in a fluorometer, with 505 nm excitation wavelength and 523 nm emission wavelength, for 5 minutes after addition of HRP or H_2O_2.

- Superoxide anion radical (O_2^-) interference: Superoxide (O_2^-) was generated chemically using ionization of potassium superoxide (KO_2) in aqueous solution. 7 mg of KO_2 was dissolved in 10 mL of DMSO containing 60 mg of 18-crown-6-ether, helping solubilization of KO_2 in DMSO. 50 μL of the KO_2 solution was mixed into 2 mL of DCFDA Ormosil PEBBLE nanoprobe solution and the change of DCFDA fluorescence was monitored for 5 minutes. As a control, 0.01 mg/mL DCFDA free dye aqueous solution, dissolved in DMSO first and diluted in buffer, was examined in same way.

- Peroxynitrite ($ONOO^-$) interference: the interference by peroxynitrite ($ONOO^-$) was tested by mixing commercially available $ONOO^-$ solution with DCFDA loaded Ormosil nanoprobe or DCFDA free dye solution. 35 mM $ONOO^-$ was stocked in strong basic solution (0.3 M NaOH) for stabililzation under -80 ℃ until future use. The $ONOO^-$ stock solution was diluted 100 folds in 0.3 M NaOH solution, kept in dry ice and melted for use immediately before the experiment. 20 μL of $ONOO^-$ solution was added to 2 mL of 0.1 mg/mL DCFDA Ormosil PEBBLE nanoprobe solution and 0.01 mg/mL DCFDA free dye solution and the fluorescence was monitored with a fluorometer with 505 nm

excitation / 523 nm emission for 5 minutes. Because of the dye's pH sensitivity, the same experiments were repeated with pure 0.3 M NaOH to confirm whether the observed responses were from $ONOO^-$ and not from basic pH.

- Nitric oxide (NO·) interference: Nitric oxide solution was prepared by dissolving NO· gas into deionized water by purging the nitric oxide gas in water for sufficient time (longer than 30 minutes). Because of the impurity of the NO· gas, preparation of this stock solution in water can easily form NO_2 and HNO_3 with oxygen and water as well as NO·, acidifying the environment, which can kill the sensitivity of DCFDA. In order to remove the acidic impurities, the NO· gas was collected after passing through 2 liquid containers filled with 50 mM NaOH and water, with gas-tight sealing, following a described method [21]. The final stock solution was around pH 6 and the concentration of dissolved NO· was about 2 mM, assuming saturation [22,23]. 20 µL NO· stock solution was added to 0.1 mg/mL DCFDA Ormosil PEBBLE nanoprobe solution or DCFDA free dye solution in a gas-tight quartz cuvette, after 20-30 minutes argon purging so as to minimize dissolved oxygen which can form further impurities and acidic conditions. The fluorescence emission change was monitored in a fluorometer, with 505 nm excitation and 523 nm emission, for 5 minutes.

Labeling with second fluorescent dye for in vitro H_2O_2 detection

A second fluorescence dye was covalently conjugated to the DCFDA loaded nanoprobes in order to visualize the location of the nanoprobes in the cells and to estimate how many nanoprobes were uptaken by the cells, because the DCFDA

nanoprobes do not have an optical signature before oxidization. Alexa 568 succinimidyl ester (SE) was chosen for this purpose because of its brightness, good photostability, insensitivity towards ROS, and its well separated excitation/emission wavelength from that of DCFDA. An aliquot of 0.1 mg/mL Alexa 568 SE dissolved in DMSO was mixed into an aliquot of 10 mL of 1 mg/mL blank Ormosil nanoparticles with primary amine groups on the surface dispersed in a buffer solution. The reaction was run with stirring for 2 hours and the product was filtered several times by an Amicon filtration system, so as to remove unbound Alexa dye molecules. The DCFDA dye was post-loaded into the Alexa dye and TAT peptide conjugated (the next paragraph) nanoparticles.

TAT peptide conjugation for cytosolic delivery

TAT is a HIV derived peptide capable of delivering external cargoes into cells, eventually into or close to the nucleus. Because of the pH dependency of DCFDA, PEBBLE nanoprobes need to be delivered directly into the cytosolic area, bypassing engulfment into endosomes by phagocytosis, which is associated with acidification [24]. In parallel with Alexa 568 SE conjugation, the TAT peptide was covalently bonded to the amine functionalized Ormosil nanoparticle surface. A heterobifunctional crosslinker, sulfo-succinimidyl 4-[*N*-maleimidomethyl] cyclohexane-1-carboxylate (sulfo-SMCC, one side amine reactive, and the other side thiol reactive), was conjugated to the nanoparticle surface together with Alexa dye. After filtration to remove unbound Alexa dye and sulfo-SMCC, cysteine capped TAT peptide was mixed into the product solution and this 2nd conjugation reaction was run, with stirring, overnight. The final product was

recovered after sufficient filtrations with an Amicon filter. Then the DCFDA dye was post-loaded into the functionalized nanoparticles, as described previously.

Cell culture and *in vitro* H_2O_2 detection

RAW264.7 murine macrophage cells were cultured in advanced-Dulbecco's modified Eagle's medium (A-DMEM) containing Glutamax (1 %), Penicillin-Streptomycin-Neomycin (PSN) (0.2 %), and heat-shocked Fetal Bobine Serum (FBS) (2 %). For the experiment, the cells were plated on 2 well chamber slides (Nunc Lab-Tek™) one day in advance. DCFDA loaded nanoprobes were added into the cell wells and incubated overnight to allow sufficient cellular uptake. Then the cell chambers were rinsed vigorously with fresh media several times so as to remove free nanoprobes from the system. The H_2O_2 generation from the macrophage cells was triggered by addition of a macrophage stimulating agent, 5 μg of *N*-formyl-Methiony-*L*-Leucyl-*L*-Phenylalanine (fMLP). The change in the DCFDA Ormosil PEBBLE nanoprobes' fluorescence was monitored for 6 hours, with 1 hour intervals, after the stimulation. In order to make sure that the response was truly induced by H_2O_2, a control experiments were achieved without stimulation by fMLP addition. Also, another control experiment with PEBBLE nanoprobes, without TAT-conjugation but with fMLP stimulation, was performed so as to examine the effect of nanoprobe localization in the phagosomes or cytosol.

Results and Discussion

Preparation of DCFDA post-loaded Ormosil PEBBLE nanoprobes

In the beginning, we have attempted to encapsulate DCFDA dye in various PEBBLE matrices. However, the simple process of encapsulation during nanoparticle synthesis caused problems. For example, Ormosil synthesis is based on a large pH swing from strong acidic conditions to strong basic conditions which happens instantly, activating and completing the oxidation of the DCFDA dye to its final oxidized form. Another matrix type, polyacrylamide (PAA) is synthesized by radical polymerization, which can also affect negatively the DCFDA. Therefore, a new method to load DCFDA into the nanoparticle matrix, which does not change the chemical structure of this dye, was necessary. The post-loading of dye into preformed nanoparticles was introduced as a solution for solving the difficulty in DCFDA dye loading. The post-loading technique basically relies on the dye's solubility in an organic-aqueous solvent, that is, a hydrophobic dye is loaded into a relatively hydrophobic but water-suspendable particle matrix, in an aqueous solvent. Because of its relative hydrophobicity the Ormosil matrix was an obvious choice for the post-loading technique. Of the diverse set of ROS sensitive molecular probes, DCFDA and dihydrorhodamine 123 (DHR) were known to be lipophilic and have been widely used for ROS detection. DCFDA was finally chosen because it showed better sensitivity towards H_2O_2 than DHR did.

Blank Ormosil nanoparticles nearly monodispersed, about 100 nm in diameter, were obtained from the described synthesis method. The DCFDA dye was doped into the Ormosil nanoparticles by post-loading (figure 3.2). The non-activated hydrophobic form

of the dye was suspended in chloroform, together with the relatively hydrophobic Ormosil nanoparticles. When this chloroform suspension was mixed with an excess amount of water, the dye and the nanoparticle matrix are localized together in the chloroform droplets dispersed in the aqueous environment. Then thechloroform was quickly evaporated by ultrasonication, leaving the dye trapped in the ormosil matrix. The principle of this post-loading method is described in a diagram below (figure 3.3). This encapsulation method was previously devised by Tyner in our group [25], based on the conventional solvent displacement method [26], which utilizes the solubility difference in the organic/aqueous mixture and was applied for our purpose with minor modifications.

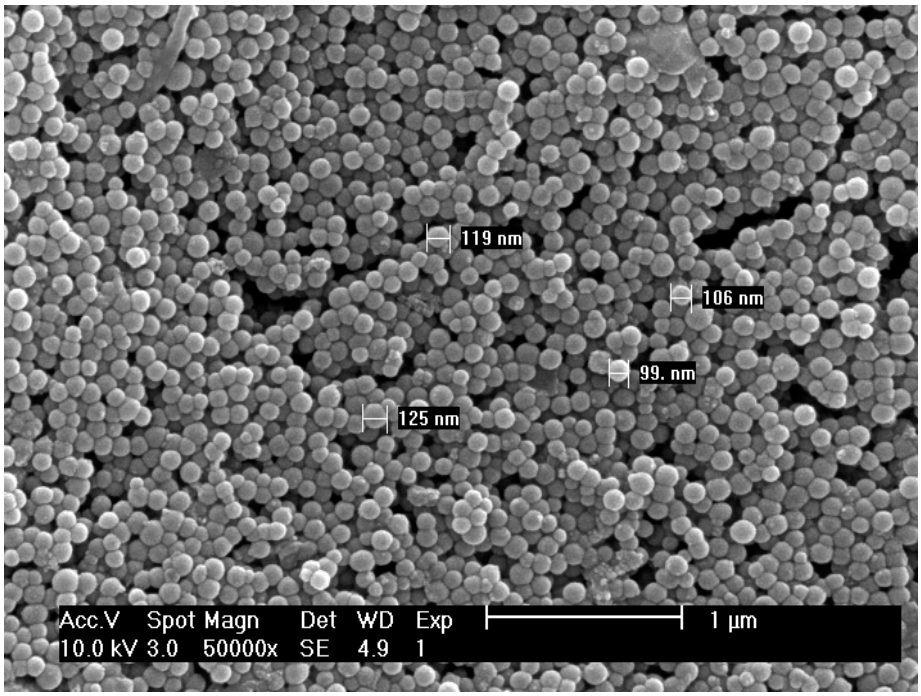

<Figure 3.2: SEM image of DCFDA loaded Ormosil nanoprobes. SEM imaging was performed with DCFDA post-loaded PEBBLE nanoprobes in XL 30 FEG SEM device after 50 seconds gold sputter coating on the sample surface>

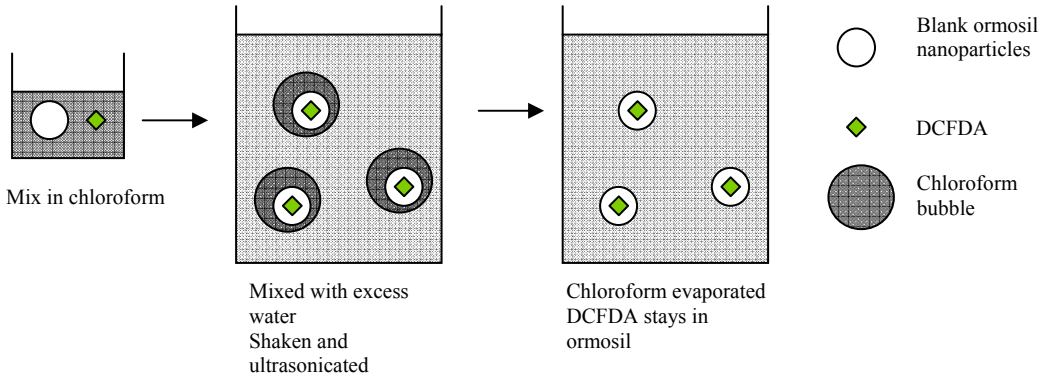

<Figure 3.3: Schematic description of the post-loading method based on the modified solvent displacement method, using pre-formed Ormosil nanoparticles. Hydrophobic Ormosil blank nanoparticles and DCFDA dye were suspended together in a volatile organic solvent, chloroform. The suspension was mixed into aqueous media immiscible with chloroform, forming an oil-in-water type emulsion. The DCFDA loaded Ormosil PEBBLEs were resulted by evaporating chloroform under stirring and ultrasonication>

H_2O_2 response

This encapsulation by post loading relies on the discovery that the hydrophobic form of the dye maintaining the diacetate group, DCFDA, can be used for H_2O_2 detection without any activation process, on which most other methods for H_2O_2 detection using this dye were based, though this form might not be as sensitive as the activated DCFH form. In order to prove that PEBBLE nanoprobes containing the DCFDA dye maintained H_2O_2 sensitivity, the fluorescence change by H_2O_2 addition was examined at various concentrations of H_2O_2. The DCFDA Ormosil PEBBLE nanoprobes showed a linear increase in fluorescence emission over time, by the simple addition of H_2O_2 shown in Figure 3.4. The rate of increase was proportional to the concentration of H_2O_2 in a dose dependent manner. The nanoprobes were able to detect H_2O_2 in the concentration range of 8.7 uM to 87 nM, but exhibited a nearly negligible difference from the control, made

by addition of water instead of H_2O_2, from 8.7 nM concentration or lower, implying that the best possible detection limit of this nanoprobe is around 10s of nM.

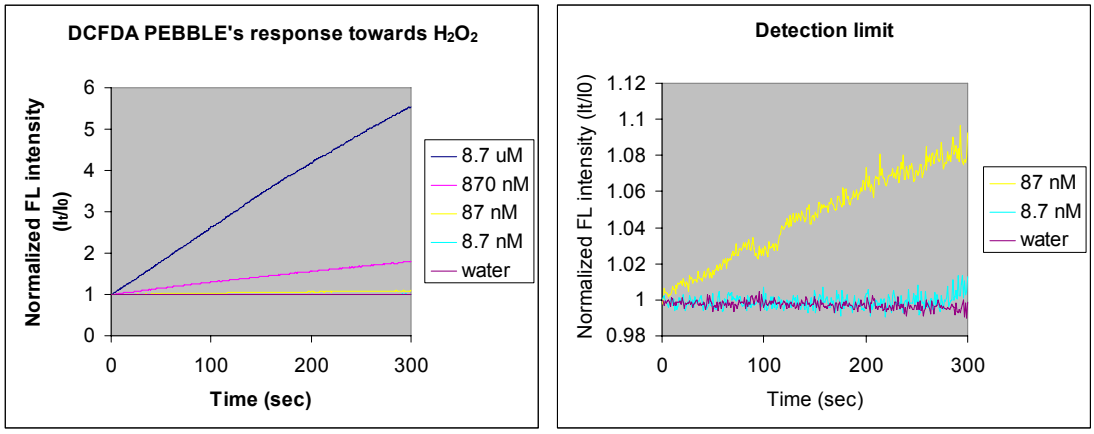

a) b)

<Figure 3.4: Time resolved acquisition of fluorescence increase of DCFDA Ormosil PEBBLE nanoprobes induced from oxidization by H_2O_2 with various concentrations in PBS buffer (pH 7) (a). The fluorescence of DCFDA Ormosil PEBBLE nanoprobes were monitored at 523 nm emission wavelength with 505 nm excitation for 5 minutes after addition of H_2O_2. The PEBBLE nanoprobes showed nearly linear increase of fluorescence intensity for 5 minutes in concentration dependent manner (proportionally). In 8.7 nM H2O2, the PEBBLE nanoprobes showed only negligible difference in response from control measurement with addition of water instead H_2O_2 solution, indicating detection limit of low 10s of nM (b). All results were normalized as I_t (fluorescence intensity at time t) / I_0 (initial fluorescence intensity) to adjust starting intensity to be same.>

Dye leaching

It was required to test if the response of this DCFDA loaded Ormosil nanoprobe towards H_2O_2 was induced from the dye located inside of the particles or from the dye leached out of the particles. In order to examine dye leaching, the nanoprobe solution was filtered and the response towards H_2O_2 of the nanoprobe solution and filtrate solution was measured. As shown in figure 3.5, the PEBBLE nanoprobe solution showed a strong

increase in fluorescence emission at 523 nm, but the filtrate solution did not show any such increase. This clearly supported the conclusion that the reaction between the DCFDA dye and H_2O_2 occurs only inside the nanoprobes and also validated the feasibility of taking advantage of the PEBBLE matrix, so as to improve the H_2O_2 selectivity, compared to that of naked molecular probes.

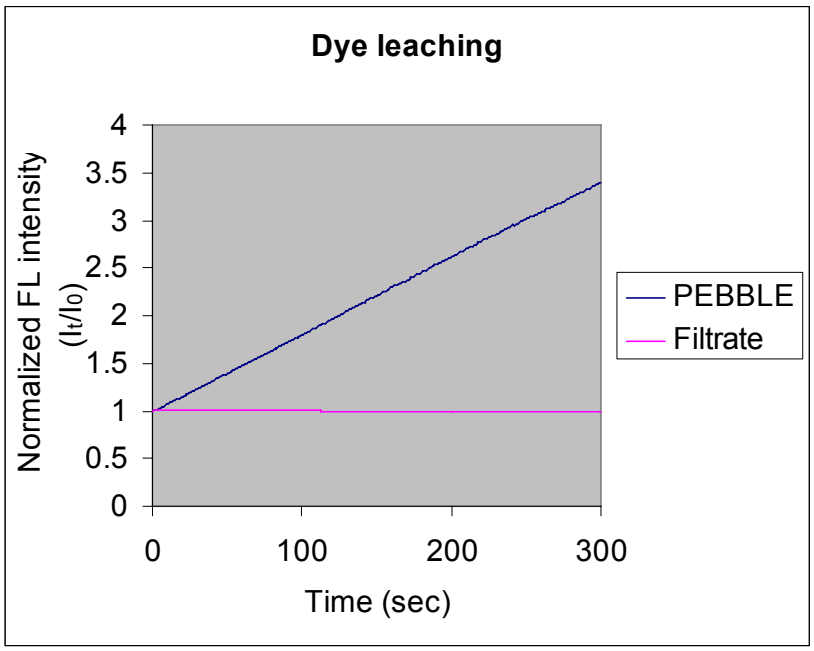

<Figure 3.5: Comparison of fluorescence emission increase induced by H_2O_2 addition between DCFDA Ormosil PEBBLE nanoprobes in PBS buffer (pH 7.4) and the filtrate solution from the nanoprobes to examine dye leaching effect. While PEBBLE solution showed rapid increase of fluorescence, the filtrate did not exhibit any notable response by addition of same amount of H_2O_2, proving the reaction between DCFDA dye and H_2O_2 only occurred inside of Ormosil matrix.>

Resistance of DCFDA Ormosil PEBBLE nanoprobes against interference from enzymes and other ROS

Many ROS sensitive molecular probes, including DCFDA, share problems such as poor selectivity and a trend for autoxidation. Further complications need to be taken

into account for measurements under physiological conditions, such as membrane permeability of the probes and unwanted enzymatic reactions. DCFDA Ormosil PEBBLE nanoprobes can be a solution to such problems; the evidence is provided below.

- HRP interference: DCFDA's reaction with ROS is often dependent on the activity of HRP. Without HRP the reactivity of DCFDA is slower, and even negligible compared to the response from the activated form, DCFH. Therefore, H_2O_2 detection using DCFDA has been usually performed with activation in the presence of HRP. However, it is well known that HRP can oxidize this dye in the absence of H_2O_2 [15-18]. Although this effect might not be a significant drawback for H_2O_2 detection when compared to the benefit from using HRP, HRP certainly makes differentiation of H_2O_2 from interferences more difficult, and thus can cause errors in the quantification of H_2O_2. We hypothesized that encapsulation of the dye into nanoparticles might reduce the interference from HRP, by blocking the contact between HRP and the dye molecules, because the size of HRP is too big for entering into the nanoparticle matrix. Figure 3.6 shows supporting results for this size based exclusion.

When only HRP was added to the PEBBLE nanoprobe solution, it did not show any increase of fluorescence intensity, indicating that no oxidization occurred. It clearly proved that the nanoparticle matrix can effectively block the internalization of enzymes, due to their size. On the other hand, when HRP and H_2O_2 were added together, the increase of fluorescence intensity was considerably faster than when only H_2O_2 was added. This means that HRP can still accelerate the reaction of DCFDA with H_2O_2 (by unclear mechanism) without interfering with the response towards H_2O_2. Because this

effect happened without influencing the reaction between DCFDA and H_2O_2, it can be a clue for the future direction of this research to improve this nanoprobe's sensitivity.

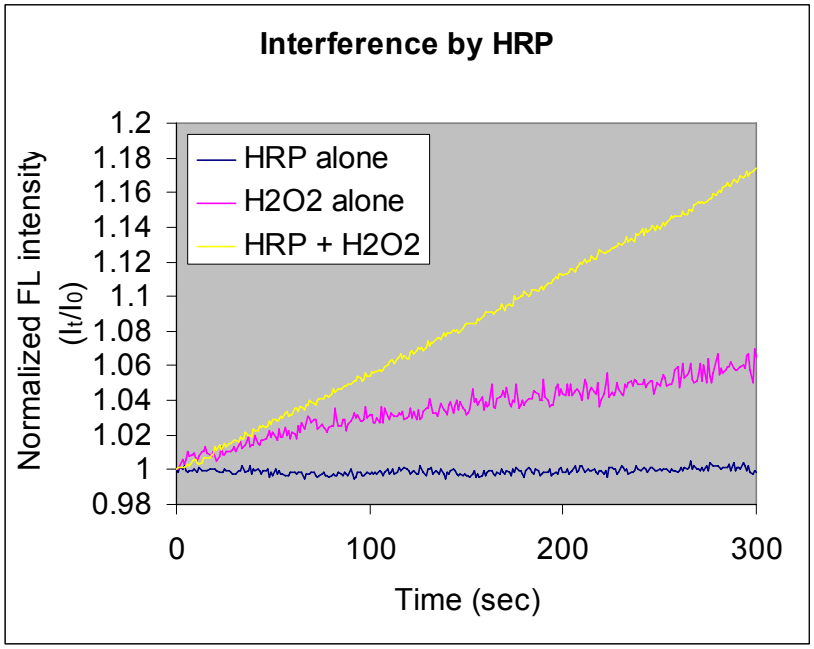

<Figure 3.6: Examination of interference by HRP: The fluorescence intensity change was monitored to test the interference from HRP when HRP, H_2O_2, or H_2O_2+HRP was added to DCFDA Ormosil PEBBLE nanoprobes suspension in PBS buffer (pH 7.4). HRP alone did not cause any change in DCFDA Ormosil PEBBLE nanoprobes' fluorescence while H_2O_2 alone and H_2O_2+HRP showed noticeable changes, indicating that HRP interference was effectively excluded by encapsulation in PEBBLEs.>

This result also indicates that possible interferences from other enzymes can be excluded as well. For example, the PEBBLE nanoprobes would be free from unwanted activation of DCFDA dye by intracellular esterase activity, which occurs in *in vitro* measurements when using DCFDA free dye and would induce dye leaching out of PEBBLE matrix. It validates one more time our premise for improvement of H_2O_2

selectivity, which is that the nanoparticle matrix functions as a screening device for the unstable ROS.

- Supereoxide (O_2^-) interference: DCFDA was known to be less sensitive towards superoxide than for other reactive oxygen species [27]. However, our experiment was based on the non-activated form of DCFDA dye, for which the reactivity towards H_2O_2 can be lower than that of the activated form (DCFH). Therefore, slight interference from superoxide cannot be neglected.

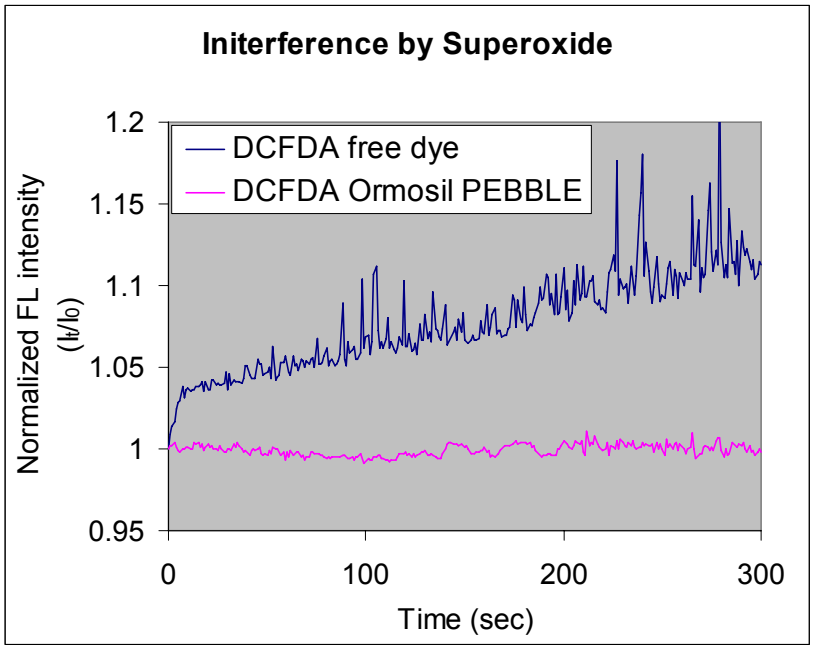

<Figure 3.7: Examination of interference by superoxide anion radical ($O2^-$) towards DCFDA free dye and DCFDA Ormosil PEBBLE nanoprobes: $O2^-$ was produced by mixing potassium superoxide (KO_2) with aqueous media (PBS buffer) containing DCFDA free dye and DCFDA Ormosil PEBBLE nanoprobes based on ionization of KO2. While DCFDA free dye showed certain increase of fluorescence intensity by addition of $O2^-$, DCFDA Ormosil PEBBLE nanoprobes only showed constant fluorescence intensity under same condition, indicating that PEBBLE nanoprobes can have resistance to the interference by $O2^-$.>

In the results (figure 3.7), DCFDA free dye showed a fast increase of fluorescence intensity at the early several seconds period, and then a gradual linear increase for the rest of the time in our measurement span. In contrast, DCFDA Ormosil PEBBLE nanoprobes did not show any time increase of emission intensity with potassium superoxide. This result shows that DCFDA Ormosil PEBBLE nanoparticles can effectively exclude any influence from superoxide interference. Superoxide is an anionic free radical and should be considered rather more hydrophilic than lipophilic. The hydrophobic matrix of the Ormosil nanoparticle might exert a repulsive effect towards the superoxide, thus resulting in insensitivity towards it.

- Peroxynitrite ($ONOO^-$) interference: According to Setsukinai's works [27], DCFDA is much more sensitive towards $ONOO^-$ than towards H_2O_2, even without acceleration by HRP. Also, $ONOO^-$ can be produced in the presence of H_2O_2 by reacting with NO_2^-, and the generation by macrophages of $ONOO^-$ in relatively high concentrations has been reported before [28,29]. Therefore, to selectively evaluate H_2O_2 generation from macrophages, the PEBBLE nanoprobes must be able to exclude the interference from $ONOO^-$. Our test results are displayed in figure 3.8. The DCFDA Ormosil PEBBLE nanoprobes showed only a slight increase of fluorescence emission due to an addition of 3.5 μM $ONOO^-$. A control measurement, by an addition of pure 0.3 M NaOH solution, supported the notion that this slight increase was entirely due to the addition of base, as there was no notable difference from the result obtained from the $ONOO^-$ solution. On the other hand, DCFDA free dye showed an immediate and significant jump of fluorescence intensity upon addition of $ONOO^-$. The increasing rate slowed down soon,

but a consistent linear increase was still observed for a long time. As done with the PEBBLE nanoprobe, 0.3 M NaOH solution was added as a control: the DCFDA free dye still showed only a slight increase, thus indicating that the notable increase of fluorescence intensity was truly from the oxidation by $ONOO^-$. This result clearly shows that DCFDA Ormosil PEBBLE nanoprobes can effectively exclude the interference from even $ONOO^-$, which could be the most severe source of interference in measurements H_2O_2.

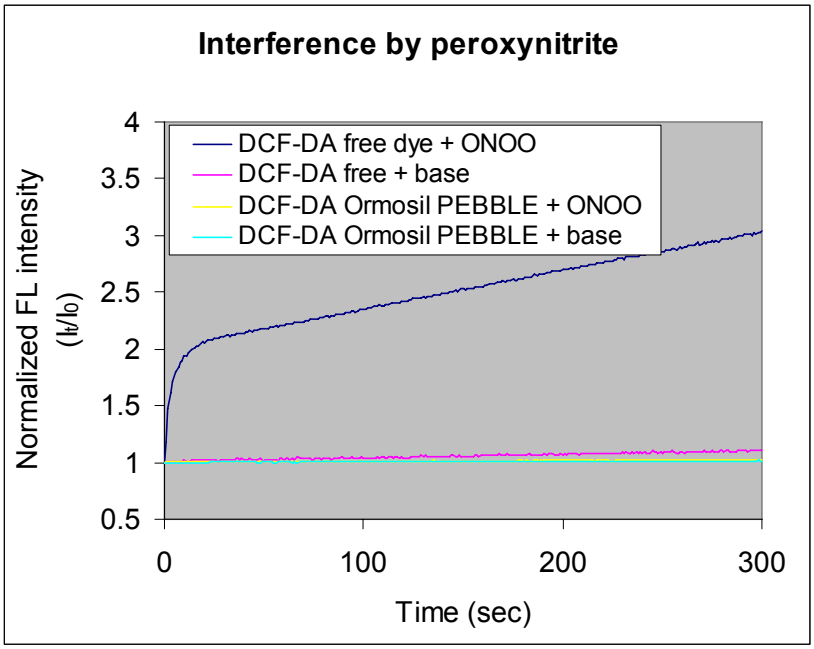

<Figure 3.8: Examination of peroxynitrite ($ONOO^-$) interference with use of DCFDA free dye and of DCFDA loaded Ormosil nanoprobes. The fluorescence change of DCFDA free dye in PBS buffer and DCFDA Ormosil PEBBLE nanoprobes in PBS buffer were monitored after addition of $ONOO^-$ for 5 minutes. DCFDA Ormosil PEBBLE showed slight increase by reaction with $ONOO^-$ but DCFDA free dye showed rapid and significantly higher increase than PEBBLE nanoprobes, indicating PEBBLE can effectively exclude the interference by $ONOO^-$. Because of the strong basic pH of the $ONOO^-$ stock solution which can interfere the response of DCFDA as well, control measurements were performed for DCFDA free dye and PEBBLE nanoprobes, using just a pure basic solution and these measurements showed that the rapid increase observed from DCFDA free dye was truly by $ONOO^-$ and the slight increase observed from DCFDA Ormosil PEBBLE nanoprobes was induced by basic pH.>

- Nitric oxide (NO·) interference: Setsukinai's work also showed that the sensitivity of DCFDA can be similar towards nitric oxide as towards H_2O_2. Thus the interference by nitric oxide needs to be evaluated. Because procedures involving with the preparation of NO· stock solutions can readily form impurities, especially HNO_3, leading to acidification of the environment, which can effectively kill the DCFDA's fluorescence and reactivity towards ROS, the stock solution was carefully prepared after treating NO· gas with a strong base, with a gas-tight sealing, following methods described in the literature [21]. The pH of the final stock solution was about 6, which is a pH still allowing sensitivity of DCFDA towards H_2O_2.

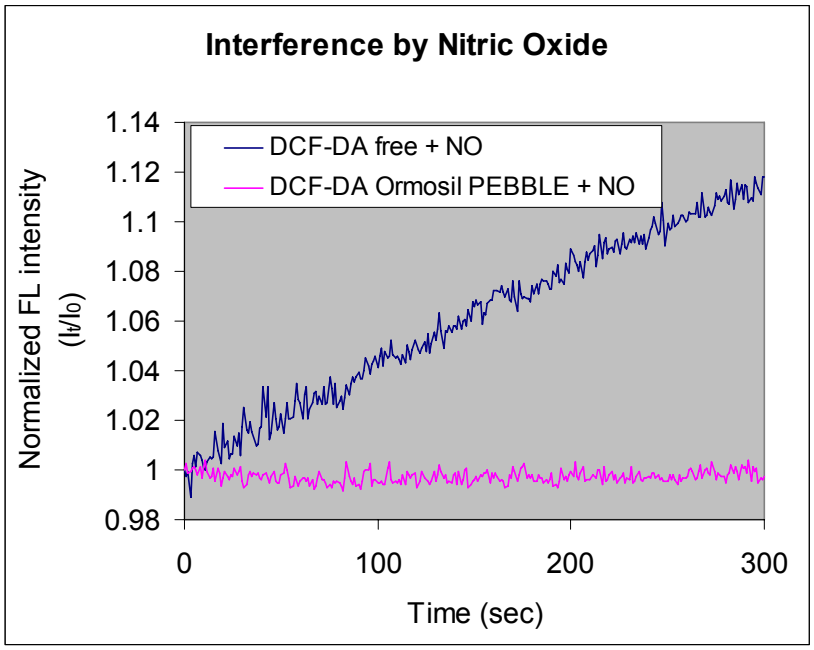

<Figure 3.9: Examination of nitric oxide (NO) interference with use of DCFDA free dye and of DCFDA Ormosil PEBBLE nanoprobes. NO stock solution with pH 6 was prepared by dissolving NO gas in DI water and the stock solution was mixed with DCFDA free dye in PBS buffer (pH 7.4) and DCFDA Ormosil PEBBLE nanoprobes in PBS buffer (pH 7.4) under gas-tight sealing. While DCFDA free dye displayed certain increase, the PEBBLE nanoprobes showed constant fluorescence intensity by addition of NO solution, indicating effective exclusion of interference by NO.>

The DCFDA Ormosil PEBBLE nanoprobes showed no noticeable increase in fluorescence intensity until the end of measurement, meaning that no fluorescence generation occurred by reaction with NO·. While the PEBBLE nanoprobes did not show any noticeable response towards NO·, DCFDA free dye showed a significant increase in fluorescence emission under identical conditions. This certainly indicated that DCFDA free dye can responsd towards NO· by forming a fluorescent product. In conclusion, DCFDA Ormosil PEBBLE nanoprobes also resist interference by NO·.

In spite of the many expected advantages of PEBBLEs over conventional molecular probes [30,31], our discovery that the non-specific ROS probe, DCFDA can be made to be H_2O_2 selective, simply by encapsulating it inside Ormosil nanoparticles, may still be surprising. This outcome is due to a synergistic effect, coming from a mutual complementarity of properties regarding the ROS and the Ormosil nanoparticles, based on analyte exclusion due to either lifetime, size, or hydrophobicity.

As mentioned above, our idea to improve H_2O_2 selectivity using PEBBLEs was inspired by two findings: 1) The nanoparticle matrix can favor the detection of more stable ROS; 2) DCFDA is still sensitive towards H_2O_2, even without activation. As discussed by King [13,14], hydroxyl radicals, the most unstable ROS with ns or shorter lifetime *in vivo* [32], could be detected by PEBBLEs only by locating the probe molecule on the surface of the nanoparticles, by a conjugation technique. It indicates that the nanoparticle matrix functions as a screening device based on 'lifetime exclusion'. Thus the encapsulation in the nanoparticle matrix favors the detection of longer lived ROS, such as H_2O_2 (lifetime of 1 sec or longer) and NO (100's of msec to 2 sec), while inhibiting the detection of all other ROS with shorter lifetime.

Also, as shown in the HRP interference section, the encapsulation by a nanoparticle matrix can effectively protect the probe molecule inside it, based on 'size exclusion' from possible attack by various biological agents of larger size. It helps to set the DCFDA dye free from one of its serious problems, HRP interference, which becomes quite advantageous for the quantitative evaluation of DCFDA's response to hydrogen peroxide. This is indeed explained by the fact that HRP cannot reach the DCFDA dye molecules by penetration through the matrix of the Ormosil nanoparticles, because of its large size.

Our results show that interferences by O_2^-, NO·, and $ONOO^-$ can all be excluded by loading the DCFDA into the Ormosil PEBBLE nanoprobes. These ROS are relatively stable, with lifetimes of miliseconds to seconds. Neither exclusion by lifetime nor by size can explain why they could not be detected by the DCFDA Ormosil PEBBLE nanoprobes, considering that we already have shown that singlet oxygen, with a lifetime of about 2 microseconds or shorter, can be successfully detected using Ormosil PEBBLE nanoprobes, as shown in chapter 2. Thus a possible characteristic we need to consider here is the hydrophobicity of the Ormosil matrix. As mentioned before, the organic portion of this matrix can make it relatively hydrophobic, even though it can be still suspended in aqueous media. This hydrophobic property can offer a more favorable environment for lipophilic ROS, such as H_2O_2 and $^1O_2$. *Vice versa*, it might mean that the Ormosil matrix can indeed have a repulsive effect towards polar ROS, such as ·OH (anionic radical), O_2^- (anion), $ONOO^-$ (also anion), and NO· (anionic radical). When this 'hydrophobic filter' and the lifetime based exclusion principle are combined, it can explain how singlet oxygen could be detected with Ormosil based nanoprobes while

superoxide could not be detected under similar conditions. In conclusion, we hypothesize that the improved H_2O_2 selectivity of DCFDA Ormosil PEBBLE nanoprobes is a consequence of the combination of **three** different exclusion principles: Size, lifetime and hydrophobicity.

In vitro H_2O_2 detection in stimulated macrophages

Macrophage is a well known phagocyte, capable of generating various ROS in an oxidative burst, in order to kill suspect foreign bodies. The oxidative burst from the macrophage can be chemotactically triggered by administering macrophage stimulants, for example, Phorbolmyristateacetate (PMA) [33], fMLP [34], Lipopolysaccharide (LPS) or gamma interferon [35]. The generation of various ROS, including H_2O_2, $ONOO^-$, O_2^- and ·OH, by macrophage has been reported [1,2,3,28,29]. The RAW 264.7 murine macrophage cell line was chosen for our experiments. DCFDA Ormosil PEBBLE nanoprobes were further functionalized by covalently attaching a secondary fluorophore, Alexa 568, for visualization of PEBBLEs, and TAT-peptide for assisted endocytosis, thus avoiding the effects of acidification accompanying macrophage phagocytosis.

After an overnight incubation with DCFDA loaded nanoprobes, with/without TAT-peptide conjugation for cytosolic delivery, the free PEBBLE nanoprobes were removed by repeated rinsing with fresh cell media. Then, the macrophage stimulating agent, fMLP was added so as to trigger an oxidative burst. Two control experiments were performed in parallel: 1) using the same TAT-conjugated PEBBLE nanoprobes but with addition of water instead of fMLP, so as to confirm whether the response was induced by an oxidative burst; 2) using PEBBLE nanoprobes without TAT peptide conjugation but

with addition of fMLP, so as to confirm whether the response was generated from the cytosolic area and not from inside of phagosomes. Virgin macrophage cells, without incubation with any PEBBLE nanoprobes, were used as a background signal.

The TAT conjugated nanoprobes showed emission maxima at 539 nm, due to DCFDA, and a weak shoulder at 595 nm due to the Alexa 568 label, for both response and control. The wavelength shift of the DCFDA's emission maxima, from the 523 nm peaks in non-biological measurements to 539 nm here, was caused by the difference in the optics between the fluorometer and fluorescence microscope. The PEBBLE nanoprobes without TAT conjugation showed a similar spectral characteristics at 539 nm due to DCFDA, but another peak at 595 nm due to the Alexa 568 label was stronger than for the PEBBLE nanoprobes with TAT, reflecting that the Alexa 568 dye was labeled more efficiently for the non-targeted nanoparticles than for the TAT conjugated ones. The DCFDA fluorescence emission change, over 6 hours monitoring, is plotted in figure 3.10.

Although DCFDA should not fluoresce before oxidization, each sample actually exhibited weak initial fluorescence of a slightly different intensity, which probably was due to the auto-oxidation of DCFDA during the overnight incubation. The difference in initial intensity can be simply explained by the difference in the number of cells containing nanoprobes in the monitored area of the microscope. So, all the data was normalized by adjusting the initial intensity to zero.

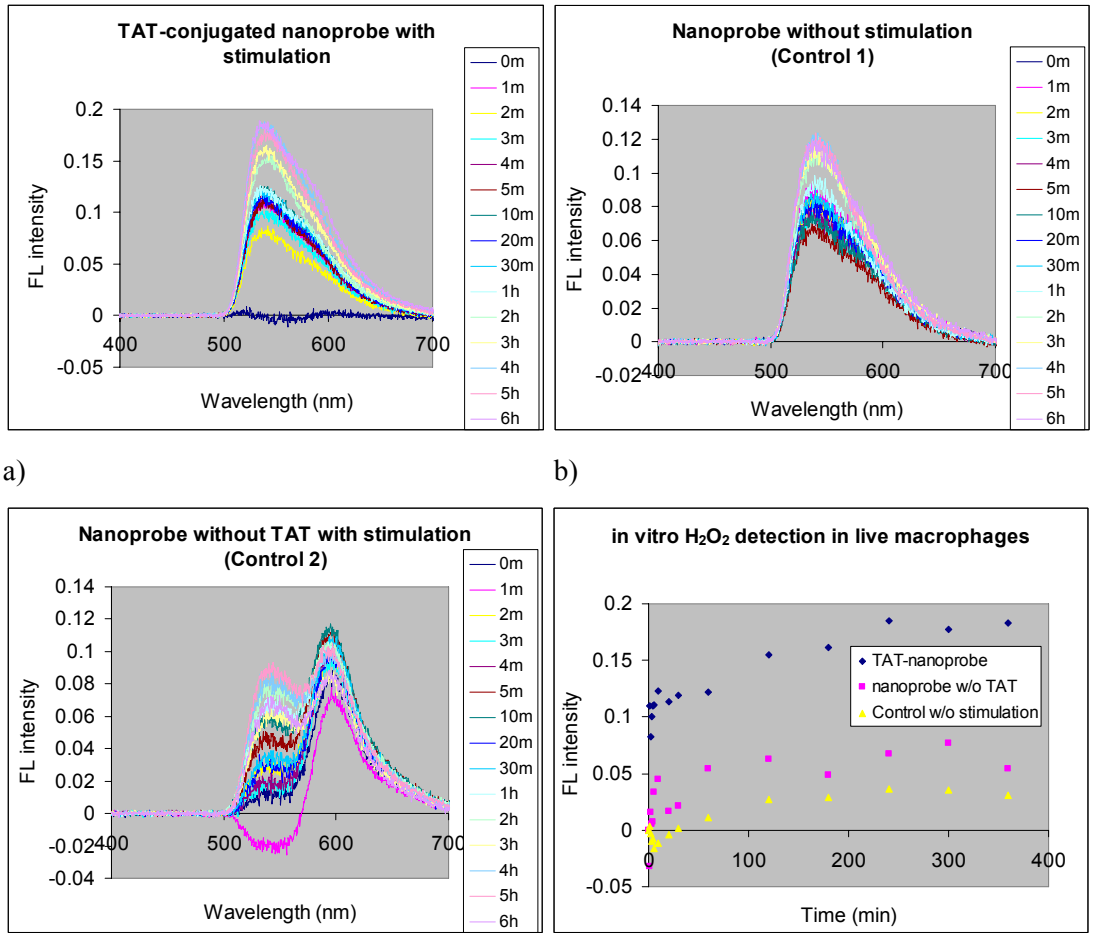

a) b)

c) d)

<Figure 3.10: *In vitro* H_2O_2 detection in fMLP stimulated live macrophages. DCFDA Ormosil PEBBLE nanoprobes were incubated with macrophage cells for an overnight and washed away. The oxidative burst from macrophages was triggered by addition of stimulating agent, fMLP, and the fluorescence intensity of DCFDA PEBBLE nanoprobes were monitored for 6 hours. a) TAT-conjugated DCFDA loaded Ormosil nanoprobes with stimulation, b) TAT-conjugated nanoprobes without stimulation for control (no H_2O_2 generation), c) nanoprobes without TAT-conjugation with stimulation for examine the difference between active cytosolic delivery by TAT and passive uptake by phagocytosis, and d) summarizing plot of fluorescence change of DCFDA for all three cases>

The TAT conjugated nanoprobes with stimulation (blue diamonds) show a fast increase of emission intensity for 1 hour, then the rate of increase slows down until the passage of 4 hours, and stabilization occurs later on. The first control (yellow triangles),

TAT conjugated nanoprobes without stimulation, shows some fluctuations for 1 hour and then a gradual increase of signal intensity for the rest of time. The reason for this fluorescence generation without stimulation can be explained by two possibilities: 1) it could be a response due to natural generation of H_2O_2 by the macrophage, without stimulating reagent, or 2) as explained previously for the initial fluorescence, it could be due to auto-oxidation of the dye over the long time measurement. Either way, this increase obtained for control samples should be subtracted for the estimation of the H_2O_2 quantity. On the other hand, with the second control (pink squares), the PEBBLE nanoprobes without TAT conjugation but with stimulation, show a positive response as well, exhibiting a certain increase of emission intensity over 6 hours. However, the degree of the increase is not as great as that of the TAT-conjugated nanoprobes.

In order to quantify the H_2O_2 detected by the DCFDA loaded Ormosil nanoprobes, a calibration curve for the relation between concentration and fluorescence intensity was constructed under identical conditions to the *in vitro* measurement (in fresh cell media), based on the fluorescent product of this reaction, DCF (2,7-dichlorofluorescein), which is hydrophilic and commercially available. By plotting the increase of the DCFDA nanoprobe's fluorescence emission on this calibration curve, the concentration of DCF formed inside the nanoprobes was estimated. Finally, the concentration of H_2O_2 could be determined assuming a 1:1 stochiometry in the reaction between the H_2O_2 and DCFDA dye molecules. The calibration procedure and the constructed standard curve are displayed in figure 3.11.

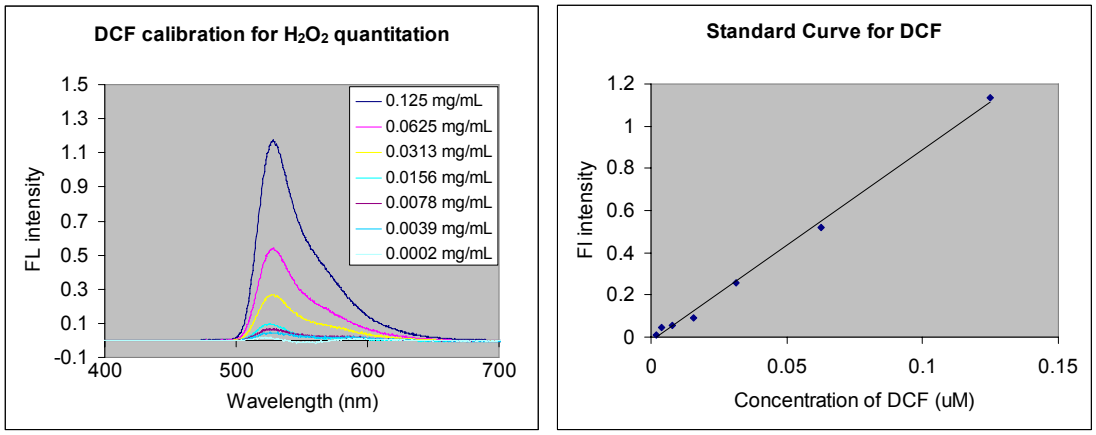

a) b)

<Figure 3.11: Estimation of H_2O_2 production from macrophages. Final product of DCFDA's oxidization, DCF are commercially available compound and the concentration of H_2O_2 was able to be determined by comparing the obtained results from in vitro detection to the standard curve constructed using DCF. a) Fluorescence emission spectra of DCF in various concentrations and b) calibration curve obtained from a)>

The TAT conjugated nanoprobes with stimulation showed an increase of about 0.18 (arbitrary unit) in the intensity while nanoprobes without TAT showed only about an 0.08 increase over 6 hours. Because the first control without stimulation also showed an increase of about 0.03, the net response for stimulated cases should be 0.15 and 0.05 after subtraction, respectively. Considering these intensity changes, the H_2O_2 concentration detected by TAT conjugated nanoprobes with fMLP stimulation was equivalent to 18 nM and that for nanoprobes without TAT was equivalent to 6 nM. This result showed that the DCFDA Ormosil PEBBLE nanoprobes are able to distinguish a low nM difference in H_2O_2 concentration. Because the PEBBLE nanoprobes showed a detection limit in 10s of nM in non-biological systems, the expanded detection limit needs to be explained. We elucidated a possible reason to be the effect of the local concentration of nanoprobes trapped in intracellular space. Unlike bulk conditions, where the PEBBLE nanoprobes are

homogenously distributed in the overall volume, the nanoprobes that were engulfed (or actively delivered by TAT-peptide) by macrophage, were only present inside of the cells after rinsing. Therefore, the local concentration of the PEBBLE nanoprobes in the intracellular space should be much higher than it seems when assuming equivalency to bulk concentration. Also, we examined the effect of the nanoprobe concentration with a fixed concentration of H_2O_2 in non-biological systems and confirmed that a stronger response can be produced with a higher concentration of nanoprobes (figure 3.12) and this trend matches well with the known reaction kinetics of DCFDA, which is known to follow 2nd order, proportionally to the DCFDA concentration and the H_2O_2 concentration [36]. This may explain why the H_2O_2 response could be improved by the local concentration elevation of the PEBBLE nanoprobes in intracellular measurement.

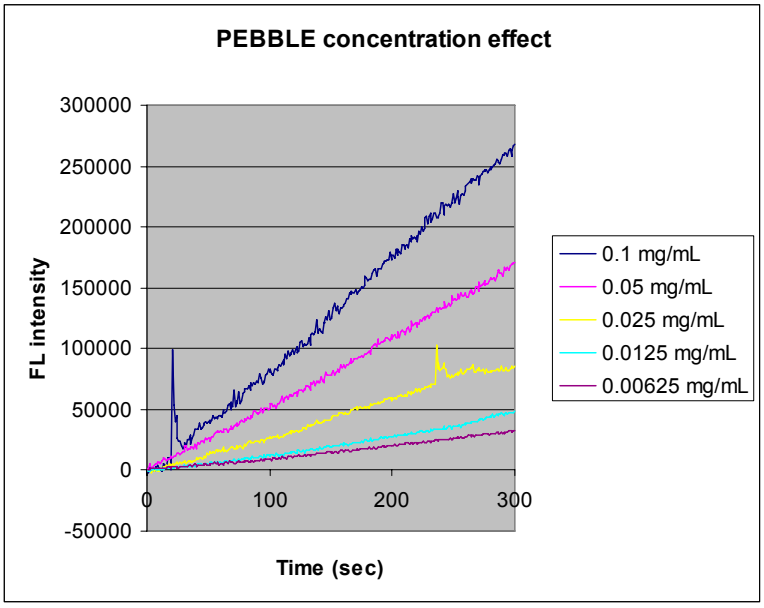

<Figure 3.12: The experimental result showing the relationship between the DCFDA Ormosil PEBBLE nanoprobe concentrations and the H_2O_2 response at a fixed H_2O_2 concentration. The rate of fluorescence of DCFDA Ormosil PEBBLE nanoprobes increased proportionally to the concentration of the PEBBLE nanoprobes.>

Figure 3.13 displays the bright field image and fluorescence image, based on Alexa 568 labeling, obtained from the exact same position monitored for the fluorescence spectra.

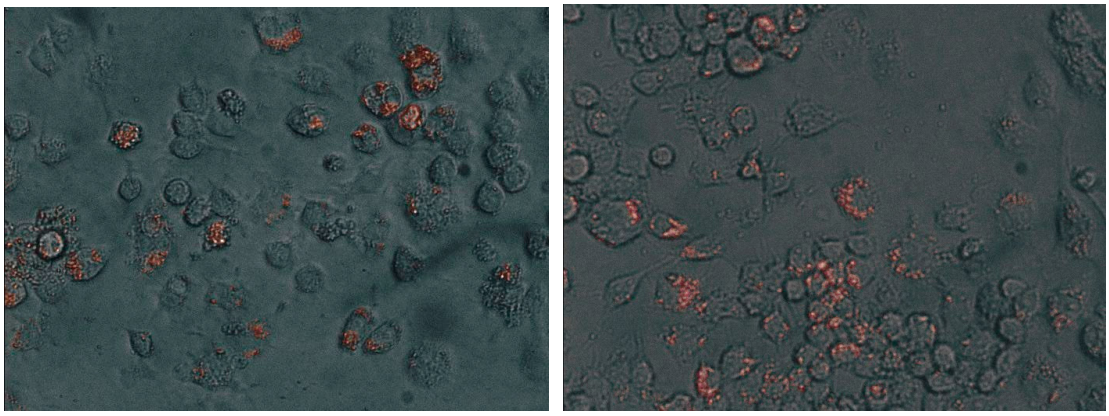

a) b)

<Figure 3.13: Bright field-fluorescence overlay image of DCFDA loaded Ormosil nanoprobes in macrophages after overnight incubation, obtained from Alexa 568 labeling. a) TAT-conjugated nanoprobes and b) nanoprobes without TAT conjugation. The unbound free PEBBLE nanoprobes were washed away by repeated rinsing with fresh cell media. The images were obtained at the same position in which the H_2O_2 detections were performed.>

In addition to the determination of the H_2O_2 quantity, the amount of nanoprobes delivered to macrophage cells in the monitored area was estimated, based on the Alexa 568 label's fluorescence intensity. Using another filter set (standard green filter cube), Alexa 568 fluorescence spectra of DCFDA Ormosil PEBBLEs were measured. Then, two calibration curves were constructed from using the same batches of the PEBBLE nanoprobes (TAT conjugated and without TAT) under conditions identical to *in vitro* measurements except the absence of cells. The results are summarized in figure 3.14.

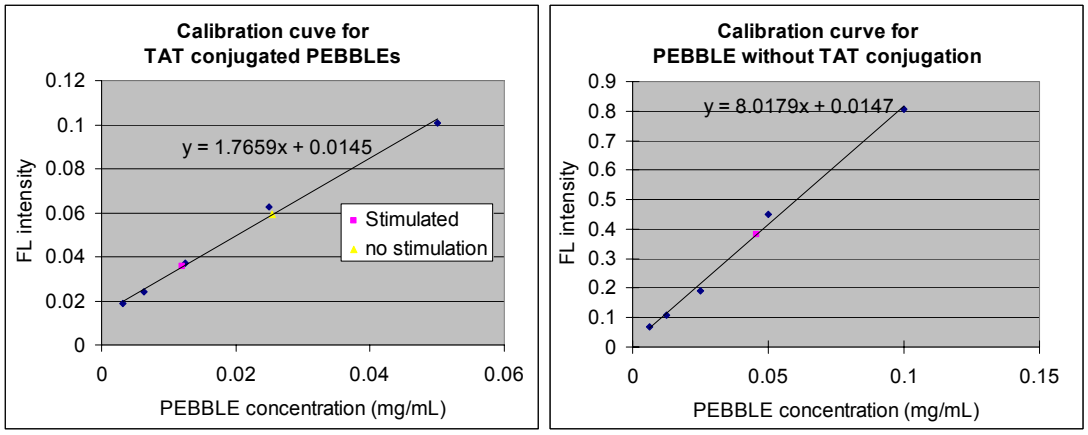

<Figure 3.14: Quantification of DCFDA Ormosil PEBBLE nanoprobes in monitored area using constructed standard curves. 2 calibration curves were constructed using TAT-conjugated PEBBLE nanoprobes (left) and PEBBLE nanoprobes without TAT conjugation (right). The concentration of PEBBLE nanoprobes used in in-vitro detections was fit to the calibration curve for estimation (pink and yellow color dots on the trend line).>

Based on these calibration curves, the concentration of DCFDA Ormosil PEBBLE nanoprobes in the monitored area was equivalent to about 0.012 mg/mL for the TAT conjugated PEBBLE nanoprobes with stimulation, and 0.046 mg/mL for nanoprobes without TAT but with stimulation. It means that macrophage engulfed about 4 times more amount of PEBBLE nanoprobes by phagocytosis than by direct delivery of nanoprobes to cytosolic area by TAT peptide. It should be noted that the measurements were performed in fixed positions and thus the results reflects only local effect occurring. When roughly same cell density of each case was assumed and the locality of results was considered, it could be concluded as the TAT conjugated PEBBLE nanoprobes detected more H_2O_2 (18 nM) with a lesser amount of nanoprobes (0.012 mg/mL) while nanoprobes without TAT detected less H_2O_2 (6 nM) with a more amount of the PEBBLE nanoprobes (0.046 mg/mL) in monitored area. In considering the effect of the PEBBLE nanoprobes concentration as described earlier, we should be able to observe a stronger

H_2O_2 response from nanoprobes when we have more PEBBLE nanoprobes in system. However, our results showed that the PEBBLE nanoprobes displayed less H_2O_2 response though their concentration in system (in monitored area) was higher than that of TAT conjugated PEBBLE nanoprobes, verifying that the sensitivity of PEBBLE nanoprobes was suppressed when they were uptaken by phagocytosis, which is typically associated with acidification.

Acknowledgements

The author would like to thank to Dr. Hao Xu and Sevanne Demirjean in Dr. Philbert's group at the University of Michigan, School of Public Health and Youxhin Zhang in Dr. Joel Swanson's group at the University of Michigan, Department of Microbiology and Immunology for their kind providing and preparing of cancer cell line for the *in vitro* experiments. The author is also grateful to the Electron Microbeam Analyasis Laboratory (EMAL) at the University of Michigan for technical support in imaging. This research was supported by the National Cancer Institute (NCI) contract NO-1-CO-37123 (R. Kopelman) and the Keck foundation contract N004497 (R. Kopelman).

References

1. B. M. Babior, Oxygen-dependent microbial killing by phagocytes, *N. Eng. J. Med.* (1978) v298(12), 659-668
2. R. Oren., M. L. Karnovsky *et al*., Metabolic Patterns in Three Types of Phagocytizing Cells, *J. Cell Biol.* (1963) v17(3), 487-501
3. M. L. Karnovsky, J. Lazdins, and S. Simmons, Metabolism of mononuclear phagocytes at rest and during phagocytosis, in *Mononuclear Phagocytes*, Edited by R. van Furth, Blackwell Scientific Publications (1975)
4. C. F. Nathan and R. K. Root, Hydrogen Peroxide Release from Mouse Peritoneal Macrophages: Dependence on Sequential Activation and Triggering, *J. Exp. Med.* (1977) v146,1648-1662
5. S. G. Rhee, H_2O_2, A Necessary Evil for Cell Signaling, *Science* (2006) v312, 1882-1883
6. R. Finkel, Oxidant Signals and Oxidative Stress, *Current Opinion in Cell Biology*, (2003) v15, 247-254
7. W. Dröge, Free Radicals in Physiological Control of Cell Function, Physiol. Rev. (2002) v82, 47-95
8. R. Colavitti, T. Galeotti et al., Reactive Oxygen Species as Downstream Mediators of Angiogenic Signaling by Vascular Endothelial Growth Factor Receptor-2/KDR, J. Biol. Chem. (2002) v277(2), 3101-3108
9. *Free Radicals in Biology* V 1, Edited by William A. Pryor, Academic Press (1976)
10. Matthew B. Grisham, *Reactive Metabolites of Oxygen and Nitrogen in Biology and Medicine*, R. G. Landes Company (1992)
11. Manfred K. Eberhardt, *Reactive Oxygen Metabolites: Chemistry and Medical Consequences*, CRC Press (2001)
12. Y. Cao, R. Kopelman *et al.*, Ratiometric Singlet Oxygen Nano-optodes and Their Use for Monitoring Photodynamic Therapy Nanoplatforms. *Photochem. Photobiol.* (2005) v81(6), 1489-1498
13. M. King, Development of Ratiometric Nanoprobes and Nanosensors for the Detection of the Hydroxyl Radical, Hydrogen Peroxide and Superoxide, Dissertation Thesis, University of Michigan, Department of Chemistry, 2005
14. M. King and R. Kopelman, Development of a Hydroxyl Radical Ratiometric Nanoprobe, Sens. Act. B, (2003) v90, 76-81
15. A. S. Kenston and R. Brandt, The Fluorometric Analysis of Ultramicro Quantities of Hydrogen Peroxide, Anal Biochem. (1965) v11(1), 1-5
16. C. P. LeBel, H. Ischiropoulos, and S. C. Bondy, Evaluation of the Probe 2',7'-Dichlorifluorescein as an Indicator of Reactive Oxygen Species Formation and Oxidative Stress, *Chem. Res. Toxicol.* (1992) v5, 227-231

17. A. Keller, R. P. Brandes et al., Analysis of Dichlorodihydrofluorescein and Dihydrocalcein as Probes for the Detection of Intracellular Reactive Oxygen Species, *Free Rad. Res.* (2004) v38(12), 1257-1267

18. M. Afri, A. A. Frimer, and Y. Cohen, Active Oxygen Chemistry within the Liposomal Bilayer Part IV: Locating 2',7'-Dichlorofluorescein (DCF), 2',7'-Dichlorodihydrofluorescein (DCFH) and 2',7'-dichlorodihydrofluorescein diacetate (DCFH-DA) in the Lipid Bilayer, *Chem. Phys. Lipids* (2004) v131, 123-133

19. H. J. Hah, S. M. Koo *et al.*, Simple preparation of monodisperse hollow silica particles without using templates. *Chem. Comm.*, (2003) (14), 1712-1713

20. Y. L. Koo, R. Kopelman *et. al.*, Real-Time Measurements of Dissolved Oxygen Inside Live Cells by Organically Modified Silicate Fluorescent Nanosensors. *Anal. Chem.* (2004) **76**(9), 2498-2505

21. J. S. Beckman, D.A. Wink, and J. P. Crow, Nitric Oxide and Peroxynitrite, in Methods in *Nitric Oxide Research*, Edited by M. Feelisch and J. S. Stamler, John Wiley & Sons (1996), 65

22. J. N. Armor, Influence of pH and Ionic Strength upon Solubility of NO in Aqueous Solution, *J. Chem. Eng. Data* (1974) v19(1), 82-84

23. I. G. Zacharia and W. M. Deen, Diffusivity and Solubility of Nitric Oxide in Water and Saline, *Annals. Biomed. Bioeng.* (2005) v33(2), 214-222

24. K. Nyberg, P. Camner *et al.*, Estimation of pH in Alveolar Macrophage Phagolysosomes, *Exp. Lung Res*. (1989) v15(4), 499-510

25. K. Tyner, R. Kopelman, and M. Philbert, "Nanosize Voltameter" Enables Cellular-Wide Electric Field Mapping, *Biophys J.* (2007) v93, 1163-1174

26. C. P. Reis, F. Veiga *et al.*, Nanoencapsulation I. Method for Preparation of Drug-Loaded Polymeric Nanoparticles, *Nanomed. Nanotech. Biol. Med.* (2006) v2, 8-21

27. K. Setsukinai, T. Nagano et al., Development of Novel Fluorescence Probe that can Reliably Detect Reactive Oxygen Species and Distinguish Specific Species, J Biol. Chem. (2003) v278(5), 3170-3175

28. H. Ischiropoulos, L, Zhu, and J. S. Beckman, Peroxynitrite Formation from Macrophage-Drived Nitric Oxide, Arch. Biochem. Biophys., (1992) v298(2), 446-451

29. Y. Xia and J. L. Zweier, Superoxide and Peroxynitrite Generation from Inducible Nitric Oxide Synthase in Macrophages, *Proc. Natl, Acad. Sci. USA*, (1997) v94, 6954-6958

30. R. Kopelman *et al.*, Subcellular optochemical nanobiosensors: probes encapsulated by biologically localised embedding (PEBBLEs). *Sensors and Actuators* B, (1998) v51(1-3), 12-16

31. Xu H., Kopelman R. *et al.,* Photoexcitation-Based Nano-Explorers: Chemical Analysis inside Live Cells and Photodynamic Therapy. *Isr. J. chem.* (2004) **44**(1-3), 317-337

32. R. Roots and S. Okada, Estimation of Life Times and Diffusion Distances Involved in the X-Ray Induced DNA Strand Breaks or Killing of Mammalian Cells, *Rad. Res.* (1975) v64, 306-320

33. G. D. Beall, F. L. Rasp *et al.*, Chemiluminscence by Human Alveola Macrophages: Stimulation with Heat-Killed Bacteria or Phorbol Myristate Acetate, *Infect. Immun.* (1977) v17(1), 117-120

34. Y. Homma, T. Takenawa et al., Evidence for Differential Activation of Arachidonic Acid Metabolism in Formylpeptide- and Macrophage-Activation-Factor-stimulated Guinea-Pig Macrophages, *Biochem. J.* (1985) v229, 643-651

35. F. Meng and C. A. Lowell, Liposaccharide (LPS)-Induced Macrophage Activation and Signal Transduction in the Absence of Src-Family Kinases, Hck, Fgr, and Lyn, *J. Exp. Med.* (1997) v185(9), 1661-1670

36. C. Loetchutinat, S. Mankhetkorn *et al*., Spetrofluorometric Determination of Intracellular Level of Reactive Oxygen Species in Drug-Sensitive and Drug-Resistant Cancer Cells Using 2',7'-Dichlorofluorescein Diacetate Assay, *Rad. Phys. Chem.* (2005) v72, 323-331

Chapter 4

Nano-PEBBLEs as Photoacoustic Imaging Agents with Simultaneous Near-Infrared Photodynamic Activity

Introduction

Photoacoustic (PA) imaging is an emerging biomedical modality based on detecting acoustic signals generated from biological tissues by optical absorption. Pulsed laser illumination is used to induce rapid thermoelastic expansion in a tissue volume, thus launching acoustic waves. An ultrasonic array transducer detects the acoustic radiation for image reconstruction. The image reflects the distribution of optical absorption in the tissue. The technique combines the high spatial resolution and penetration of ultrasonic imaging with the high contrast related to the optical properties of tissue. PA imaging has been used mainly to image blood vessels [1], the brain [2,3], cancers of the breast [4] and skin [5,6], the eye [7], and small animals [8]. These applications are based on naturally occurring light absorbers, such as hemoglobin and melanin.

Photoacoustic imaging using near-infrared (NIR) illumination in the range of 700 – 1000 nm has attracted the most attention because light can penetrate several centimeters into tissue at these wavelengths, thus avoiding intense absorption by natural tissue pigmenting components and water. Ideally, the tissue medium should

have low optical absorption for deep penetration, while the objects of interest (such as tumors in cancer detection) should have high absorption for best image contrast. Exogenous staining can provide high contrast when the natural optical contrast is not sufficient. Several PA imaging studies utilized various NIR absorbing agents, such as Indocyanine Green (ICG) [9], and gold nanoparticles [10,11].

Photodynamic therapy is another field for which the NIR region can be significantly beneficial. Short tissue penetration of the illumination light has limited the application of PDT to only for a few types of cancer, such as skin cancer, lung cancer, neck cancer and others that are located where the illumination source (fiber) can be close. Also, PDT has been mainly used to treat small volume tumors, because of limitation in tissue penetration depth. A number of efforts have been made to develop advanced photosensitizers with NIR excitation, so as to overcome this problem. Various NIR photosensitizers, including benzochlorin iminium salts (798 nm excitation) [12], Lutetium texaphyrin (700 – 760 nm excitation) [13], and bacteriochlorins (739 nm excitation) [14] have been synthesized and investigated for this purpose. NIR 2-photon excitation has also been used for PDT [15]

ICG is a water-soluble, FDA approved dye which has a strong absorption around 800 nm and has been widely used for retinal angiography [16], liver function testing [17], and cardiac output determination [18]. ICG has NIR fluorescence [19] and PDT using ICG has been reported recently.[20-22].

We present here a dual-function, nano-sized agent, capable of both early stage cancer detection by PA imaging and localized cancer treatment by PDT, thus combining two functions in one by PEBBLE technology. Further multifunctionality is easily

achieved by adding PEBBLE targeting, as has been demonstrated before in the Kopelman Lab [23,24]. These PEBBLEs are designed by encapsulating ICG dye in an Ormosil matrix incorporating an antibody on its surface for cancer targeting. We note that the PA imaging can be used to detect the nanoparticles without significant activation of the toxic singlet oxygen generation, because PDT light doses are typically in the range of 10 – 100 J/cm^2 [25], which is 10^3 to 10^4 times higher than the required light fluence for a single acquisition of a photoacoustic image. An additional continuous wave (CW) laser can be used for PDT activation.

We have developed ICG-embedded PEBBLEs that are incorporated with cancer specific targeting as a contrast agent for PA imaging. Nano-encapsulation of ICG has been reported for a few different applications, such as improvement/stabilization of ICG properties, drug delivery of ICG and photodynamic therapy [26-29]. Dye encapsulation in PEBBLEs has several advantages for the dual functionality of photoacoustic imaging and PDT when we aim for *in vivo* applications. First, the nanoparticle surface can be engineered for specific purposes, for example, incorporation of a targeting moiety and/or PEGylation for extended blood circulation time [30]. Second, superior contrast is achieved by dye encapsulation because of its high concentration in the nanoparticle. Finally, encapsulation into a nanoparticle stabilizes the ICG dye molecules against aqueous media and other destabilizing effects from the biological environment [26]. Here we describe our investigations on ICG-embedded Ormosil PEBBLEs for cancer targeted photoacoustic imaging and their potential use in photodynamic therapy.

Experimental

Materials

Indocyanine Green (ICG) and ninhydrin were purchased from Fluka and 1,3-diphenylisobenzofuran (DPIBF), phenyltrimethoxysilane (PTMS), methyltrimethoxysilane (MTMS), aminopropyltrimethoxysilane (APTMS), ammonium hydroxide, nitric acid, and 2-iminothiolane hydrochloride (2-IT) were obtained from Aldrich. Sulfosuccinimidyl 4-[*N*-maleimidomethyl]cyclohexane-1-carboxylate (Sulfo-SMCC) was purchased from Pierce. PBS buffer was self made. Other materials used are Agarose (GPG/LE, American Bioanalytical), and Intralipid (Lyposin 10 %, Abbott laboratories). All dyes and chemicals were used without further purification.

ICG PEBBLE synthesis

ICG-embedded Ormosil PEBBLEs were synthesized based on a sol-gel process combined with micro-emulsion polymerization [31-33]. Although most protocols followed the method described in previous chapters, some procedures were carefully modified as follows to maximize the efficiency of dye loading and minimize the deactivation of ICG's optical properties, as ICG is known to be quite unstable 26,34]. Specifically, an aliquot of 80 μL of PTMS was added to 31 mL of water containing 34 μL of nitric acid. The mixture was heated to 60 °C in a water bath and stirred at 1000 RPM for 30 minutes on a hot plate stirrer (Signature 575, VWR Int., West Chester, PA). The reaction mixture was maintained under constant heating and stirring for 2 more hours, after quick addition of 6 mL of preheated 30 % ammonium hydroxide. Then, the reaction

mixture was cooled to 35 °C or less, to avoid deactivation of the dye by heat. An aliquot of 1 mL of water solution containing 6 mg of ICG and 100 μL of MTMS was added to the mixture. The reaction was run for another 1 hour and 10 μL of APTMS were added, to give primary amine functionality to the surface of the PEBBLEs, for conjugation with antibody. After 1 hour, the product was filtered with a Magna nylon membrane filter (pore size 0.1 um) with air suction by a respirator. The products were re-suspended in water and rinsed in an Amicon filtration system 5 times, to remove impurities such as non-reacted monomers, dyes, and other soluble chemicals. The resultant PEBBLEs were recovered by additional suction filtration and dried under a nitrogen atmosphere or in a lyophilizer. The final product needed to be stored in dried form for two reasons; in order to avoid deactivation of the ICG dye contents in the liquid environment and also to obtain accurate particle number density information from controlled concentrations.

Quantitation of dye loading efficiency with ICG Ormosil PEBBLE's absorbance

To estimate the ICG dye loading capacity of the Ormosil nanoparticles, we prepared a set of calibration samples consisting of a known concentration of free ICG dye and blank Ormosil nanoparticles. Blank particles are added to the calibration samples so as to match their light scattering coefficient to that of the ICG Ormosil PEBBLEs. UV-VIS absorption spectra of several calibration samples, with various dye concentrations, were measured and compared to the absorption spectrum of the ICG Ormosil PEBBLE sample. Absorbance values at 790 nm were plotted and fitted with a linear dependence on dye concentration.

Aqueous stability measurements

Solutions of 0.1 mg/mL ICG Ormosil PEBBLEs in water and 1 μM free ICG dye in water were prepared. They were covered with aluminum foil and stored at room temperature for 5 days. Absorption spectra of both PEBBLEs and free dye solutions were measured daily and compared, after ultrasonication for several minutes so as to minimize aggregation.

Photosensitization

The photodynamic efficacy of the ICG dye has been investigated recently [20 - 22]. To evaluate singlet oxygen generation from ICG Ormosil PEBBLEs, the singlet oxygen sensitive molecular probe, 1,3-diphenylisobenzofuran (DPIBF), described in chapter 2, was used. DPIBF can rapidly quench singlet oxygen, reducing its fluorescence emission near 450 nm. Because of the hydrophobicity of DPIBF, the photodynamic effect was measured in an EtOH-water (50:50) mixture, instead of pure water. A 0.1 mg/mL suspension of ICG Ormosil PEBBLEs in an EtOH-water mixture and a 1 μM (concentration was arbitrarily chosen) solution of free ICG dye in an EtOH-water mixture were examined for photodynamic capability. 0.2 mL of 10 μM DPIBF in EtOH-water solution was mixed with 2 mL of either ICG PEBBLEs or free dye solution in a 4 mL capacity fluorescence quartz cuvette. The free ICG dye-DPIBF or PEBBLE-DPIBF mixture, with shaking, was illuminated by a Ti-Sapphire laser around 800 nm wavelength with a 1.4 mm beam width and 700 mW beam power (light fluence 1.36 kJ/cm^2), in continuous wave (CW) mode, for 30 seconds. Fluorescence spectra of DPIBF were

measured with a fluorometer in the 420-620 nm range, with a 412 nm excitation wavelength, before and after laser illumination.

PEBBLE-antibody conjugation

Specific binding of ICG Ormosil PEBBLEs to cancer cells is achieved by conjugating HER-2 antibody (*neu* Ab-17, Labvision Corp.) onto the PEBBLE surface. The HER-2 antibody is known to have a good affinity for breast cancer and prostate cancer cells [35]. PEBBLE-antibody conjugation was performed following 3 steps: attaching a crosslinker on the PEBBLE surface, thiolization of the antibody, and crosslinking between the linker attached PEBBLEs and the thiolized antibody.

First, 2 mL of an ICG-embedded amine functionalized Ormosil PEBBLE (12 mg) solution was added into 2 mL of PBS buffer (10 mM, pH 7.5) in a 20 mL scintillation vial. The solution was purged with argon and then treated with 3 mg of a crosslinking agent, sulfo-SMCC (heterobifunctional, amine reactive on one side and thiol reactive on the other side). The glass vial was sealed with parafilm and covered with aluminum foil. The mixture was stirred in a 37 °C water bath for 1 hour. The reaction mixture was washed twice in a 10 mL Amicon (100 kDa MWCO filter membrane) with sodium phosphate buffer (100 mM, pH 7.2). The final volume of the solution was 4 mL.

Second, to add a free thiol group (-SH) onto the antibody available for conjugation with an SMCC attached ICG PEBBLE, the antibody was treated with 2-iminothiolane hydrochloride (2-IT). Next, 0.1 mL of a 1 mg/mL antibody ($6.7 \cdot 10^{-7}$ mmol) solution was mixed with 2 mL of 2-IT in PBS buffer solution containing the same number of 2-IT molecules. The vial was sealed with parafilm, and the mixture was stirred

at room temperature for 2 hours. Finally, 4 mL of SMCC attached ICG PEBBLE solution and 2 mL of thiolized antibody solution were mixed together. This mixture was purged with argon for 1-2 minutes and stirred overnight, sealed with parafilm. Then, the mixture was washed in a 10 mL Amicon filter with sodium phosphate buffer (pH 7.2) 2 times and with DI water 3 times. The washed solution was carefully transferred back to a scintillation vial and lyophilized for 3 days. The prepared antibody-conjugated ICG Ormosil PEBBLEs sample was stored in a freezer (-20 ℃) until future use.

Cell targeting efficiency of antibody-conjugated ICG PEBBLEs

We have tested the conjugation efficiency of antibodies to the PEBBLE surface and their binding to target cells. LNCaP cells, a cell line extracted from a lymph node metastasis of prostate cancer, was provided by Dr. Kathlyn Day in Dr. Mark Day's group at The University of Michigan, Department of Urology and Comprehensive Cancer Center, and cultured in a cell chamber with two compartments (CultureSlides, BD Falcon^{TM}, BD BioCoat^{TM}) . Cells were attached to the bottom of the chamber and their surface density was less than 50 %. A 0.2 mg/mL sample of antibody-conjugated ICG Ormosil PEBBLEs and a sample of bare ICG Ormosil PEBBLEs (from the same batch), in PBS buffer solution, were prepared and filtered with 5 μm pore diameter syringe filters. They were adjusted to give similar absorption intensity at 800 nm by the added buffer solution. A 1 mL antibody-conjugated PEBBLE solution was added into one compartment and a 1 mL non-conjugated PEBBLE solution was added into the other compartment. The cell solutions were incubated for 1 hour, at room temperature, and the free PEBBLEs were removed from the cell chamber by washing 2 times with PBS buffer.

The efficiency of antibody targeting was confirmed by measuring the photoacoustic signal from cells treated with antibody-conjugated PEBBLEs and bare PEBBLEs (control). In the collaboration with Dr. Shai Ashkenazi in Dr. Matthew O'Donnell's group at The University of Michigan, Biomedical Engineering Department, photoacoustic imaging with a scanning photoacoustic microscope was performed, producing high resolution images of the cells in the two compartments. The setup is shown in figure 4.1.

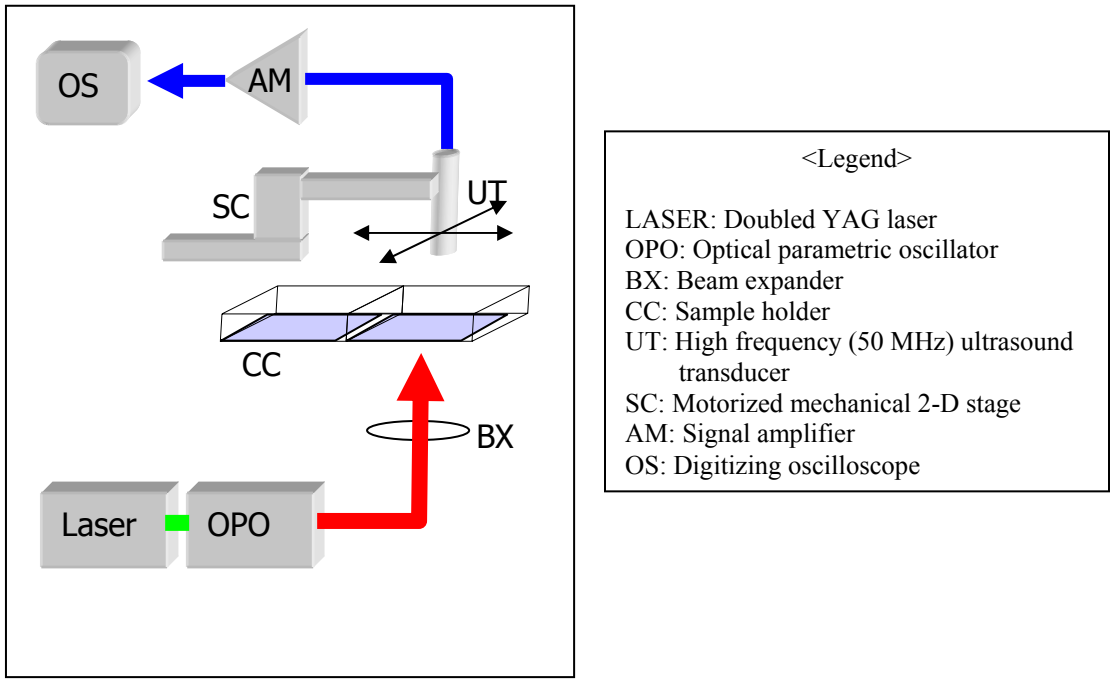

<Figure 4.1: A high resolution photoacoustic scanning system configuration>

In more detail, a doubled YAG pulsed laser (Continuum, I-20) pumps an optical parametric oscillator (OPO) (Continuum, Surelite OPO Plus) to produce 5 ns pulses with a tunable wavelength in the range of 690 nm to 980 nm. The output pulse energy was set to 8 mJ and the beam diameter was expanded to 20 mm cross section in diameter. The

beam was directed to illuminate the cell chamber bottom. A single element, focused, high frequency ultrasound transducer ($LiNbO_3$ 50 MHz, focal length = 4 mm, f/1.5) detected the photoacoustic signal at the top of cell solution. The transducer focal plane was aligned with the chamber bottom surface. The transducer was mounted on a motorized XYZ translation stage to accurately scan the total volume of the cell chamber. The transducer signal is amplified (Panametrics, model 5910PR), digitized by a digital oscilloscope (LeCroy, WaveSurfer 432), and transferred to a computer for storage. The computer was also used to control scanning.

Photoacoustic imaging setup

The scanning photoacoustic microscope described above is designed for imaging of tissue culture specimens. Given its limited depth of field (60 μm for the low f# transducer used) and long data acquisition time (limited by mechanical scanning), this instrument is not appropriate for clinical applications. To explore the potential of PEBBLEs for clinical applications, a second photoacoustic imaging system built by Dr. Shai Ashkenazi and Dr. Sheng-Wen Huang in O'Donnell group, with lower spatial resolution but more appropriate for clinical applications, was introduced. The detailed description about this imaging system, as follows, was provided by Dr. Ashkenazi and quoted from our co-publication in the Journal of Biomedical Optics [36]. This new imaging system is more practical than the scanning photoacoustic microscope in three respects: electronic scanning for high frame rate; electronic focusing, providing uniform resolution; and the ability to change probes for different medical applications. The system uses a clinical ultrasound scanner (Ultrasonix, Sonix RP). A software development kit,

available from the scanner manufacturer, allows full control over the ultrasound beam former operation and signal acquisition hardware using C/C++ programming language. We have utilized this feature to customize the scanner for a dual-mode operation where both B-mode ultrasound and photoacoustic imaging modes are implemented. Figure 4.2 shows the schematic of the dual-mode imaging system.

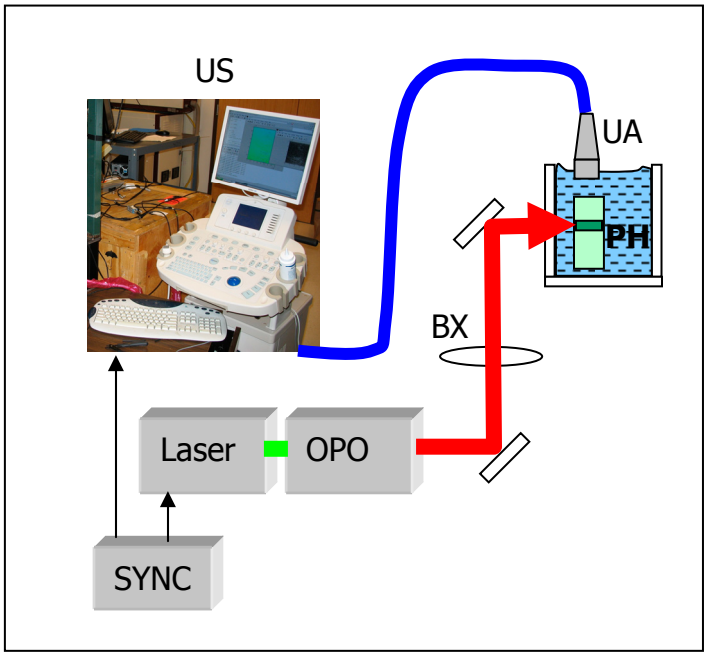

<Figure 4.2: Schematic of the photoacoustic imaging setup based on a clinical ultrasound scanner and a doubled YAG pulsed laser pumping an OPO. The beam is expanded (BX) before illuminating the phantom (PH). An ultrasound array probe (UA) detects the laser generated acoustic waves. The ultrasound scanner (US) acquires signals in synchronization with the laser pulses. The scanner employs a beam forming algorithm to form the photoacoustic image.>

In the photoacoustic mode, the ultrasound scanner receives the acoustic emission (generated by the pulsed laser) using a linear array ultrasound probe (Ultrasonix L-14-5/38, 128 elements, bandwidth 5 – 14 MHz). Laser pulses and ultrasound signal acquisition are synchronized using a common clock source (Agilent function generator)

and a field programmable gate array (ezFPGA-C6-8 Module, Dallas Logic, Plano TX). The system is programmed to acquire the ultrasound signal on a single array element for every laser pulse. A complete data set is acquired every 128 laser pulses (6.4 sec). To reduce noise, 16 data sets are averaged before processing. A beam forming algorithm, employing Coherent delay-and-sum and implemented using MATLAB (Mathworks Inc.) code, was applied to reconstruct the photoacoustic image [37].

Preparation of tissue phantom containing ICG Ormosil PEBBLEs for 2-dimensional and 3-dimensional photoacoustic imaging

In order to demonstrate the feasibility of photoacoustic imaging using ICG Ormosil PEBBLEs as a contrasting agent, we have performed imaging of phantoms containing ICG Ormosil PEBBLEs in tissue mimicking structures, made of agarose gel. Phantoms containing small gelled ICG PEBBLE solutions were implanted in optically diffusive gel (Agarose 2%, Intralipid 5%), following the geometries for 2-D and 3-D, as shown in figure 4.3. For 2-D phantoms, the preformed agarose gel cylinder was punctured through to form 3 holes and the holes were filled with half melted agarose gel containing ICG Ormosil PEBBLEs. For 3-D phantoms, several pieces of PEBBLE containing gel were put on the top of a background gel cylinder (gel without PEBBLEs) and, then, melted agarose gel was poured onto them, forming another layer of gel bearing PEBBLE phantoms inside. The phantoms were illuminated from the side while immersed in a water tank and the ultrasound transducer was positioned above the phantom to perform photoacoustic imaging.

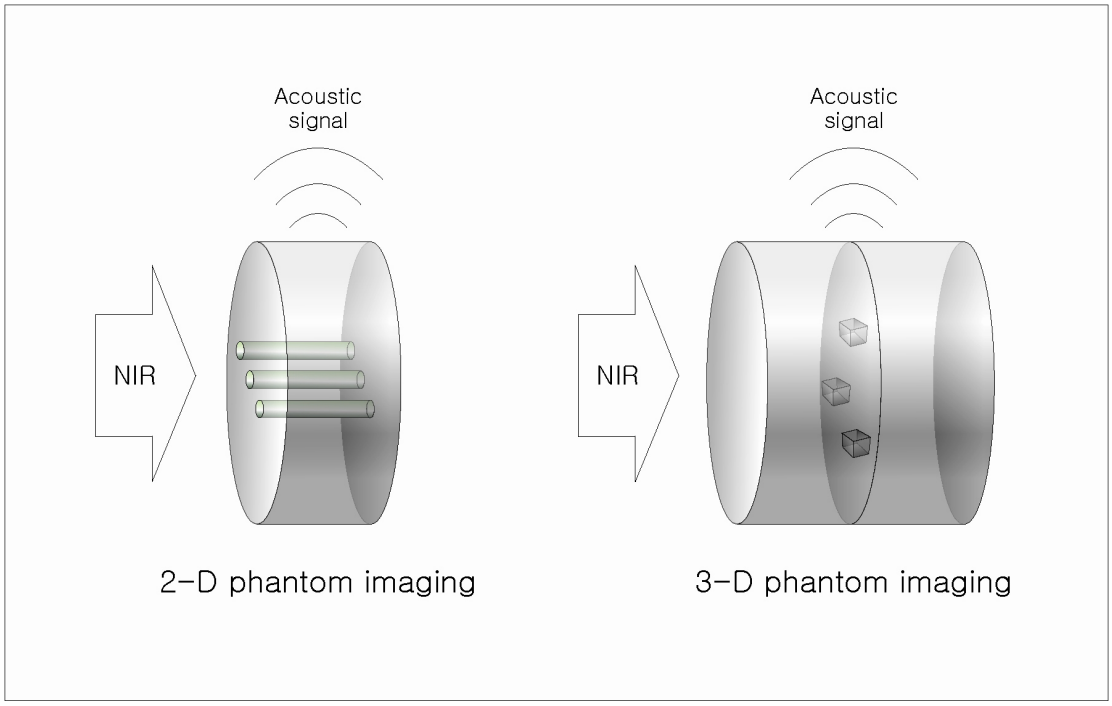

<Figure 4.3: Schematic for tissue mimicking phantom for 2-D and 3-D photoacoustic imaging.>

Results and Discussion

ICG PEBBLE synthesis and characterization

ICG Ormosil PEBBLEs were synthesized based on sol-gel chemistry and yielded 70 mg of nearly mono-dispersed nanoparticles with 100 nm diameter. A scanning electron microscope (SEM) image of the particles (dried phase) and a particle size distribution curve obtained from a dynamic light scattering (DLS) particle sizer (wet phase) are given in figure 4.4. Only a negligible difference in the mean particle size was observed between the dried and wet phase, implying negligible swelling of the particle matrix.

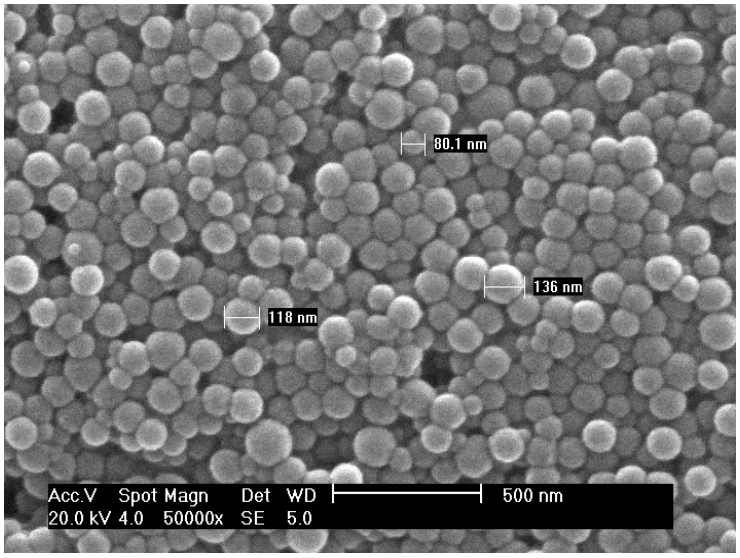

(a)

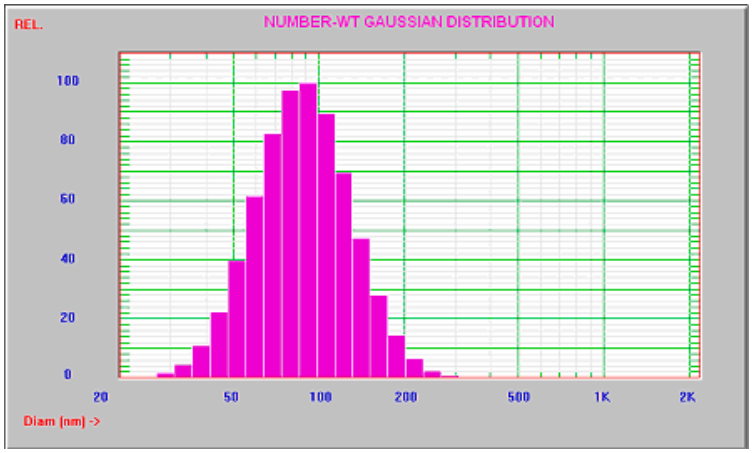

(b)

<Figure 4.4: SEM image of ICG Ormosil PEBBLEs (a) and particle size distribution obtained from dynamic light scattering particle sizer (b). Both results consistently showed that ICG Ormosil PEBBLEs are nearly monodisperse, 100 nm in diameter.>

Unlike the other Ormosil PEBBLEs described in chapters 2 and 3, the preparation for ICG Ormosil PEBBLEs was needed to be considerably modified to avoid the deactivation of ICG dye. ICG has been well known for being relatively unstable and susceptible to various factors, including the aqueous solvent, photobleaching, pH

(especially acidic), and heat [26,34]. The Ormosil synthesis is based on a sol-gel method which relies on the balance of two different reaction mechanisms; hydrolysis of silane monomer at acidic conditions and condensation to form nanoparticles at basic conditions. Furthermore, the synthesis requires heating to 60 ℃ to supply sufficient reaction energy and the dye content needs to be exposed to the aqueous environment for more than 2 days, from synthesis to recovery. In early trials for PEBBLE synthesis, the loss of the ICG absorption characteristics at the 800 nm region and the change of color from green to brown, indicating chemical transformation, were observed, resulting in failure. Also, the attempt to develop ICG embedded PEBBLEs using a PAA matrix failed as well, because we found out that the ICG dye can be effectively destroyed by the radicals on which the PAA synthesis is based. In order to overcome these problems stemming from ICG's instability, the Ormosil synthesis protocol was modified. The ICG dye was put into the reaction under basic conditions, after a 2 hour condensation of the PTMS monomer, to avoid acidic pH, as well as after cooling down the reaction temperature to 35 ℃ or lower, to avoid overheating. Also, the rinsing and recovery procedures were achieved in an Amicon filtration system, which takes much less time than suction filtration, to reduce the time period during which the ICG dye needs to be exposed to an aqueous solution. As a consequence, the ICG Ormosil PEBBLEs could be obtained while maintaining both a good NIR absorption and its green color.

Quantification of dye loading efficiency by ICG Ormosil PEBBLE's absorbance

Dye loading of a PEBBLE particle was tested by comparing its optical absorption with that of free ICG dye at different concentrations (see figure 4.5 left). Blank Ormosil particles were added to the free ICG solutions, to match the scattering coefficient to that of ICG PEBBLEs. Linear curve fitting for peak absorption (at λ=790 nm) was evaluated, so as to estimate the dye concentration in the PEBBLE particle (figure 4.5 right).

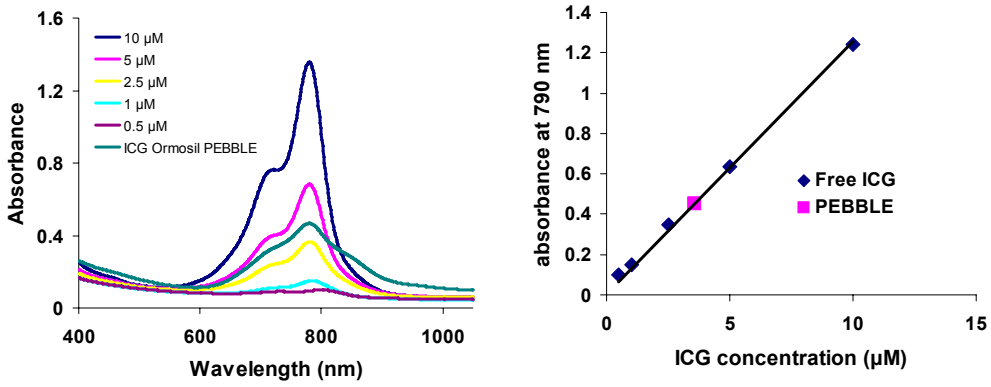

<Figure 4.5: Dye loading inside a PEBBLE particle was tested by comparing optical absorption of PEBBLE particles with optical absorption of free ICG dye at different concentrations (left). Linear curve fitting for the peak absorbance (at λ=790 nm) was evaluated, so as to estimate the dye concentration in the PEBBLE particle (right).>

The estimated dye concentration in the PEBBLE sample, in a 0.1 mg/mL ICG Ormosil PEBBLE solution, is 3.6 μM. When assuming that the density of the Ormosil nanoparticle matrix is about 2.0 g/cm^3 [38,39], and considering the average particle size of 100 nm, the particle number density of 10^{11} particles/mL can be computed, using the weight of particles in the solution, particle volume and density. This dye concentration corresponds to 23,000 ICG molecules per 1 Ormosil nanoparticle. High loading capacity is advantageous for gaining a strong enough contrast effect, in cell targeting applications.

As the number of cell membrane receptors per area is limited, a high loading per particle provides a mechanism for enhancing the signal from each targeted cell.

The characteristics of the ICG Ormosil PEBBLEs' absorption spectrum remained the same as those of the ICG free dye, although minor changes were observed, reflecting an effect stemming from the Ormosil matrix. According to Landsman *et al.* and Zhou *et al.*, at concentrations above 1 mM, ICG can produce dimers or higher aggregated forms (oligomers) resulting in changes in the absorption peak shape, represented by a rise of a dimer peak around 700 nm and a decline in the monomer peak at 790 nm [40,41]. The shape and location of the ICG PEBBLE's absorption spectrum indicates that the dye molecules are mostly present in monomer form, in spite of their high packing density in the nanoparticles. In order to verify that the observed absorption spectrum corresponds to ICG molecules encapsulated in nanoparticles, rather than by free dye in the solution, due to dye leaching, the following leaching test was performed, following the method described earlier.

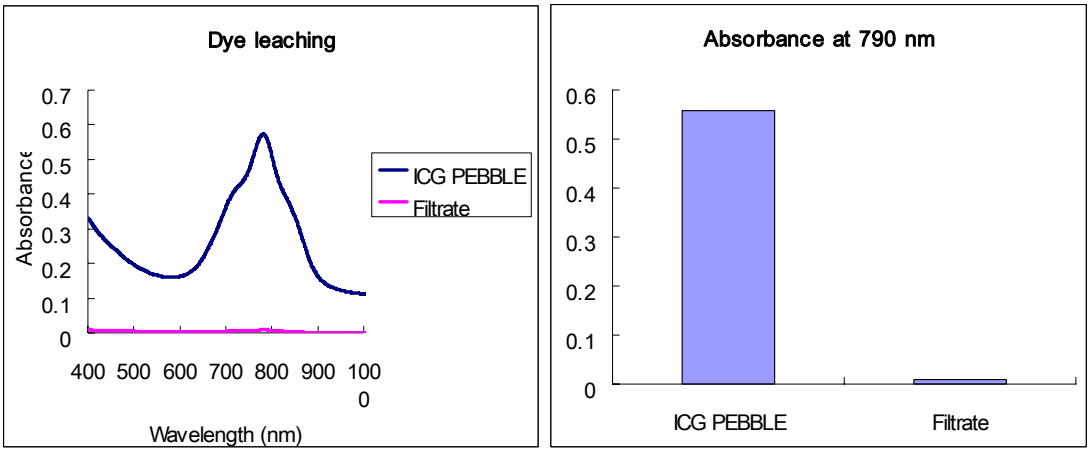

<Figure 4.6: Comparison of UV-VIS absorption spectra between ICG Ormosil PEBBLEs and filtrate at the absorption maxima near 800 nm. Filtrate solution showed only a trace of absorbance at 800 nm, verifying negligible dye leaching>

The PEBBLE solution was filtered by suction, using a Whatman Anodisc filtration membrane with 0.02 μm pore diameter, and absorbance of the filtrate was measured. Only negligible dye leaching was observed (figure 4.6), supporting the notion that the ICG molecules in the nanoparticle are present in monomer form. As it will be explained in more detail in the next section, the enhanced stability of ICG in the nanoparticle is attributed to the interaction of the dye molecules with the Ormosil matrix, which favors the monomer form by isolating individual dye molecules and preventing dye-dye interactions.

Aqueous stability measurements

The enhanced stability of ICG nanoparticles is a major advantage over free ICG dye, regarding clinical applications. Several environmental conditions are known to affect ICG and reduce its optical absorption. Free ICG dye is unstable in aqueous media and sensitive to pH [26,34]. This instability can limit its application as an optical contrast agent in medicine. Saxena *et al.* [26] have reported that ICG doped nanoparticles based on PLGA (poly latic-glycolic acid) biodegradable polymer could improve stability of ICG. To test the stability of ICG Ormosil PEBBLEs in aqueous media, we have monitored their optical absorption in a water solution for 5 days. The absorption intensity of ICG Ormosil PEBBLE decreased by less than 10 % over 5 days, while free ICG dye showed an over 70 % decrease, indicating severe deactivation in water (figure 4.7). This result shows that encapsulation of ICG in Ormosil nanoparticles improves the ICG stability in aqueous media by a large factor.

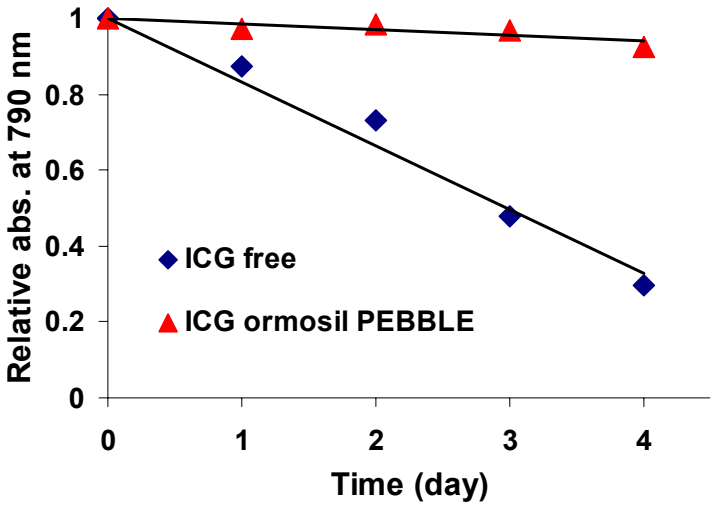

<Figure 4.7: Relative optical absorption of free ICG dye (diamonds) and ICG PEBBLE (triangles), measured over 5 days. Stabilization due to PEBBLE encapsulation is evident.>

Photosensitization

The photodynamic efficacy of ICG Ormosil PEBBLEs was evaluated by monitoring the change of fluorescence intensity of a DPIBF chemical probe, as explained in chapter 2. As shown in figure 4.8, for laser illumination at 800 nm, over 30 seconds, the fluorescence emission of DPIBF decreased with either free ICG dye or ICG Ormosil PEBBLEs present. In contrast, no such decrease was observed from controls with DPIBF but without free ICG dye or ICG Ormosil PEBBLEs, indicating that the decrease of DPIBF fluorescence intensity was induced by the ICG. This measurement confirms the potential of ICG Ormosil PEBBLEs as a photosensitizer for PDT. The irradiated light fluence of our experiment was about 1.36 kJ/cm^2 and the PDT dose can be roughly estimated to be 2×10^{19} photons absorbed by ICG/mL, which is relatively higher than the typical levels of clinical PDT. The system will be optimized for more acceptable

condition in clinical applications and the PDT efficacy of ICG Ormosil PEBBLE will be investigated in more detail in the future.

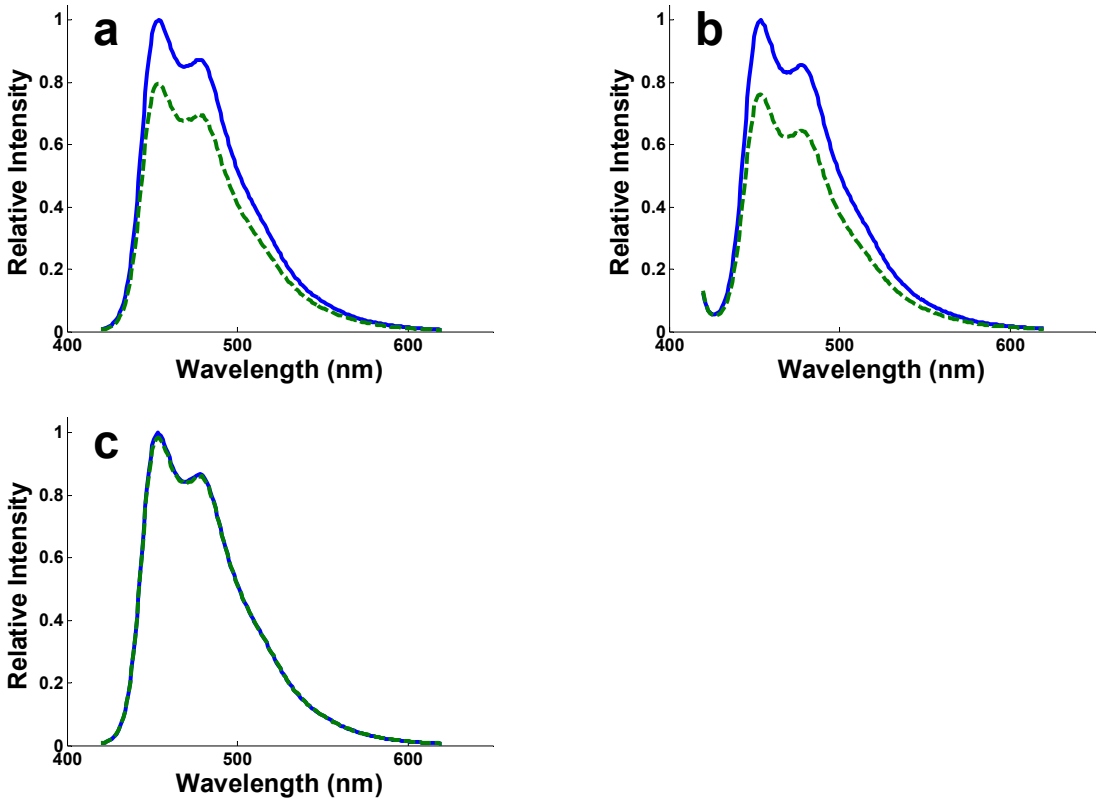

<Figure 4.8: Fluorescence intensity of singlet oxygen detecting probe, DPIBF with free ICG dye (a), DPIBF with ICG Ormosil PEBBLEs (b), and pure DPIBF (c). As mentioned in chapter 2, DPIBF can lose its fluorescence by reacting with singlet oxygen. In each case the intensity was measured before (solid line) and after (dashed line) Ti-Sapphire laser illumination tuned at a wavelength of 800 nm, for 30 seconds. Reduced fluorescence intensity indicates singlet oxygen generation and ICG Ormosil PEBBLEs and ICG free dye both showed notable fluorescence reduction while control did not shown any decrease under same illumination.>

Cell targeting efficiency of antibody-conjugated PEBBLEs in *in vitro* photoacoustic imaging

ICG PEBBLEs were conjugated with HER-2 antibody to test targeting of prostate cancer cells (LNCaP cell line). Cells were incubated with conjugated particles and with bare particles (control) to compare specific and non-specific binding of PEBBLEs to cells. In both cases we used a high resolution photoacoustic scan to detect and image a single cell layer. The scanned image of cells targeted by conjugated particles (figure 4.9 top) has a mean signal energy 22 dB higher than that of the control cells sample (figure 4.9 bottom), for an illumination wavelength of 800 nm. This result indicates that the antibody molecules were successfully conjugated to the PEBBLEs surfaces and maintained their targeting ability. The experiment also demonstrates the potential of photoacoustic imaging for *in vitro* single cell detection using ICG Ormosil PEBBLE cell tagging. The photoacoustic signal from cells in the control sample was higher than the noise level, indicating some degree of non-specific binding, or insufficient washing to remove all PEBBLEs. The specificity of the targeting moiety will be further investigated in our future works.

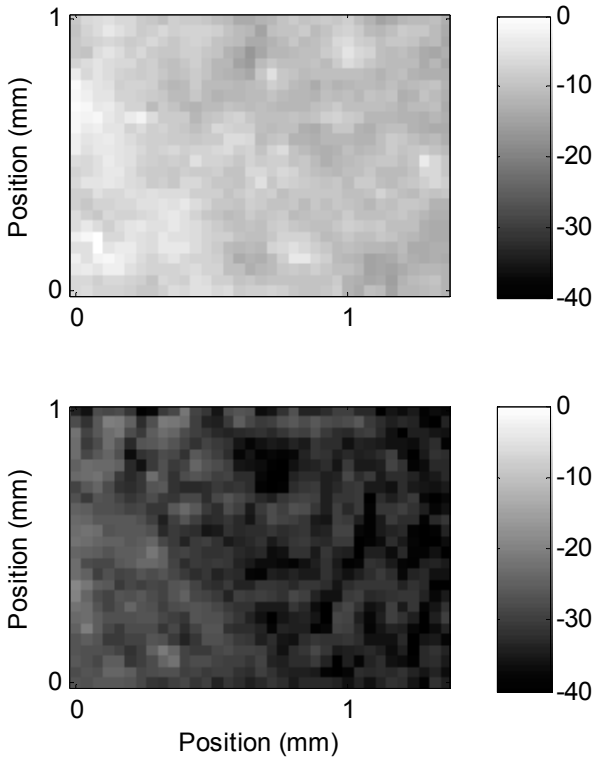

<Figure 4.9: Photoacoustic images of LNCaP cells incubated with antibody-conjugated PEBBLEs (top), and LNCaP cells incubated with un-conjugated PEBBLEs (bottom). In both cases cells were incubated for 1 hour and than washed twice. Signal gray scale is in dB. 22 dB stronger PA signal intensity was obtained from ab-conjugated PEBBLEs than un-conjugated PEBBLEs, indicating efficient tumor targeting.>

2-D and 3-D photoacoustic phantom imaging

We have studied the 2-D photoacoustic imaging by imaging phantom objects with inclusions of PEBBLE nanoparticles in varying concentrations. As shown in figure 4.3, a phantom with three cylindrical inclusions, each 1.5 mm in diameter, with PEBBLE concentrations of 1 mg/mL (10^{12} PEBBLEs/cm^3), 0.1 mg/mL (10^{11} PEBBLEs/cm^3), and 0.01 mg/mL (10^{10} PEBBLEs/cm^3) were constructed with agarose gel with Intralipid, to mimick tissue's scattering nature. A 2-D photoacoustic image was acquired using a laser pulse energy of 12 mJ, a beam width of 25 mm (light fluence is 2.6 mJ/cm^2), and an

illumination wavelength of 800 nm. The 2-D photoacoustic image of the phantom is shown in figure 4.10. The result demonstrates that the PA signal intensity is clearly correlated with the PEBBLE concentration of the inclusions. The instrumental detection limit of ICG PEBBLEs, for the current conditions, is estimated to be about 0.01 mg/mL (10^{10} PEBBLEs/cm^3), which is equivalent to 0.36 μM of free ICG dye, based on a particle density calculation and the calibration curve in section 3.2. At this concentration the absorption coefficient is 0.1 cm^{-1}, which is lower than the absorption coefficient of typical tissue. For example, a recent study on the optical properties of the human prostate gland shows a mean absorption coefficient of 0.23 cm^{-1}, with inter-subject and intra-subject (different locations within the prostate gland) variations on the order of 0.2 cm^{-1} [42]. In this case, the minimal concentration required to provide sufficient contrast (estimated as 4 times the mean tissue background) is about 0.1 mg/mL (10^{11} PEBBLEs/cm^3).

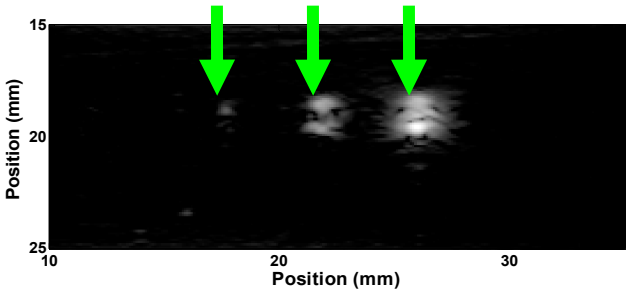

<Figure 4.10: Photoacoustic image of a gel phantom with three, 1.5 mm diameter, cylinders of different PEBBLE concentrations: $1{\cdot}10^{10}$ (PEBBLEs/cm^3) (left), $1{\cdot}10^{11}$ (PEBBLEs/cm^3) (middle), and $1{\cdot}10^{12}$ (PEBBLEs/cm^3) (right). The dynamic range of the gray scale is 40 dB.>

3-D phantom photoacoustic imaging was performed using 0.1 mg/mL which the estimated PEBBLE concentration appropriate for prostate gland as a target object. The phantom for 3-D photoacoustic imaging was prepared as designed in figure 4.3, and the thickness of the background gel (distance between phantom surface to the PEBBLE-containing gels inside) was more than 1 cm in any orientation. The instrumental configuration for 3-D imaging was almost the same as for 2-D imaging, except for the changeable transducer position. The transducer was moved back and forth in the direction of the NIR laser, with 0.05 mm intervals, performing 2-D imaging at multiple positions. The 3-D imaging was obtained by stacking up the 2-D images in a sequence of positions. As displayed in figure 4.11, the result clearly shows that 4 different pieces of objects, containing 0.1 mg/mL ICG Ormosil PEBBLEs with random shape, could be successfully detected through more than 1 cm depth by the 3-D photoacoustic imaging.

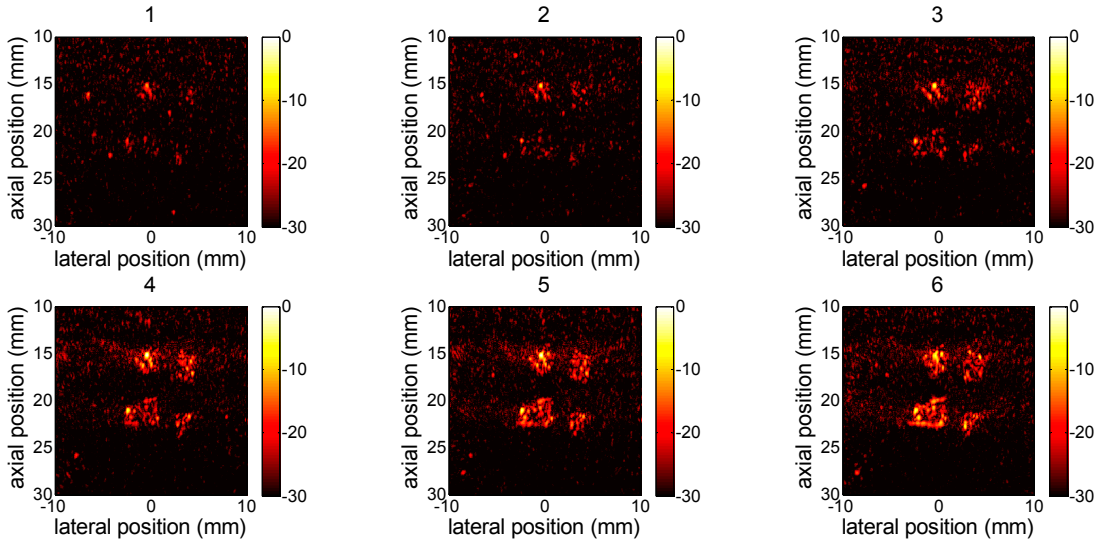

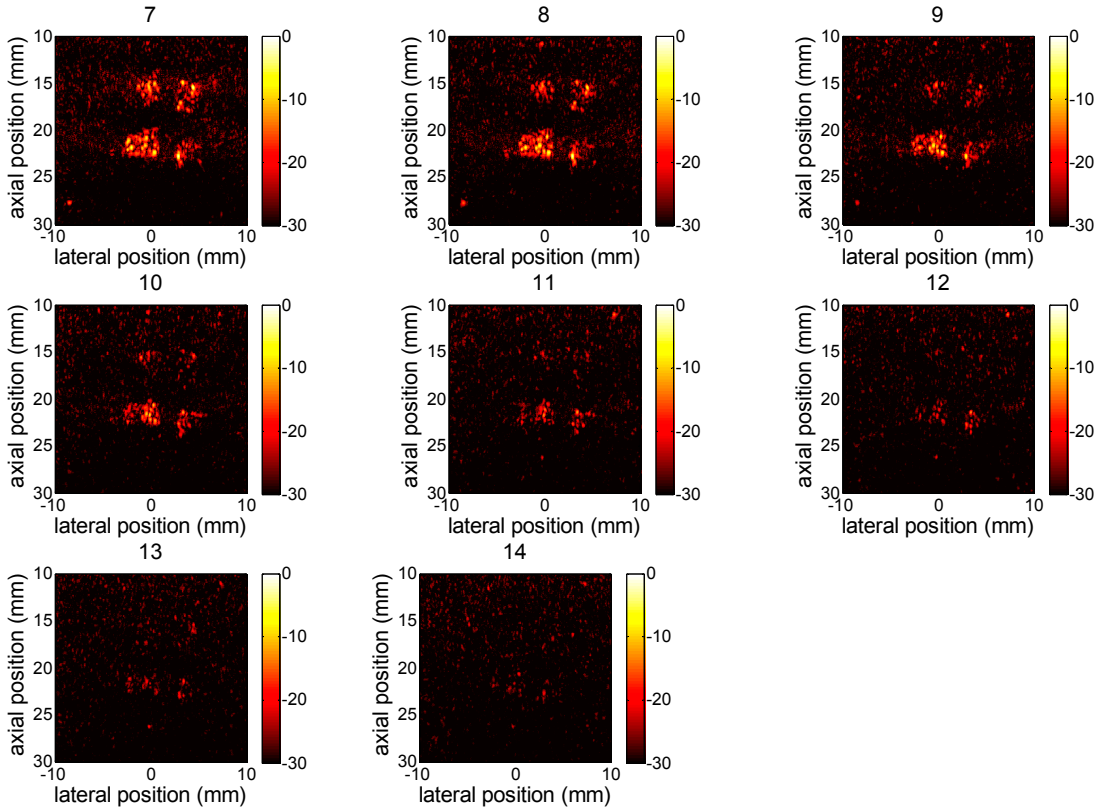

<Figure 4.11: 3-D photoacoustic imaging of ICG embedded Ormosil PEBBLE phantoms designed as figure 4.3. 4 pieces of gel containing ICG Ormosil PEBBLEs with random shape were planted inside tissue mimicking background gel cylinder and imaged. The illumination and acoustic signal reading were both achieved through more than 1 cm thickness of background gels>

Acknowledgements

The author deeply thanks Dr. Shai Ashkenazi and Dr. Sheng-Wen Huang, in Dr. Matthew O'Donnell's group at The University of Michigan, Biomedical Engineering Department, for collaborating in all the aspects of photoacoustic imaging instrumentations, and Dr. Kathlyn Day in Dr. Mark Day's group at The University of Michigan, Urology Department and Comprehensive Cancer Center, for providing prostate cancer cell lines. The author also thanks to Dr. Yong Eun Koo and Dr. Wenzhe Fan for helpful discussions and acknowledges support from NCI contract NO-1-CO-37123 (Kopelman) for partial support.

References

1. R. I. Siphanto, K. K. Thumma, R. G. M. Kolkman, T. G. van Leeuwen, F. F. M. de Mul, J. W. van Neck, L. N. A. van Adrichem, and W. SteenbergenSerial "Noninvasive photoacoustic imaging of neovascularization in tumor angiogenesis" *Optics Express*, **13**(1), 89-95, (2005)
2. X. Wang, X. Xie, G. Ku, L. V. Wang, and G. Stoica, "Noninvasive imaging of hemoglobin concentration and oxygenation in the rat brain using high-resolution photoacoustic tomography", *J. Biomed. Opt.* **11**, 024015 (2006)
3. X. Wang, G. Ku, M. A. Wegiel, D. J. Bornhop, G. Stoica, and L. V. Wang, "Noninvasive photoacoustic angiography of animal brains in vivo with near-infrared light and an optical contrast agent", *Optics Letters*, **29**(7), 730-732 (2004)
4. R. O. Esenaliev, A. A. Karabutov, F. K. Tittel, B. D. Fornage, S. L. Thomsen, C. Stelling, and A. A. Oraevsky, "Laser optoacoustic imaging for breast cancer diagnostics: limit of detection and comparison with x-ray and ultrasound imaging", *Proc. SPIE* **2979**, 71 (1997)
5. J. A. Viator, L. O. Svaasand, G. Aguilar, B. Choi, and J. S. Nelson, "Photoacoustic measurement of epidermal melanin", *Proc. SPIE* **4960**, 14 (2003).
6. P. C. B. Rompe, F. H. dos Anjos, A. A. Martin, A. M. Mansanares, E. C. da Silva, D. Acosta-Avalos, and P. R. Barja, "Characterization of human skin through photoacoustic spectroscopy", *Proc. SPIE* 5325, 136 (2004)
7. U. Oberheide, B. Jansen, I. Bruder, H. Lubatschowski, H. Welling, and W. Ertmer, "Optoacoustic imaging for ophthalmology", *Proc. SPIE* 4434, 1 (2001)
8. B. Liu, V. H. Gattone II, R. A. Kruger, and K. M. Stantz, "Assessment of photoacoustic computed tomography to classify tissue in a polycystic-kidney disease mouse model", *Proc. SPIE* 6086, 608607 (2006)
9. K. M. Stantz, B. Liu, M. Cao, D. Reinecke, K. Miller, and Robert Kruger, "Photoacoustic spectroscopic imaging of intra-tumor heterogeneity and molecular identification", *Proc. SPIE* 6086, 608605 (2006)
10. P.-C. Li, C.-W. Wei, C.-K. Liao, C.-D. Chen, K.-C. Pao, C.-R. C. Wang, Y.-N. Wu, and D.-B. Shieh, "Multiple targeting in photoacoustic imaging using bioconjugated gold nanorods", *Proc. SPIE* 6086, 60860M (2006)
11. A. Conjusteau, S. A. Ermilov, D. Lapotko, H. Liao, J. Hafner, M. Eghtedari, M. Motamedi, N. Kotov, and A. A. Oraevsky, "Metallic nanoparticles as optoacoustic contrast agents for medical imaging", *Proc. SPIE* 6086, 60860K (2006)
12. G. M. Garbo, A. R. Morgan et al. "In Vivo and *In Vitro* Photodynamic Studies with Benzochlorin Iminium Salts Delivered by a Lipid Emulsion" Photochem. Photobiol., (1998) v68(4), 561-568

13. K. W. Woodburn, S. W. Young *et al.* "Photodynamic Therapy of B16F10 Murine Melanoma with Lutetium Texaphyrin" J. Investig. Dermatol. (1998) v110, 746-751

14. J. P. Rovers, M. F. Grahn *et al. In Vivo* Photodynamic Characteristics of the Near-Infrared Photosensitizer 5,10,15,20-Tetrakis(*M*-Hydroxyphenyl) Bacteriochlorin, Photochem. Photobiol. (2000) v72(3), 358-364

15. D. Gao, R. Kopelman et al, Nanoparticles for Two photon Photodynamic Therapy in Living Cells, Nano Lett. (2006), v6(11), 2383-2386

16. W. R. Freeman, D. U. Bartsch, A. J. Mueller, A. S. Banker, R. N. Weinreb, "Simultaneous Indocyanine Green and fluorescein angiography using a confocal scanning laser ophthalmoscope", *Arch Ophthalmol.* (1998), v116, 455-463,.

17. T. Nonami, A. Nakao, T. Kurokawa, H. Inagaki, Y. Matsushita, J. Sakamoto, H. Takagi, "Blood loss and ICG clearance as best prognostic markers of post-hepatectomy liver failure", *Hepatogastroenterology*., (1999), v46(27), 1669

18. T. Iijima, T. Aoyagi, Y. Iwao, J. Masuda, M. Fuse, N. Kobayashi and H. Sankawa, "Cardiac output and circulating blood volume analysis by pulse dye-densitometry", *J. of Clinic. Monit. and Comp.* (1997), v13(2), 81-89

19. R. C. Benson and H. A. Kues, "Fluorescence properties of Indocyanine Green as related with angiography", *Phys. Med. Biol.* (1978), v23(1), 159-63

20. S. Fickweiler, R. Szeimies, W. Bäumler, P. Steinbach, S. Karrer, A. E. Goetz, C. Abels, S. Hofstädter, and M. Lanthaler, " Indocyanine Green: Intracellular uptake and phototherapeutic effects in vitro", *J. Photochem. Photobiol.* B, (1997), v38(2-3), 178-183

21. L. Varriale, E. Crescenzi, V. Paba, B. Mazziotti di Celso, G. Palumbo, "Selective light-induced modulation of Bcl-XL and Bax expressions in Indocyanine Green-loaded U937 cells: effects of continuous or intermittent photo-sensitization with low IR-light using a 805-nm diode laser", *J. Photochem. Photobiol.* B, (2000), v57(1), 66-75

22. C. Ables, "Targeting of the vascular system of solid tumours by photodynamic therapy (PDT)", *Photochemical & photobiological sciences*, (2004), v3, 765-771

23. R. Kopelman *et al.* Subcellular optochemical nanobiosensors: probes encapsulated by biologically localised embedding (PEBBLEs). *Sensors and Actuators* B, (1998), v51(1-3), 12-16

24. Xu H., Kopelman R. *et al.* Photoexcitation-Based Nano-Explorers: Chemical Analysis inside Live Cells and Photodynamic Therapy. *Isr. J. chem.* (2004), v44(1-3), 317-337

25. J. H. Pinthus, A. Bogaards, R. Weersink, B. C. Wilson, and J. Trachtenberg, "Photodynamic therapy for urological malignancies: past to current approaches", *The J. of Urology*, (2006), v175(4), 1201-1207

26. V. Saxena, M. Sadoqi, and J. Shao, "Enhanced photo-stability, thermal stability and aqueous stability of Indocyanine Green in polymeric nanoparticulate systems", *J. Photochem. Photobiol.* B, (2004), v74, 29-38

27. V. Saxena, M. Sadoqi, and J. Shao, "Indocyanine Green-loaded biodegradable nanoparticles: preparation, physiochemical characterization and in vitro release", *Int. J. Pharm.* (2004), v278(2), 293-301

28. V. Saxena, M. Sadoqi, and J. Shao, "Polymeric nanoparticulate delivery system for Indocyanine Green: biodistribution in healthy mice", *Int. J. Pharm.* (2006), v308(1-2), 200-204

29. A. J. Gomes, L. O. Lunardi, J. M. Marchetti, C. N. Lunardi, and A. C. Tedesco, "Indocyanine Green nanoparticles useful for photomedicine", Photomed. *Laser Surg.* (2006), v24(4), 514-521

30. R. Kopelman, H. Xu, F. Yan, E. Monson, W. Tang, R. Schneider and M. Philbert, "Preparation and Characterization of Poly (ethylene glycol)-Coated Stöber Silica Nanoparticles for Biomedical Applications", *SPIE (International Society of Photonic Engineering) Proc.* (2002), v4626, 383-393

31. H. J. Hah, J. S. Kim, B. J. Jeon, S. M. Koo and Y. E. Lee, "Simple preparation of monodisperse hollow silica particles without using templates", *Chem. Comm.* (2003), v14, 1712-1713

32. Y. L. Koo, Y. Cao, R. Kopelman, S. M. Koo, M. Brasuel, and M. A. Philbert "Real-time measurements of dissolved oxygen inside live cells by organically modified silicate fluorescent nanosensors" *Anal. Chem.*, (2004), v76(9), 2498-2505

33. Y. Cao, Y. L. Koo, S. M. Koo, and R. Kopelman, "Ratiometric Singlet Oxygen Nano-optodes and Their Use for Monitoring Photodynamic Therapy Nanoplatforms" *Photochem. Photobiol.* (2005), v81(6), 1489-1498

34. V. Saxena, M. Sadoqi, and J. Shao, "Degradation kinetics of Indocyanine Green in aqueous solution", *J. Pharm. Sci.* (2003), v92, 2090-2097

35. M. J. van de Vijver, J.L. Peterse, W.J. Mooi, P. Wisman, J. Lomans, O. Dalesio, and R. Nusse, "*Neu*-protein overexpression in breast cancer. Association with comedo-type ductal carcinoma in situ and limited prognostic value in stage II breast cancer", *New England Journal of Medicine*, (1988), v319(19), 1239-1245

36. Gwangseong Kim, Shai Ashkenazi et al., Indocyanine-green-embedded PEBBLEs as a contrast agent for photoacoustic imaging, J. Biomed. Optics (2007), v12(4), 044020

37. M. Xu, Y. Xu, and L. V. Wang, "Time-domain reconstruction algorithms and numerical simulations for thermoacoustic tomography in various geometries", IEEE Trans. Biomed. Eng. (2003), v50(9), 1086-1099

38. B. Fei, H. Lu, R. H. Wang, J. H. Xin, "Monodisperse organosilica microcapsules with functional groups by self-catalysis", *Chem. Letters*, (2006), v35(6), 622-623

39. A. van Blaaderen and A. Vrij, “Synthesis and characterization of mondisperse colloidal organo-silica spheres”, *J. Colloid Interface Sci.*, (1993), v156, 1-18

40. M. L. J. Landsman, G. Kwant, G. A. Mook, and W. G. Zijlstra, “Light-absorbing properties, stability, and spectral stabilization of Indocyanine Green”, *J. Appl. Physiol.* (1976), v40, 575-583

41. J. F. Zhou, M. P. Chin, and S. A. Schafer, “Aggregation and degradation of Indocyanine Green”, *Proc. SPIE*, (1994), v2128, 495-505

42. T. C. Zhu, A. Dimofte, J. C. Finlay, D. Stripp, T. Busch, J. Miles, R. Whittington, S. B. Malkowicz, Z. Tochner, E. Glatstein, and S. M. Hahn, “Optical properties of human prostate at 732 nm measured in vivo during motexafin lutetium–mediated photodynamic therapy”, *Photochemistry and Photobiology*, (2005), v81, 96–105

Chapter 5

Summary and Future Directions

Summary

This work exhibits nano-encapsulation techniques to explore reactive oxygen species for biosensing, bioimaging, and therapeutics, based on PEBBLE technology and using an Ormosil matrix. Because of the unique characteristics of ROS, high reactivity and instability, research on ROS, especially its quantitative aspects, typically requires tools with extraordinary sensitivity and specificity. Ormosil PEBBLEs are suggested here as a solution to these obstacles. Three examples were discussed: highly sensitive singlet oxygen detecting PEBBLE nanoprobes, highly specific hydrogen peroxide detecting PEBBLE nanoprobes, and dual-function PEBBLEs for both photoacoustic imaging contrast and photodynamic cancer therapy.

In Chapter 2, the development of DPIBF Ormosil PEBBLE nanoprobes for singlet oxygen detection in *in vitro* PDT was described. The improvement in sensitivity was achieved by introducing DPIBF, which is the most sensitive singlet oxygen probe, but not appropriate for biological use, by encapsulation in an Ormosil PEBBLE matrix. The latter showed improved sensitivity towards singlet oxygen, compared to other common singlet oxygen probes used in aqueous media. By utilizing these PEBBLE nanoprobes, we were able to quantify the steady-state singlet oxygen concentration in the given PDT

system. Also, this revealed numerical evidence that an increase in photosensitizer amount does not guarantee better PDT efficiency. Furthermore, by discovering the difference in steady-state singlet oxygen concentration between cells and absence of cells, we could estimate the cellular consumption of singlet oxygen, which can be a direct and objective measure for cellular damage by singlet oxygen in a PDT system. We found a correlation of singlet oxygen consumption with cell survival (or death), which can be used to predict the cellular damage, depending on given conditions. This result can provide critical information to improve the current PDT dose-metric methods, enhancing therapeutic efficiency.

In Chapter 3, we presented evidence that the H_2O_2 selectivity of a nonspecific ROS molecular probe, DCFDA can be significantly improved by encapsulating it in a, relatively hydrophobic, Ormosil PEBBLE matrix. The use of the non-activated, hydrophobic DCFDA form, enables changing the simple post loading method into preformed Ormosil nanoparticles, using modified solvent displacement technique. The encapsulation of this dye into PEBBLEs suppressed an interference by HRP (with or without H_2O_2) while still catalyzing the nanoprobe's response towards H_2O_2. The PEBBLE matrix can protect the dye from interfering with those of very short lifetime,/ like the hydroxyl radical. The relatively hydrophobic Ormosil matrix can improve the sensitivity of the dye towards lipophilic ROS, like H_2O_2, and effectively repulse polar ROS, including superoxide , peroxynitrite, and nitric oxide, thus resulting in a significant improvement in the H_2O_2 specificity of DCFDA. The DCFDA Ormosil PEBBLE nanoprobes could measure quantitatively the H_2O_2 generation in stimulated macrophages, which is in the nanomolar concentration range. The PEBBLE nanoprobes were actively

delivered into the cytosolic area of macrophage cells by TAT peptide conjugation, thus avoiding effects of acidification during the phagocytosis of the macrophage.

In Chapter 4, a new type of PEBBLEs, for combined photoacoustic imaging and photodynamic therapy, was introduced. The photoacoustic contrast agent was developed based on Ormosil PEBBLEs, encapsulating a high concentration of the NIR absorbing photosensitizer dye, indocyanine green (ICG). These PEBBPEs provide efficient signal enhancement for photoacoustic imaging. Based on a photoacoustic imaging system appropriate for potential clinical applications, the instrumental detection limit was determined to be 10^{10} PEBBLEs/cm^3 at an illumination intensity of only 2.6 mJ/cm^2 and a diagnostically relevant wavelength of 800 nm. To provide sufficient contrast in tissue, at least a 10 times higher concentration is required. For typical cells with 20 μm in extent, this estimation corresponds to a concentration of 400 particles per cell, which is not excessive, representing an exciting prospect for molecular imaging in clinically relevant applications. A targeting antibody (anti-Her-2/neu) was conjugated to the surface of the nanoparticles. Specific binding of these nanoparticles to prostate cancer cells was demonstrated *in vitro*. Targeted cells were imaged by a high resolution photoacoustic scanner. High contrast was observed between targeted cells and non-targeted cells. ICG Ormosil PEBBLEs combine an additional feature that makes them especially attractive for future applications in cancer detection and treatment: They provide high contrast for photoacoustic imaging, can easily be designed to target specific cell membrane receptors, and can be used to generate singlet oxygen for PDT. Typical applications include: prostate cancer, bladder cancer, and cancers in the gastro-intestinal tract.

Future Directions

As described in Chapter 2, DPIBF Ormosil PEBBLE nanoprobes enable one to directly quantify the amount of singlet oxygen generated from a PDT system and thus present a new methodology for PDT dosimetry that is based directly on the singlet oxygen quantity, rather than on an indirect light dose and singlet oxygen quantum yield, which can be biased by the complexity of biological systems. However, it should be noted that this method can only be applied to a PDT system with certain assumptions. For example, the PDT system used for our research was based on an adherent cell line, where most cells were attached to the bottom of system, which means that the PDT effect occurred in a nearly 2-dimensional system. Thus, additional considerations should be required for studying a cell suspension or a 3-dimensional mass of cancer. Also, our experiments were based on non-targeted photosensitizers (in our case, MB PAA DNPs) and the photosensitizers were homogeneously distributed throughout the entire system, with DPIBF Ormosil PEBBLE nanoprobes. If the photosensitizers are targeted or delivered into cancer cells, the configuration of singlet oxygen detection with DPIBF Ormosil PEBBLE nanoprobes must be redesigned, corresponding to the localization of photosensitizers.

Also, the effect of other factors on singlet oxygen generation should be studied using DPIBF Ormosil PEBBLE nanoprobes. The current results were obtained under fixed conditions, including 2 mW excitation power, 5 minutes illumination time, 1 mg/mL and 0.1 mg/mL photosensitizer concentrations, a single cancer cell type, and so on. A variation of those factors should be comprehensively investigated and analyzed, so

as to build a complete data set for PDT dosimetry, which could be applied to any situation. With accumulation of such data, a prospective aim that may be achieved in the near future would be the determination of the cell type specific threshold level of singlet oxygen that is required for cell kill. Various cell types should be investigated, using the method proposed here. If this threshold level could indeed be determined, the PDT efficiency could be improved.

In Chapter 3 it was discussed that DCFDA Ormosil PEBBLE nanoprobes can have an improved H_2O_2 specificity, over other ROS, and 3 principles: size exclusion, lifetime exclusion, and hydrophobic interaction, were hypothesized to explain the mechanism of better H_2O_2 selectivity. Further investigations to demonstrate these principles would be an important task for H_2O_2 research. In order to do it, the properties of the Ormosil matrix need to be understood. Such understanding would not only be important for H_2O_2 research but also beneficial for developing new PEBBLE nanosensors or nanoprobes that are selective towards other ROS. Based on achieved H_2O_2 selectivity, DCFDA Ormosil PEBBLE nanoprobes can be a powerful tool for ROS research. Various physiological events related to H_2O_2, such as oxidative cell signaling and phagocytosis, could be investigated and understood, using these PEBBLE nanoprobes. Furthermore, a better understanding of H_2O_2 may result in a better understanding of other ROS as well.

Unlike the DPIBF Ormosil PEBBLE nanoprobes in Chapter 2 and the DCFDA Ormosil PEBBLE nanoprobes in Chapter 3, the ICG Ormosil PEBBLEs in Chapter 4 were basically developed for *in vivo* applications. The plan is as followed. The ICG Ormosil PEBBLEs would be injected into a blood vessel (vein) and then actively delivered to the tumor region, by targeting. The cancer tissue would be imaged and

diagnosed with photoacoustic imaging, and then would be destroyed with photodynamic therapy, by increasing the excitation of the beam power. In order to achieve these tasks, the biocompatibility of the Ormosil PEBBLE matrix should be studied and improved. Ormosil nanoparticles have a tendency to form aggregates in a solvent with high ionic strength, like biological media, and it can thus cause clogging of the blood vessel, non-specific binding with various biological matters, and immune reactions. In order to improve colloidal stability of the ICG Ormosil PEBBLEs, the surface of the PEBBLEs should be modified. A typical method for this surface modification is PEGylation. PEGylation of Ormosil PEBBLEs is already being studied. Utilization of a biocompatible surfactant, to improve the quality of PEBBLE suspension, is being investigated as a second approach. After that, *in vivo* photoacoustic imaging and PDT would be attempted.

Overall it has been shown here how to apply nano-encapsulation techniques to improve properties of molecular probes for ROS research. The developed PEBBLEs described in each chapter could initiate various new approaches for ROS and could contribute to expand our understanding about them.

Appendices

Appendix 1

PEBBLE to PEBBLE Detection of Singlet Oxygen in PDT

The Kopelman group has been developing an advanced photodynamic therapy (PDT) system based on PEBBLE technology, called Dynamic Nanoplatforms (DNPs). DNPs are typically PEBBLEs, made of biocompatible polyacrylamide (PAA) matrix, containing (1) photosensitizers such as Photofrin (PF) [1], methylene blue (MB) [2], disulfonated 4,7-and diphenyl-1,10-phenantroline ruthenium (Ru(dpp(SO3)2)3)) [3] for singlet oxygen generation, (2) targeted to cancer by incorporating tumor homing moieties on the surface of these PEBBLEs, and (3) multi-functional by including functional materials for different purposes together, such as imaging. Because encapsulation in the PEBBLE matrix often influences the properties of the dye contents, the singlet oxygen generation from these DNPs must be evaluated to determine their PDT efficiency prior to actual *in vitro* or *in vivo* PDT. A commercial water-soluble molecular probe, ADPA (9,10-antheracenedipropionic acid) has been mainly used to examine singlet oxygen generation from the given DNPs in our group.

For actual *in vitro* and *in vivo* PDT experiments, we have sometimes experienced poor PDT outcomes from DNPs that showed good singlet oxygen generation efficiency determined by ADPA. We now understand the reason of this mismatch: ADPA free

dye can readily diffuse into the DNP matrix and detect generated singlet oxygen inside of the DNP matrix, which however does not exit the PEBBLE, resulting in overestimated singlet oxygen generation efficiency.

This problem can be solved by using the DPIBF Ormosil PEBBLE nanoprobes described in Chapter 2. The detection of singlet oxygen using PEBBLE type probes can effectively exclude the singlet oxygen generated that did not come out of the DNP matrix, and thus a more accurate evaluation of the efficiency of singlet oxygen generation from DNPs can be achieved. This requires the singlet oxygen PEBBLE nanoprobes to have high sensitivity. As explained in Chapter 2, the sensitivity towards singlet oxygen of DPIBF Ormosil PEBBLE nanoprobes was verified to be better than that of other common probes. Based on this method, the singlet oxygen generation from various DNPs was evaluated with DPIBF Ormosil PEBBLE nanoprobes and compared to results from DPIBF free dye.

Experimental

Dye loading efficiency of PF embedded DNPs

Singlet oxygen generation is basically proportional to the amount of Photosensitizer, unless aggregation of dye is predominant. The quantity of PF dye encapsulated in 0.1 mg/mL PAA DNPs was estimated by comparing UV-VIS absorption intensity with calibration curve constructed by PF with known concentrations.

Evaluation of singlet oxygen generation from PF embedded DNPs

Various batches of photofrin embedded DNPs were examined. Suspensions of these PF DNPs were prepared in EtOH-water mixture (50:50) to give 2 different concentrations (1 mg/mL and 0.5 mg/mL). 200 uL of 0.2 mg/mL DPIBF Ormosil PEBBLE nanoprobes solution or 10 uM DPIBF free dye solution was mixed into 2 mL of each PF DNPs solution. The photosensitization was performed in fluorometer with 630 nm excitation for 5 minutes and the fluorescence of DPIBF Ormosil PEBBLE nanoprobes or DPIBF free dye was monitored in 420 – 620 nm range at various time points with 412 nm excitation wavelength. These experiments were done in the EtOH-water mixture to solubilize DPIBF free dye.

Results and Discussion

0.1 mg/mL of various PF PAA DNPs, including standard PF PAA DNP, PF embedded GBA-PAA DNP(GBA represents a cross-linker, glycerol dimethacrylate, used for the synthesis of this PAA DNP), PF embedded AHM-PAA DNP prepared from powder (AHM as well represents a cross-linker 3-acryloyloxy-2-hydroxypropyl methacrylate), PF embedded AHM-PAA prepared from solution (batch #10, #11, and #12) were examined. The UV-VIS spectra were measured in the range of 200 – 800 nm.

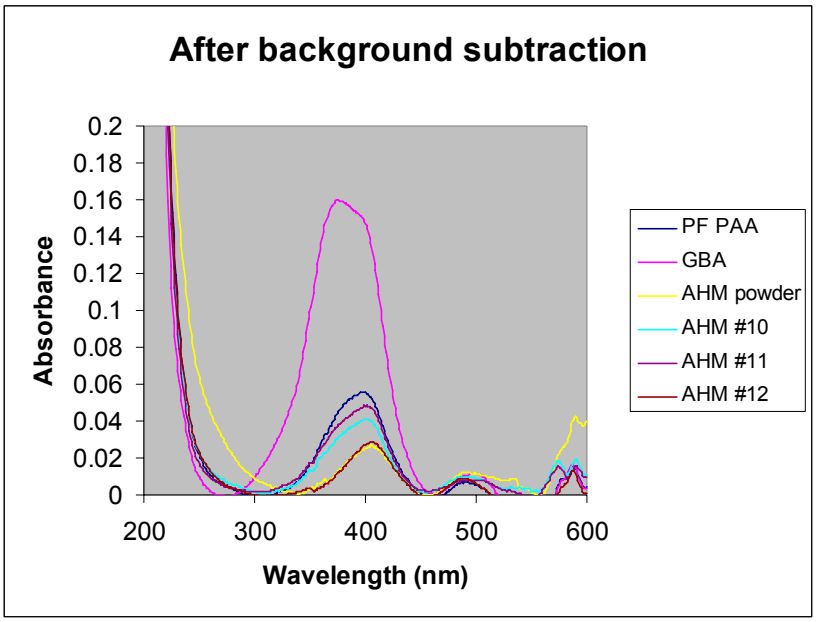

<Figure A1.1: UV-VIS absorption spectra of PF PAA DNPs, showing difference in dye loading capacity>

Several samples like PF PAA and PF AHM-PAA powder looked cloudy even after long ultrasonication (over 1 hour) and showed corresponding background effects induced by light scattering. This background effect must be subtracted for accurate estimation and comparison. The normalized result is displayed in figure A-1. The comparison was performed using the absorption peak located around 400 nm, which is maximum peak of PF absorption. It should be noted that the excitation wavelength for PDT with PF should be at 630 nm but it is not the strongest maximum in PF absorption. The concentration of embedded PF in each PEBBLE was calculated based on the calibration curve obtained from PF free dye with blank PAA nanoparticles and the estimated results are summarized in table A-1 as below.

Sample type	Absorbance	est. conc. (mg/mg)
PF PAA	0.056	0.004
GBA	0.160	0.016
AHM powder	0.027	0.001
AHM #10	0.041	0.003
AHM #11	0.048	0.004
AHM #12	0.029	0.001

<Table A1.1: Estimated dye loading (mg PF/mg PEBBLE) of PF in PAA DNPs based on the UV-VIS absorption intensity shown in figure A1.1>

Because of the inaccuracy in background subtraction procedure, this result should be relevant only for relative comparisons of PF dye loading among different batches of PF PAA DNPs. The PF embedded GBA-PAA showed highest dye loading, compared to the other batches, thus a higher singlet oxygen production can be expected as well.

Singlet oxygen production from each DNPs was examined using DPIBF free dye and DPIBF Ormosil PEBBLE nanoprobes under identical conditions. The fluorescence emission decay was monitored for 5 minute illumination times and the rate constant of this decay (k) was calculated, based on 1st order reaction kinetics, following the described method in Chapter 2. The results are displayed in figure A-2.

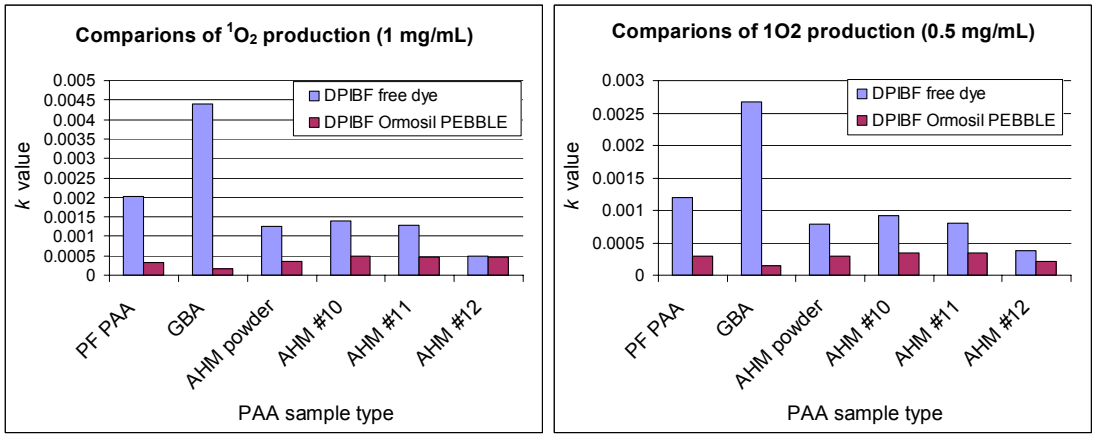

<Figure A1.2: Singlet oxygen production efficiency by various PF PAA DNPs at different PEBBLE concentrations (1 mg/mL and 0.5 mg/mL DNPs in water). The singlet oxygen production from various DNPs was significantly reduced when they were evaluated by DPIBF Ormosil PEBBLE nanoprobes compared to when they were evaluated by DPIBF free dye.>

When examined by DPIBF free dye, the singlet oxygen generation represented by the *k* value matched relatively well the PF concentration determined by UV-VIS absorption, though minor discrepancies were shown as well. Especially, the PF embedded GBA-PAA, which was the highest one in dye loading, showed a remarkably higher *k* value than the others. However, when examined by DPIBF Ormosil PEBBLE nanoprobes, a dramatic difference was observed. PF embedded GBA-PAA, which showed the best singlet oxygen production efficiency obtained from DPIBF free dye, turned out to be the least effective one when obtained from DPIBF Ormosil PEBBLE nanoprobes. Similar effects were observed in standard PF PAA DNP. In contrast, PF embedded AHM-PAA batch # 10 and # 11 exhibited much stronger singlet oxygen production when they were evaluated by DPIBF Ormosil PEBBLE nanoprobes. The same trend was observed from both concentrations of DNPs (1 mg/mL and 0.5 mg/mL), supporting the consistency of the data. This result clearly verifies that the singlet oxygen generation efficiency can be

significantly distorted when it is evaluated by a free dye probe of singlet oxygen, due to internalization of the dye in the DNP matrix. Based on this improved method of singlet oxygen production determination, an *in vivo* PDT experiment was carried out by Dr. Brian Ross' group at the University of Michigan, Department of Radiology, in a collaborative research, and a successful PDT outcome was obtained [4]. In conclusion, DPIBF Ormosil PEBBLE nanoprobes can provide a more accurate and credible singlet oxygen production determination for a DNP based PDT system, and it should be considered as another important advantage of using PEBBLEs.

References

1. Y-E. Koo, R. Kopelman et al., National Cancer Institute (NCI) project reports (unpublished).
2. W. Tang, M. Philbert et al., Photodynamic characterization and *in vitro* application of Methylene Blue-containing nanoparticle platforms, *Photochem. Photobiol.* (2005), v81, 242-249
3. M. J Moreno, R. Kopelman et al., Production of singlet oxygen by $Ri(dpp(SO_3)_2)_3$ incorporated in polyacrylamide PEBBLEs, *Sensors and Actuators* B, (2003), v90, 82-89
4. B. Ross, R. Kopelman et al., Photonic and magnetic nanoexplorers for biomedical use: from subcellular imaging to cancer diagnostics and therapy, *Proc. SPIE* (2004), v5331, 76-83

Appendix 2

Singlet Oxygen Detection in Live Macrophage *in vitro*

While singlet oxygen production and its mechanism *in vivo* are still largely unclear, there are several reports on singlet oxygen production in certain situations. According to Steinbeck *et al*., singlet oxygen production from stimulated macrophage and neutrophils has been detected by a singlet oxygen probe doped film and by micro beads [1,2]. Based on this finding, we attempted to detect production of singlet oxygen in live macrophage, using the DPIBF Ormosil PEBBLE nanoprobes described in Chapter 2

Experimental

A RAW264.7 murine macrophage cell line was used for singlet oxygen detection. The macrophage cells were cultured in a 6 well plate with glass cover slip, following the method described in Chapter 3. DPIBF Ormosil PEBBLE nanoprobes were added to the cell plate and incubated overnight, to allow sufficient cellular uptake. The cover slip was set into a cell chamber. The free PEBBLE nanoprobes were removed by repeated rinsing with fresh cell media. Then, 2.5 μL of a 1 mg/mL macrophage stimulating reagent, Phorbolmyristateacetate (PMA) solution in DMSO, was added to trigger oxidative bursts in macrophages. The change of the DPIBF Ormosil PEBBLE nanoprobes'

fluorescence intensity was monitored in an Olympus IMT II fluorescence microscope that is incorporated with a spectrometer using customized violet filter cube sets (415 nm exciter and > 450 nm dichroic mirror and emitter combination). Data were taken at various time points after the addition of PMA, until the DPIBF fluorescence intensity was stabilized. The same procedures were repeated by adding pure DMSO instead of PMA in DMSO for the control measurement.

Results and Discussion

Before doing the singlet oxygen detection in PMA stimulated macrophage, the cellular localization of Ormosil PEBBLE nanoprobes needed to be investigated, using confocal microscopy. Because appropriate filter sets, for visualizing DPIBF Ormosil PEBBLE nanoprobes directly, were not available, the localization of the PEBBLE nanoprobes was simulated using an Ormosil PEBBLE containing another fluorophore, DiI (a lipophilic long-chain carbocyanine dye with excellent brightness and stability). Also, the localization of DiI PEBBLEs inside of cells was further investigated, using a Z-series scanning function, which is a quantitative analysis of the fluorescence intensity at a certain spot during variation of the focal plane in the z-direction. The confocal fluorescence image of DiI Ormosil PEBBLEs and Z-series plot were displayed in figure A2.1.

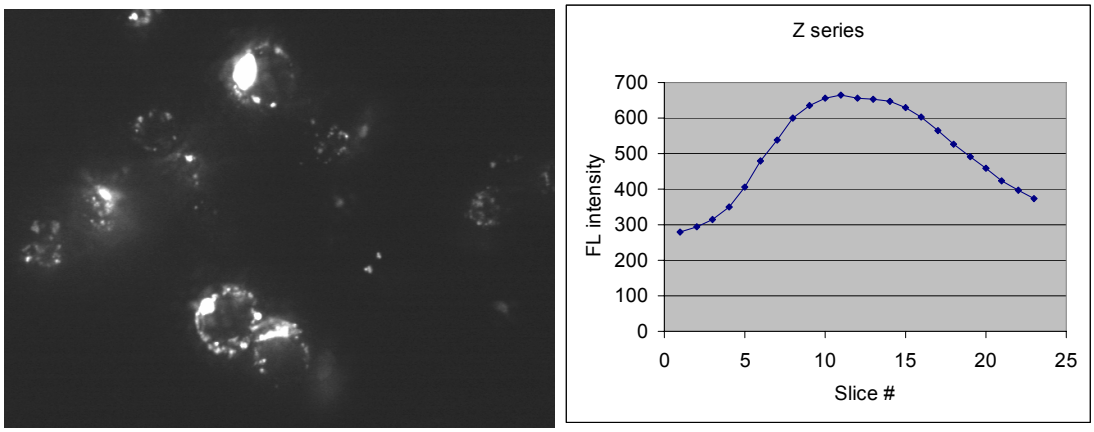

a) b)

<Figure A2-1: Intracellular localization of Ormosil PEBBLEs based on DiI fluorescence. a) confocal imaging of DiI Ormosil PEBBLEs to simulate DPIBF Ormosil PEBBLE nanoprobes, and b) a Z-series scanning, indicating highest distirubtion of PEBBLEs in the central region of intracellular space.>

The confocal images of macrophage incubated with DiI Ormosil PEBBLEs clearly revealed the shape of cells, indicating that the PEBBLEs were effectively delivered to cells. Because confocal images do not distinguish PEBBLEs located inside of cells from PEBBLEs that are attached to the cell membrane, a Z-series was necessary to be viewed. As shown in figure A2.1-b), The Z-series measured about bright spots in the cells showed that a majority of PEBBLEs were located in the central space, inside of cells, supporting that the Ormosil PEBBLEs were truly engulfed by the macrophage cells. Although this measurement was achieved using DiI Ormosil PEBBLEs instead of actual DPIBF Ormosil PEBBLE nanoprobes, the cellular uptake should mainly depend on the surface property of the PEBBLE matrix and thus it should be acceptable enough to conclude that DPIBF Ormosil PEBBLE nanoprobes would be localized in the same way as the DiI Ormosil PEBBLEs were.

Then, an *in vitro* singlet oxygen detection using DPIBF Ormosil PEBBLE nanoprobes was attempted. The fluorescence intensity changes of DPIBF Ormosil PEBBLE nanoprobes, monitored from PMA stimulated macrophages and from non-stimulated controls, are displayed in figure A2.2.

As summarized in figure A2.2, PMA stimulated macrophages showed rapid reduction of the DPIBF Ormosil PEBBLE nanoprobes' fluorescence, over 50 % from initial intensity after 30 minutes, while the controls showed only minor fluctuations over the same period. The fluorescence reduction mainly occurred within the first 5 minutes and then the fluorescence intensity was relatively stabilized. It is not certain whether the minor decrease during the later period (5 – 30 min) was caused by singlet oxygen production or by photobleaching of the PEBBLE nanoprobes. Because the DPIBF Ormosil PEBBLE nanoprobes are highly specific to singlet oxygen, over other ROS which can be generated during an oxidative burst, the decay of their fluorescence intensity must be induced by singlet oxygen. Therefore, this result provides definite evidence that macrophage can produce singlet oxygen in certain amounts when stimulated.

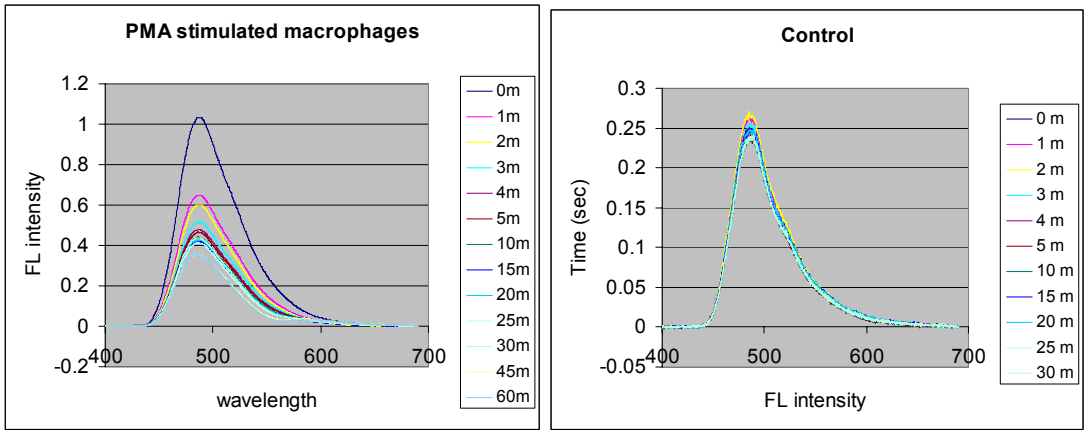

a) b)

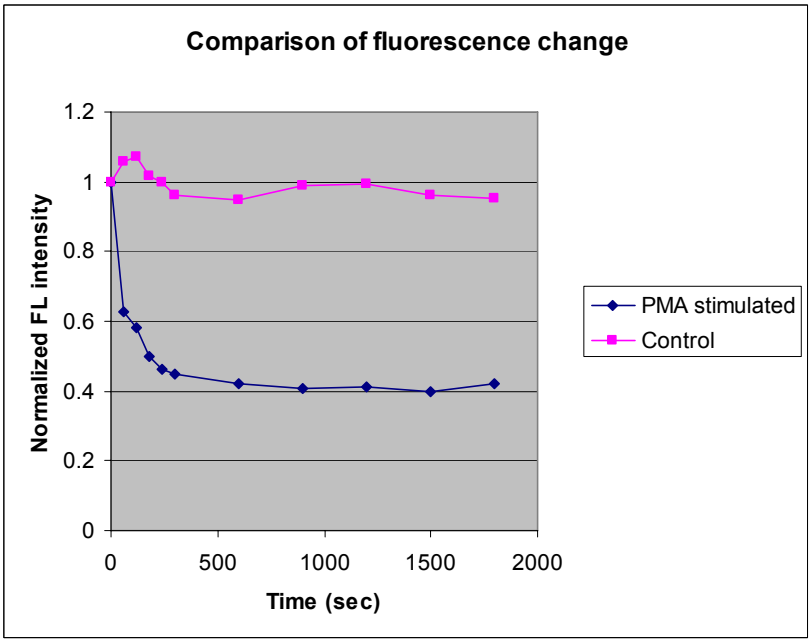

c)

<Figure A2.2: Fluorescence time change of DPIBF Ormosil PEBBLE nanoprobes, due to singlet oxygen produced from macrophage: a) response from PMA stimulated macrophage, b) response from non-stimulated macrophage (control), and c) comparison of fluorescence intensity changes between a) and b). The fluorescence intensity was normalized as I_t/I_0.>

In order to estimate the amount of singlet oxygen generated from the macrophage, a calibration curve between the DPIBF Ormosil PEBBLE nanoprobes, at various known concentrations, and their fluorescence intensity, was constructed under conditions

identical to those of the *in vitro* measurements above. Unlike for the PDT system, the singlet oxygen generation in stimulated macrophages is not in a steady-state and the methodology of singlet oxygen quantification based on the *k* value, described in Chapter 2, is not valid for this system. Thus, the amount of singlet oxygen was determined by estimating the amount of endoperoxides produced from the reaction between singlet oxygen and the DPIBF dye in the PEBBLE nanoprobes, and by applying a 1:1 stoichiometry between them, following known reaction mechanism [3]. The calibration curve is shown in figure A2.3.

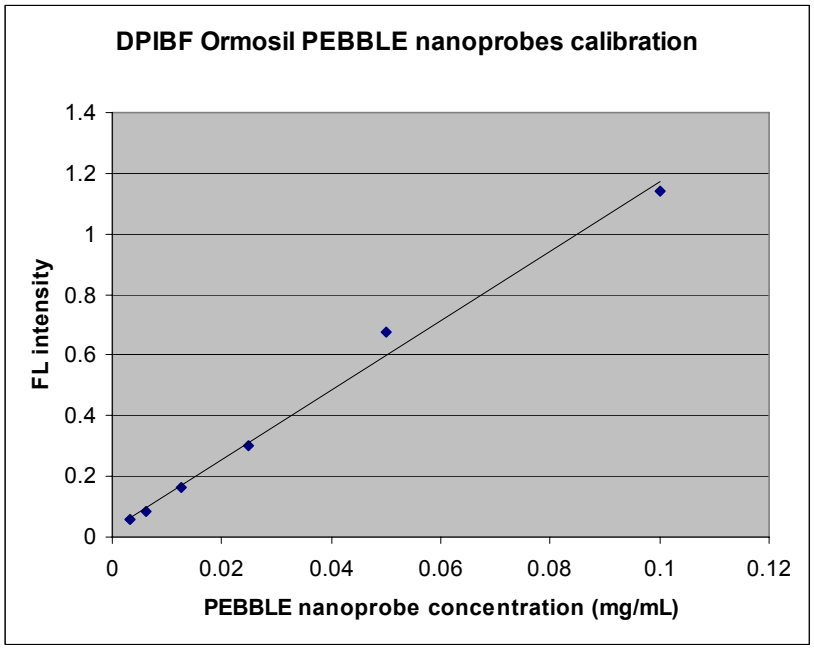

<Figure A2.3: A calibration curve showing the relation between the DPIBF Ormosil PEBBLE nanoprobe concentration and their fluorescence intensity for estimation of singlet oxygen production from stimulated macrophages>

According to the fluorescence spectra in figure A2.2-a), the fluorescence intensity value of DPIBF Ormosil PEBBLE nanoprobes in the given macrophage was initially

about 1.02 and then reduced to about 0.42 at 30 minutes; these values are equivalent to 0.087 mg/mL of the PEBBLE nanoprobes for the initial and 0.034 mg/mL for the final period. In other words, an amount of DPIBF molecules contained in 0.053 mg/mL of the Ormosil PEBBLE nanoprobes disappeared by reacting with singlet oxygen. The dye loading of DPIBF Ormosil PEBBLE nanoprobes has already been determined, in Chapter 2, as 0.1 mg/mL DPIBF Ormosil PEBBLE nanoprobe solution contains about 9.91 μM of DPIBF free dye. Based on this calculation, roughly, 5.25 μM of singlet oxygen was detected by the DPIBF Ormosil PEBBLE nanoprobes, in the given macrophage system. Because these results were obtained without considering cell density and assuring appropriate doses of PMA that depend on the cell density, the quantity of singlet oxygen produced by a single macrophage could not be determined. However, these results clearly showed that DPIBF Ormosil PEBBLE nanoprobes can be used to detect singlet oxygen production from an oxidative burst in live phagocytes. This opens up the possibility of further quantitative investigations of singlet oxygen mechanisms in biological systems, with high sensitivity and high specificity.

References

1. M. J. Steinbeck, M. J. Karnovsky *et al*., Extracellular production of singlet oxygen by stimulated macrophages quantified using 9,10-diphenylantheracene and perylene in a polystyrene film, *J. Biol. Chem.* (1993), v268(21), 15649-15654
2. M. J. Steinbeck, M. J. Karnovsky *et al*. Intracellular singlet oxygen generation by phatocytosin neutrophils in response to particles coated with a chemical trap, *J. Biol. Chem.* (1992), v267(19), 13425-13433
3. B. B. Merkel and D. R. Kearns, Rate constant for the reaction between 1,3-diphenylisobenzofuran and singlet oxygen. *J. Am. Chem. Soc.*, (1975), v97(2), (1975), 462-463